Design and Control of A DC Grid for Offshore Wind Farms

Deng, Fujin

Publication date:
2012

Document Version
Publisher's PDF, also known as Version of record

Design and Control of A DC Grid for Offshore Wind Farms

By

Fujin Deng

A dissertation submitted to

The Faculty of Engineering, Science, and Medicine, Aalborg University

in partial fulfilment of the requirements for the degree of

Doctor of Philosophy

Department of Energy Technology
AALBORG UNIVERSITY
Aalborg, Denmark 2012

Thesis title:

Design and Control of A DC Grid for Offshore Wind Farms

Name of PhD student:

Fujin Deng

Name and title of supervisor and any other supervisors:

Prof. Zhe Chen

List of published papers:

- Paper 1: Fujin Deng and Zhe Chen: "Low-voltage ride-through of variable speed wind turbines with permanent magnet synchronous generator". In *Proc 35th Annual Conference of Industrial Electronics*, 2009, pp. 621-626.

- Paper 2: Fujin Deng and Zhe Chen: "A new structure based on cascaded multilevel converter for variable speed wind turbine". In *Proc. 36th Annual Conference on IEEE Industrial Electronics Society*, 2010, pp. 3167-3172.

- Paper 3: Fujin Deng and Zhe Chen: "Variable speed wind turbine based on multiple generators drive-train configuration". In *Proc. IEEE PES Innovative Smart Grid Technologies Conference*, 2010, pp. 1-8.

- Paper 4: Fujin Deng and Zhe Chen: "An offshore wind farm with DC grid connection and its performance under power system transients". In *Proc. IEEE Power and Energy Society General Meeting*, July, 2011, pp.1-8.

- Paper 5: Fujin Deng and Zhe Chen: "Control of improved full-bridge three-level DC/DC converter for wind turbines in a DC grid". *IEEE Transaction on Power Electronics*, vol. 28, no. 1, pp. 214-324, January 2013.

- Paper 6: Fujin Deng and Zhe Chen: "Design of protective inductors for HVDC transmission line within DC grid offshore wind farms". Accepted, *IEEE Transactions on Power Delivery*.

- Paper 7: Fujin Deng and Zhe Chen. “Operation and control of a DC-grid offshore wind farm under DC transmission system faults”. Submitted to *IEEE Transactions on Power Delivery*, February 2012.

- Paper 8: Fujin Deng and Zhe Chen: “A control method for voltage balancing in modular multilevel converters”. Submitted to *IEEE Transactions on Power Electronics*, August 2012.

This thesis has been submitted for assessment in partial fulfilment of the PhD degree. The thesis is based on the submitted or published scientific papers which are listed above. Parts of the papers are used directly or indirectly in the extended summary of the thesis. As part of the assessment, co-author statements have been made available to the assessment committee and are also available at the Faculty. The thesis is not in its present form acceptable for open publication but only in limited and closed circulation as copyright may not be ensured.

Abstract

Wind power is growing rapidly around the world, and the offshore wind farm is currently seen as a promising solution to satisfy the growing demand for renewable energy source. Along with the increase in the capacity of offshore wind farms and the distance between offshore wind farms and land, the high-voltage direct current (HVDC) is attractive. In addition, the DC grid may also be interested for interconnecting the wind turbines in the collection level. As a consequence, a DC grid can be established for the offshore wind farm, where the wind power collection system and power transmission system both adopt DC technology. S far, the existing grid codes for wind turbines are mainly focused on AC system. Therefore, the faults analysis in the DC grid and the appropriate fault protections are required for the DC grid.

This thesis focuses on the design and control of the DC grid for offshore wind farms. The DC grid layout for offshore wind farm is introduced. The wind turbine configurations in DC grid are studied. A DC/DC converter is proposed for the wind turbine directly integrating to the DC grid. The operation principle of the DC/DC converter and the control of the wind turbine in DC grid are proposed as well. The HVDC transmission system configuration is studied. A DC/DC converter is proposed as the offshore converter to step up the collection level voltage to the transmission level voltage. The control strategies for the offshore converter and the onshore converter are proposed. The control of the DC grid under AC grid faults is discussed, and the improved control is presented to ride-through the AC grid faults for the DC grid. The cable fault in the HVDC transmission system is discussed. The performances of the HVDC system under faults are analyzed. And then, the protective inductor is proposed and designed for the HVDC system. Afterwards, the redundancy of the HVDC system under cable faults is studied, and a fault ride-through strategy is proposed for the DC grid under cable faults.

Throughout the thesis, the DC grid for offshore wind farms examples are modeled with the professional tool PSCAD/EMTDC, and the DC/DC converter prototype was built and tested in the laboratory, and the results verify the theoretical analysis.

Acknowledgements

The financial support for this research project given by the Department of Energy Technology and the China Scholarship Council is gratefully acknowledged.

I would like to express my deepest gratitude to my supervisor Prof. Zhe Chen for all support, guidance and encouragement during the project. I would also like to thank my colleagues Zhou Liu and Yunqian Zhang for lots of help in life and work. Thanks also to the people in the Department of Energy Technology for help during my PhD period.

Finally, I would like to thank my family and friends for their love and support.

Fujin Deng
Aalborg, Denmark
August, 2012

Contents

Abbreviation

AC	Alternating current
CB	Circuit breaker
DAB	Dual active bridge
DC	Direct current
DFIG	Doubly fed induction generator
EMF	Electric and magnetic field
EMI	Electromagnetic interference
FSWT	Fixed speed wind turbine
HB	Half bridge
FB	Full bridge
FBTL	Full bridge three level
HVAC	High voltage alternating current
HVDC	High voltage direct current
IFBTL	improved full-bridge three-level
IGBT	Insulated gate bipolar transistor
kV	Kilovollt
LCC	Line Commutated converter
MFT	Medium frequency transformer
MMC	Modular multilevel converter

MPPT	Maximum power point tracking
NPC	Neutral point clamped
NOFC	Negative offshore converter
NONC	Negative onshore converter
PCC	Point of common coupling
PD	Phase disposition
PMSG	Permanent magnet synchronous generator
POFC	Positive offshore converter
PONC	Positive onshore converter
PS	Phase shifted
PSC-SPWM	Phase-shifted carrier-based sinusoidal pulse width modulation
PWM	Pulse width modulation
SAB	Single active bridge
SCIG	Squirrel cage induction generator
SM	Submodule
SPWM	Sinusoidal pulse width modulation
VSC	Voltage source converter
VSWT	Variable speed wind turbine
WRIG	Wound rotor induction generator

Chapter 1

Introduction

1.1 Background

Wind power has been developed for a long time and kept the rapid growth around the world [1]. All existing offshore wind farms have an AC collection system so far, the collected power is then sent to an onshore AC grid through high-voltage alternating current (HVAC) or HVDC transmission technology [2-4].

With the increase in the capacity of offshore wind farms and the distance between the offshore wind farm and the land, the DC transmission, with the advantages such as reactive power and harmonics and so on, becomes attractive under the growing trends of the offshore wind farm development [5-8]. On the other hand, it may be an interesting and cost-effective solution that the DC grid for the interconnection of the wind turbines in the wind farm [9-15]. The DC grid only uses two cables which reduces the cost and the loss. In addition, the DC/DC converters would be applied in the DC grid as the voltage transformer instead of the large and heavy AC transformer. In DC grid, the output voltage of the wind turbine will be boosted to the collection level voltage by a DC/DC converter, and the collection level voltage will be further boosted to the transmission level voltage by a DC/DC converter. Owing to the application of the medium frequency transformer in the DC/DC converters, the size and weight of the component will be reduced, which is very significant for the application of DC grid for the offshore wind farm [9-15].

Recently, the grid codes have been issued for the grid connected wind turbines or wind farms to realize the continuity and security of transferring the wind power into the grid. However, the wind turbines are collected with AC grid in all existing offshore wind farms and the existing grid codes for the wind turbines are established for AC system, and there are rarely grid codes published for wind turbines in DC grid [16-18]. The

protective devices, such as DC circuit breakers, are still under development and not commercially available [19-20]. As a consequence, many aspects related to DC grid need to be studied, including the configuration and the control of the DC grid for offshore wind farms under normal situation and cable faults situation, the redundancy of the DC transmission system, and the operation of the DC grid after faults.

1.2 Overview of Previous Work

Regarding to the DC grid for offshore wind farms, the early solutions are mainly focused on the HVDC transmission system, which is used to transmit the offshore wind farm power to the land with the DC technology, especially for the large-scale offshore wind farm and the long distance between the offshore wind farm and the land. Through the HVDC technology, the loss and cost for the wind power system can be reduced [5-8].

Recently, the DC grid becomes attractive for the interconnection of the wind turbine in the offshore wind farm, where the output of the wind turbine is DC instead of AC, and the output of the wind turbine is directly connected into the DC grid.

The DC grid may offer some advantages for offshore wind farms in comparison with the AC grid, such as costs, reactive power, and harmonics etc. Especially, the DC/DC converter would be used in the DC grid instead of the ac transformer. In the DC grid, the modern DC/DC converter with the medium frequency transformer would be used to step up the voltage. Compared with the bulky 50 Hz transformer used in the traditional AC grid, the frequency of the DC/DC converter in the DC grid is much higher than 50 Hz, and the size and weight of the DC transformer can be reduced in comparison with the 50 Hz AC transformer. The size and weight of the device is very important in the development of the offshore wind farm [9-15].

A few DC/DC converters for the offshore wind farm have been presented in literatures [21-25], where the efficiency of the wind farm with different DC/DC converters was evaluated. Further, based on the DC/DC converter, the layouts of the DC grid for the offshore wind farm have been discussed. Besides, the basic control of the DC grid for the offshore wind farm has been introduced as well.

The protection for the DC grid is an important issue, for example, the DC cable faults would be severe and may damage the system, which becomes more challenging for such a DC grid [26]. A few protection methods have been introduced, for example, the DC switches and DC circuit breakers for isolating the faulty section of a DC system [27]. Especially, the passive and active DC breakers for high-voltage transmission system have

been developed [28]. On the other hand, a few measures are presented to monitor the DC fault and handle the DC faults in [26], [29-31].

As to the DC grid for offshore wind farms, further research is needed considering the design and control of the wind turbine suitable for the DC grid. Although a few DC/DC converters have been introduced before, there are still some challenges for the integration of wind turbines into the DC grid. The HVDC transmission system should be studied for the DC grid, which is obviously different from the existing offshore wind farms, because the offshore converter in the DC grid is a DC/DC converter not an AC/DC converter as in the existing HVDC transmission system. The design and control for the HVDC transmission system in the DC grid is also an important issue. Although a few literatures have reported the faults situation in the DC grid, the measures for the system protection is not enough, for example, the DC circuit breaker is being developed and not suitable for the perfect protection for the DC grid. Furthermore, the redundancy and the operation of the DC grid under cable faults have been rarely reported in detail.

1.3 Aims and Main Contributions of the Thesis

- **Objective 1:** To investigate the difference between the DC grid for offshore wind farms and the existing offshore wind farm configurations, and the design and control requirement for the DC grid
  Contribution: The basic information of the DC grid for offshore wind farms including layout, the important electrical components, protective devices, and cable are discussed.

- **Objective 2:** To develop the suitable wind turbine for DC grids
  Contribution: The wind turbine for DC grid has been studied. A suitable DC/DC converter associated with its operation principle applied for integrating the wind turbine into the DC grid is presented. The control of the wind turbine in the DC grid is also studied.

- **Objective 3:** To develop the HVDC transmission system for DC grids
  Contribution: The HVDC transmission system is developed in the DC grid for the offshore wind farm, which is different from that in the existing wind farm system. A DC/DC converter associated with its operation principle is presented for the HVDC transmission system in the DC grid. The basic control of the HVDC system in the DC grid is presented as well.

- **Objective 4:** To develop the control of the DC grid under AC grid faults
  Contribution: The AC grid fault is studied. The control of the DC grid of offshore wind farms to ride-through the AC grid fault is presented, which includes the wind turbine control, offshore converter control, and the onshore converter control. It has been proven that the wind farm can reconnect after the fault is cleared within the time specified in existing grid codes.

- **Objective 5:** To develop the protection for the HVDC system under cable faults
  Contribution: The performance of the DC grid under cable faults has been studied including the onshore converter and the offshore converter. The corresponding protections for the onshore converter and the offshore converter are presented and analyzed. The selection of the converter capacity and the protective devices size is studied.

- **Aim 6:** To develop the redundancy and the control for the DC grid under HVDC transmission system faults
  Contribution: The redundancy of the DC grid under the HVDC transmission system fault is investigated, and the corresponding operation of the switchgears for redundancy is studied. Furthermore, the control for the DC grid under HVDC system faults is presented, which can effectively ride-through the HVDC system faults for the DC grid.

1.4 Layout of the Thesis

The thesis studies the DC grid for offshore wind farms. Firstly, an overview of the DC grid for offshore wind farms is presented in Chapter 2, where the system layout of the DC grid is discussed. The main difference between the DC grid for offshore wind farm and the existing offshore wind farm is investigated, and the main components in the DC grid are indicated.

In Chapter 3, the variable-speed wind turbine (VSWT) for the DC grid is studied. The improved full-bridge three-level isolated DC/DC converter is indicated as a possible better option to integrate the wind turbine into the DC grid. In addition, the corresponding modulation strategies, voltage balancing control, as well as the wind turbine control are introduced. The simulation study and experimental test in the laboratory are both conducted, and the results verify the feasibility of this wind turbine configuration.

In Chapter 4, the HVDC transmission system is investigated. The onshore converter and the offshore converter associated with their control are discussed respectively. A

DC/DC converter is studied and presented for the offshore DC/DC converter. The performance of the DC grid under AC grid faults is analyzed, and the corresponding fault ride-through control for the DC grid is presented.

The HVDC transmission system fault in the DC grid is investigated in Chapter 5. The performances of the onshore converter and the offshore converter under faults are analyzed, and the corresponding protections for the onshore converter and the offshore converter are analyzed and designed. The redundancy for onshore station and offshore station under HVDC system faults is presented, which can be realized with the actions of the switchgears. The corresponding control for the wind turbine, the onshore converter, and the offshore converter under HVDC system faults are presented, which can effectively ride-through the HVDC system faults for the DC grid.

1.5 Publications

The publications are:

1. Fujin Deng and Zhe Chen, "Low-voltage ride-through of variable speed wind turbines with permanent magnet synchronous generator," in *Proc 35th Annual Conference of Industrial Electronics*, 2009, pp. 621-626.

2. Fujin Deng and Zhe Chen, "A new structure based on cascaded multilevel converter for variable speed wind turbine," in *Proc. 36th Annual Conference on IEEE Industrial Electronics Society*, 2010, pp. 3167-3172.

3. Fujin Deng and Zhe Chen, "Variable speed wind turbine based on multiple generators drive-train configuration," in *Proc. IEEE PES Innovative Smart Grid Technologies Conference*, 2010, pp. 1-8.

4. Fujin Deng and Zhe Chen, "An offshore wind farm with DC grid connection and its performance under power system transients," in *Proc. IEEE Power and Energy Society General Meeting*, July, 2011, pp.1-8.

5. Fujin Deng and Zhe Chen, "Control of improved full-bridge three-level DC/DC converter for wind turbines in a DC grid," *IEEE Transaction on Power Electronics*, vol. 28, no. 1, pp. 214-324, January 2013.

6. Fujin Deng and Zhe Chen, “Design of protective inductors for HVDC transmission line within DC grid offshore wind farms,” accepted, *IEEE Transactions on Power Delivery*.

7. Fujin Deng and Zhe Chen, “Operation and control of a DC-grid offshore wind farm under DC transmission system faults,” submitted to *IEEE Transactions on Power Delivery*, February 2012.

8. Fujin Deng and Zhe Chen, “A control method for voltage balancing in modular multilevel converters,” submitted to *IEEE Transactions on Power Electronics*, August 2012.

Chapter 2

DC Grids for Offshore Wind Farms

2.1 Introduction

Along with the increase in the capacity of offshore wind farms and the distance between the offshore wind farm and the land, the DC collection and the DC transmission grid, with the advantages such as reactive power and harmonics etc., becomes attractive under the growing trends of the offshore wind farm development [5-8].

Recently, the HVDC technology is being attractive for the long distance power transmission of the large-scale offshore wind farm, which can effectively reduce the cable loss and cost [5-8]. Owing to the benefits of the DC grid, the conception that using DC grid for the interconnection of the wind turbine instead of AC collection grid in the wind farm would be interesting for offshore wind farms [9-15]. As a consequence, the DC grid for the offshore wind farm may be developed with the DC technology, where the wind power in the wind farm are collected with DC network and transmitted to the offshore station. And then, the wind farm power is sent to the on land grid with the HVDC transmission system.

Similar to the existing offshore wind farm with AC collection system, the design and control of the DC grid layout, and the key components and so on will be an important issue, and should be considered.

2.2 DC-Grid Layout

The layout of the DC grid for offshore wind farms is still a matter of research and discussion. A few DC-grid layouts have been indicated in some literatures as shown in Fig. 2.1 [10]. In Fig. 2.1(a), a DC/DC converter is equipped in each wind turbine to step up the DC-link voltage of the wind turbine to the medium voltage level for power collection. And then, the collection voltage is boost up again by the DC/DC converter at the offshore station to the transmission voltage level. In Fig. 2.1(b), only a DC/DC converter is installed at the offshore station, which is used to step up the collection voltage level to the transmission voltage level. In Fig. 2.1(c), the DC/DC converter at the offshore station is omitted, and each wind turbine is equipped with a DC/DC converter to step up its output voltage.

In Fig. 2.1(a), owing to the DC/DC converter is equipped in each wind turbine, the collection voltage level can be set as a high voltage, which can reduce the cable losses at the collection level. The DC-link voltage in the wind turbine can be controlled, which can effectively increase reliability and improve system performance at the expense of the additional DC/DC converter in the wind turbine. In Fig. 2.1(b), there is only one DC/DC converter at the offshore station. The collection level voltage is the DC-link voltage of the wind turbine, which is normally as low as a few kilovolts (kV). Especially, at the large-scale offshore wind farm, the Fig. 2.1(b) may result in high current in the collection level system, which may have a high requirement for the DC cable. As to Fig. 2.1(c), where the DC/DC converter is only equipped in each wind turbine and the DC/DC converter at the offshore station is removed, the DC/DC converter in each wind turbine would step up the DC-link voltage of the wind turbine to the transmission voltage level, which would have a high requirement for the wind turbine.

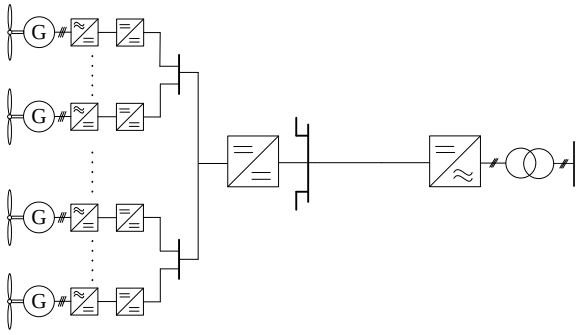

(a)

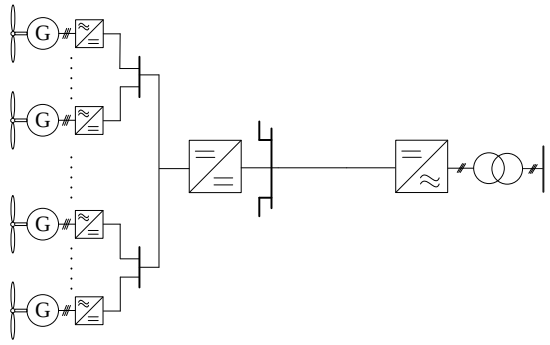

(b)

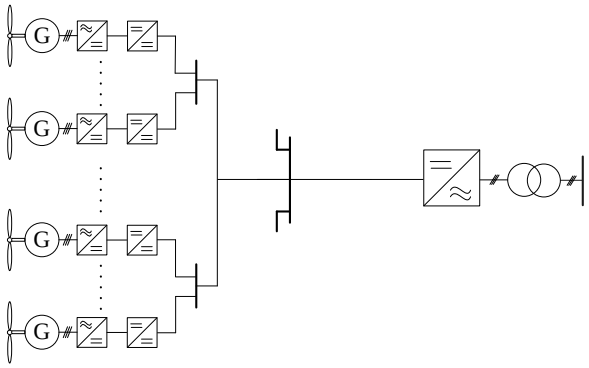

(c)

Fig. 2. 1. Block diagram of three DC-grid configurations for offshore wind farms. (a) Configuration A. (b) Configuration B. (c) Configuration C.

Recently, the AC distribution and transmission are commonly used with mature technologies. Hence, the DC grid for offshore wind farms can be designed in a similar way as a wind farm with an AC grid, where the wind turbines are connected in radials to a common DC/DC converter at the offshore station, and each DC cluster is in string connection as shown in Fig. 2.2 [2-15]. In the DC grid, the AC output of the generator in the wind turbine is converted into DC by the power converter and integrated into the DC collection system. And then, the output power of the wind turbines is collected and transferred to the offshore station, where the DC/DC converter is installed for stepping up the voltage from the collection level to the transmission level. Afterwards, the wind farm power is transmitted to the onshore converter with the HVDC technology and fed into the AC grid.

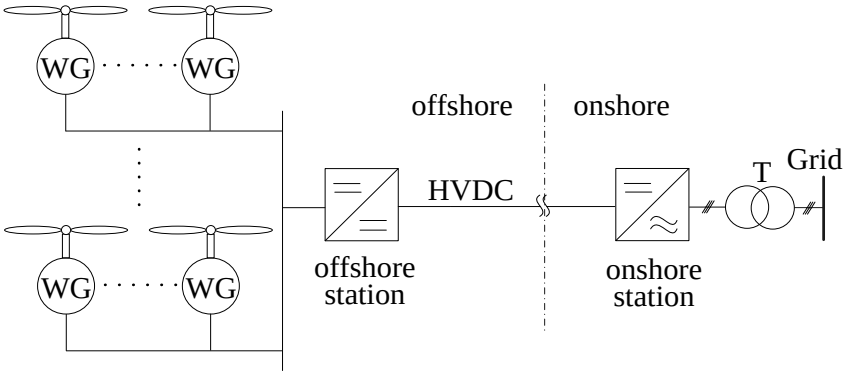

Fig. 2.2. Block diagram of the DC grid for offshore wind farms.

2.3 Wind Turbine

As shown in Fig. 2.2, in order to achieve the DC grid for offshore wind farms, the DC-grid wind turbine is an important component.

2.3.1 Wind Turbine Overview

With the rapid development of the wind power industry, the main three types of typical generator systems including Squirrel cage induction generator (SCIG), doubly fed induction generator (DFIG), and permanent magnet synchronous generator (PMSG), are widely used for the wind turbine development. Owing to the difference of the rotation speed range among the wind turbines, the wind turbine can be referred to as fixed speed, limited variable speed, and variable speed [33].

Fixed Speed Concept

Fig. 2.3 shows the Fixed speed wind turbine (FSWT) system, where the SCIG stator windings are directly connected to the grid through a transformer. A multiple-stage gearbox is equipped in the FSWT system and the SCIG is only operated around the synchronous speed. Therefore, the wind turbine, as shown in Fig. 2.3, is called fixed speed wind turbine system. Normally, a capacitor bank is equipped for reactive power compensation because the SCIG always draws reactive power from the grid. Although there are a few advantages for the FSWT including robust, easy and cheap for mass production and so on, a number of disadvantages also exist for the FSWT as follows [33].

- The wind turbine speed is only in a narrow range

- High mechanical and fatigue stress
- High flicker
- The grid voltage cannot be supported by this wind turbine system

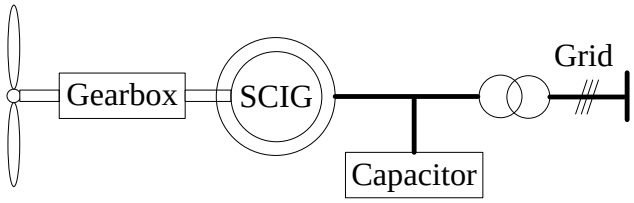

Fig. 2.3. Block diagram of the FSWT generation system.

Limited Variable Speed Concept

Fig. 2.4 shows the limited VSWT with a wound rotor induction generator (WRIG), where the WRIG stator is directly connected to the grid through a transformer. The power electronic converter is used to realize the variable rotor resistance. Through controlling the power extracted from the WRIG, the variable speed operation can be realized [33].

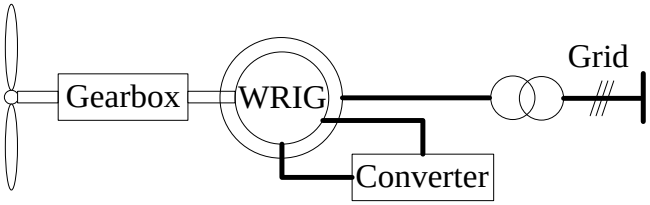

Fig. 2.4. Block diagram of limited VSWT generation system.

Variable Speed Concept with DFIG

Fig. 2.5 shows the VSWT based on DFIG, where the generator stator is directly connected to the grid, and the generator rotor is connected to the grid through a power electronic converter. The power converter controls the rotor speed. This type of wind turbine can be operated in a wide speed range. Normally, the speed range of the DFIG-based wind turbine is ±30% around the synchronous speed. The power converter is approximately 25~30% of the wind turbine capacity. As a consequence, this type wind turbine is attractive and popular from the view of economics. In addition, the power electronic converter can compensate the reactive power and support the grid voltage. However, the VSWT based on DFIG has the following disadvantages [33].

- A multi-stage gearbox is necessary in the drive train
- The slip ring may result in machine failure

- Large stator current may be caused during grid faults owing to the stator is directly connected to the grid

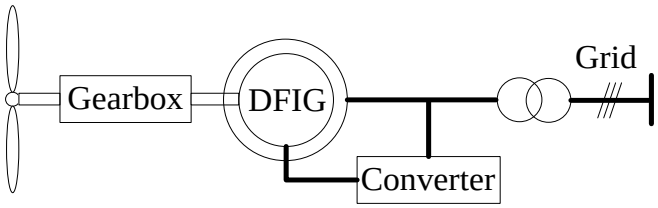

Fig. 2.5. Block diagram of VSWT generation system based on DFIG.

Variable Speed Concept with PMSG

Fig. 2.6 shows the VSWT based on PMSG, where the direct-drive PMSG is connected to the grid through a full-scale power converter. The generator is decoupled from the grid by the power converter, which ensures that the grid disturbances have no direct effect on the generator [33]. As a consequence, this type wind turbine can have a good performance over the entire speed range.

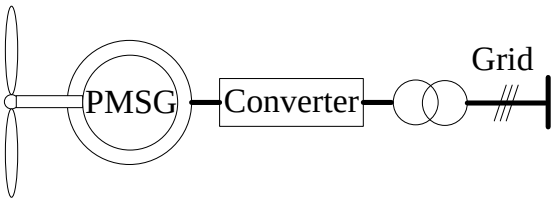

Fig. 2.6. Block diagram of VSWT generation system based on PMSG.

2.3.2 DC-Grid Wind Turbine

Various wind turbines for the AC-grid integration have been developed and commonly used with mature technologies, which is mainly consists of the generator and the power converter. The DC-grid wind turbine can also be designed in a similar construction.

Generator for DC-grid wind turbine

According to the aforementioned introduction, three main generator including SCIG, DFIG, and the PMSG associated with different wind turbine configurations are popular in wind power industry. With large-scale exploration and integration of wind sources, VSWT system is becoming more popular than FSWT system [34], which results in that

the DFIG and PMSG may be interesting for the DC-grid wind turbine. On the other hand, in comparison with the DFIG, the PMSG has a few advantages as follows [35].

- High efficiency
- High reliability such as no slip rings
- Application of PM for rotor

Recently, the performance of the PMSG is being improved and the cost of the PM is decreasing, which makes PMSG more attractive for the wind turbine. As a consequence, the PMSG with a full-scale power converter will be a promising construction for the DC-grid wind turbine.

AC/DC Converter for DC-Grid Wind Turbine

The power converter is a key component in the VSWT. So far, a few literatures report the power converters for the VSWT based on PMSG, which are mainly contains two types as shown in Fig. 2.7 [36-43]. In Fig. 2.7(a), the PMSG is connected to the DC grid only with an AC/DC converter. In Fig. 2.7(b), the PMSG is connected to the DC grid through an AC/DC converter and a DC/DC converter. In comparison with Fig. 2.7(a), a grid-side DC/DC converter is used in Fig. 2.7(b).

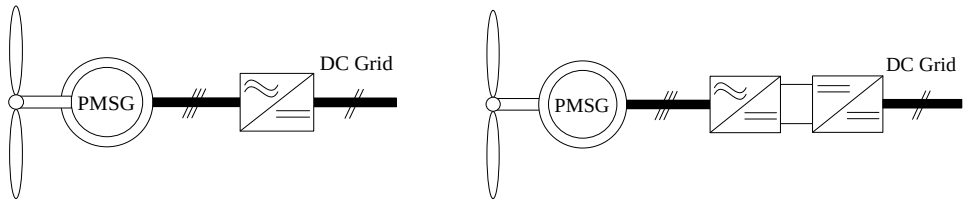

(a) (b)

Fig. 2.7. Block diagram of DC-grid wind turbine. (a) Topology A. (b) Topology B.

So far, a few AC/DC converters and DC/DC converters have been reports for the wind turbine generation system. Figs. 2.8(a) and (b) show the wind turbine configuration based on the two-level and three-level voltage source converter (VSC) respectively, which are widely used for the wind power generation system [36-40]. Fig. 2.8(c) shows another wind turbine configuration with the diode rectifier and the boost converter [40-43].

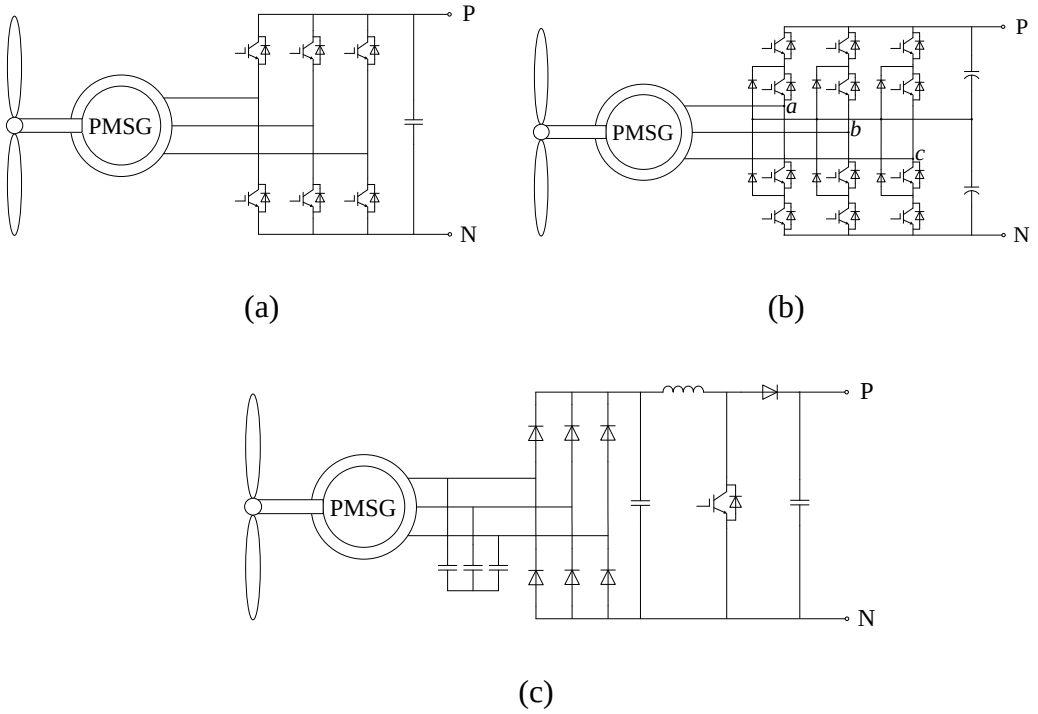

Fig. 2.8. Block diagram of PMSG with (a) Two-level VSC. (b) Three-level VSC. (c) Diode rectifier and boost converter.

Fig. 2.8(c) is the simplest configuration among the three types, which requires the least number of switches and reduces the cost. However, the switch in Fig. 2.8(c) has to take the full DC-link voltage, and the voltage change rate dv/dt is high. In addition, the use of the diode rectifier as the generator side converter may cause high THD of the generator output [44]. The two-level VSC, as shown in Fig. 2.8(a), is commonly used in the wind turbine system because of its simple structure and few components. However, along with the increase of the power and voltage range of the wind turbine, the two-level VSC may suffer from larger switching losses and lower efficiency such as the MW and MV power levels. In addition, the only two voltage stages cause higher dv/dt stresses to the generator, and the bulky output filters may be required [45]. Three-level neutral point clamped (NPC) topology, as shown in Fig. 2.8(b), is one of the most commercialized multi-level converters for wind power systems. The switches in the three-level VSC only take half of the DC-link voltage, which effectively reduces the dv/dt in comparison with the other two configurations [45].

DC/DC Converter for DC-Grid Wind Turbine

The high power DC/DC converters are key components for realizing the DC-grid wind turbine. In the DC grid, the DC/DC converters equipped with the medium

frequency transformer would replace the large and heavy AC transformers to boost the output voltage of the wind generator to the medium voltage level for the collection system. The application of DC/DC converters has a number of advantages since they can eliminate the large AC transformers, and reduce the size and weight of the system.

To date, a number of DC/DC converters have been reported including isolated and non-isolated configurations [21-25], [45-66], while most of the DC/DC converters are for the low voltage and low power application, and the DC/DC converters for these high power levels are still under development. The development of the DC/DC converter for the DC grid will be an important issue.

2.4 HVDC System

2.4.1 HVDC System Overview

The HVDC technology is an efficient and flexible method to transmit large amounts of electric power over long distances by overhead transmission lines or underground/submarine cables.

Recently, there are mainly two types of HVDC transmission technologies. One is the classical HVDC transmission system based on current source converters with naturally commutated thyristors as shown in Fig. 2.9 (a), and called Line Commutated converter (LCC) [2]. From Fig. 2.9(a), it can be seen that the classical HVDC transmission system is naturally able to withstand short circuit currents due the DC inductors limiting the current during faults condition. The other one is the new HVDC transmission using VSC (Self-Commutated Voltage Source Converter) with pulse-width modulation as shown in Figs. 2.9 (b)~(d) [3-5], [67].

These days, the VSC-HVDC transmission system becomes more and more attractive, which are marked by ABB with the name “HVDC Light” and by Siemens with the name “HVDC Plus”. In the VSC-HVDC technology, the Insulated gate bipolar transistors (IGBTs) are used, and can switch off currents, which means that there is no need for an active commutation voltage. The VSC-HVDC transmission does not requires a strong offshore or onshore AC grid. Besides, the active and reactive power can be controlled independently in the VSC-HVDC transmission system, which can reduce the need for reactive power compensation and contribute to the stability of the AC grid. Furthermore, owing to the use of IGBT semiconductors, the VSC-HVDC transmission system may have a high switching frequency and reduce the harmonic content of the system, which results in a reduced size of the filter required at the AC side.

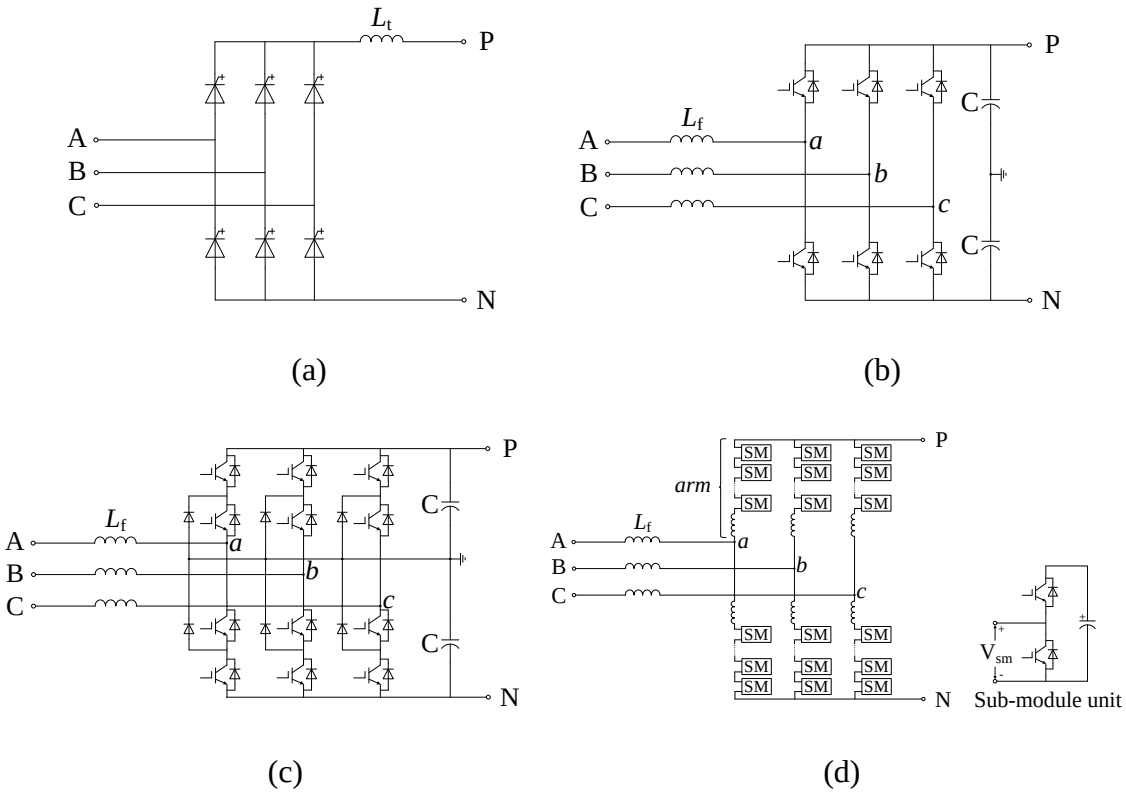

Fig. 2.9. Block diagram of (a) Six-pulse valve LCC-HVDC. (b) Two-level VSC-HVDC. (c) Three-level VSC-HVDC. (d) Modular multilevel converter (MMC)-based HVDC.

Normally, the DC/AC converter for the VSC-HVDC transmission system contains two-level VSC, three-level VSC, and the MMC-based VSC as shown in Figs. 2.9(b)~(d).

Two- and Three-Level VSC for HVDC

As shown in Figs. 2.9(b) and (c), the two-level VSC is the simplest configuration and only consists of six valves, which can create two voltage levels. The three-level topology is currently a popular converter, which can generate three voltage levels. The two- and three-level VSCs have been used in the commissioned projects [68], where the two- or three-level pulse width modulation (PWM) are used to approximate the desired waveform. For such converter topologies a high number of semiconductor devices with blocking capability of several kilovolts are connected in series. In order to ensure uniform voltage distribution, all devices connected in series in one converter arm must be switched simultaneously. As a consequence, high and steep voltage steps are applied at the AC side, which causes high component stresses and extensive filters are required.

MMC for HVDC

The MMC configuration is a novel multilevel configuration as shown in Fig. 2.9(d), which has been introduced by Siemens into HVDC applications during recent years [69], [70]. The MMC consists of six converter arms, each of which comprises a high number of SMs and one converter reactor connected in series. The converter arm acts as a controllable voltage source produced by a number of identical but individually controllable SMs to create a high number of discrete voltage steps, which forms an approximate sine wave with adjustable magnitude of the voltage at the AC terminal. Due to the converter reactor in each arm, the effects of faults arising within or outside the converter can be reduced [71]. As a consequence, the MMC technology provides significant benefits for HVDC transmission systems.

2.4.2 HVDC System for DC Grid

As shown in Fig. 2.2, the HVDC transmission system contains an offshore station, transmission cables, and an onshore station. At the offshore station, the offshore converter is used to collect the DC clusters and convert the DC voltage from the collection voltage level to the transmission voltage level. At the onshore station, the DC power is converted into AC and sent into the AC grid. As a consequence, the HVDC transmission system in the DC grid is different from the existing HVDC transmission system, where the AC/DC or DC/AC power conversion is used at each point of the HVDC transmission system. Hence, a HVDC transmission system configuration is required for the DC grid as shown in Fig. 2.10, and a DC/DC converter should be developed for the offshore converter in the DC grid.

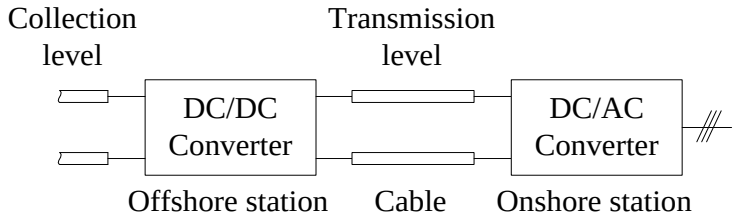

Fig. 2.10. Block diagram of HVDC transmission system in the DC grid.

2.5 Protective Devices

In the DC grid for offshore wind farms, the wind turbine, the offshore converter, and the onshore converter are connected through submarine cables. In case of a cable fault, it may take a long time to clear the fault. As a consequence, the protection in the DC grid

for offshore wind farms must be a priority. The protection of the offshore wind farm can be done with AC circuit breakers, DC switches, and DC circuit breakers and so on. In addition, the chopper resistor for discharging a DC link may be used for protection.

AC Circuit Breaker

The AC circuit breaker (CB) is widely used. It is the most economical way to protect the DC system using the AC CB at the AC side. However, it requires a long time for the AC CB to interrupt the circuit because of their mechanical restrictions, and the best interrupting time for an AC CB is two cycles these days [72].

DC Switch

The DC switch is fast operating mechanical switch. However, the DC switch has no capability of interrupting a fault current [30].

DC Circuit Breaker

The DC CB is different from the AC CB because of the absence of a natural current zero crossing in the DC system. The DC CB has to interrupt short-circuit current very quickly. Currently, the DC CB is only widely available for the low- and medium-voltage range. The breaker interrupting HVDC short-circuit current is not commonly available and has very limited ratings. A few proposals for the DC CB design have been presented in the literatures, which comprise different series and parallel connections of classical AC interrupters, resonance circuits with inductors and capacitors, semiconductors, charging units, or resistors. For example, the passive and the active DC breaker based on standard SF_6 AC circuit breakers with auxiliary circuits for high-voltage transmission system has been developed, which normally needs tens of milliseconds to interrupt the DC circuit [27], [28]. Fig. 2.11 shows the circuit breaker with a passive auxiliary circuit. In the circuit breaker with an active auxiliary circuit, the capacitor *C* is pre-charged prior to the switching and one circuit breaker is inserted between capacitor *C* and inductor *L* [28].

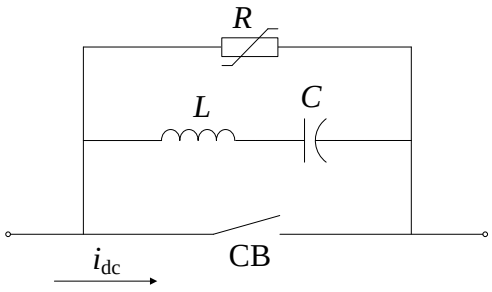

Fig. 2.11. Block diagram of a HVDC circuit breaker with a passive auxiliary circuit.

2.6 Summary

In this chapter, the DC grid for offshore wind farms is introduced, including its layout, and the key components. The layout of the DC grid for offshore wind farms may be similar to the AC-grid structure. The wind turbine configuration and the HVDC transmission system configuration in the DC grid are different from that in the existing AC offshore wind farm. In the DC grid, the DC/DC converter should be developed for the DC integration of wind turbines and the HVDC transmission system.

Chapter 3

Wind Turbine for DC Grids

3.1 Introduction

The wind turbine is an important component in the DC grid, which is required to produce a DC output and can be integrated into the DC grid directly. As introduced in Chapter 2, a DC-grid wind turbine configuration is shown in Fig. 2.7(b), where the AC output of the generator is converted into DC with the generator-side converter, and a DC/DC converter is used as the grid-side converter to step up the DC-link voltage to a high value. Two types of generator-side converter are introduced for the DC-grid wind turbine. The first one is with the uncontrollable diode rectifier as the generator side converter. The second one is with the VSC as the generator-side converter.

In the wind turbine with uncontrollable diode rectifier, the AC output of the generator is converted to DC by the diode rectifier, and the generator is controlled by the DC/DC converter. Although the wind turbine with the uncontrollable diode rectifier as the generator-side converter has reduced cost in comparison with the wind turbine with the VSC as the generator-side converter, the output THD of the generator with the diode rectifier is much high in comparison with the generator with VSC. In the wind turbine with the VSC as the generator-side converter, the generator is controlled with the VSC, and the DC-link in the wind turbine is kept by the grid-side DC/DC converter, which can reduce the disturbance of the DC grid on the wind turbine. In a word, a high efficient DC/DC converter is required to realize the DC connection and power delivery for the DC-grid wind turbine.

These days, most exist DC/DC converters are used in the low power applications. The low power DC/DC converters are common but the high-voltage and high-power

DC/DC converters in the MW-level are rarely available on the market. So far, a lot of DC/DC converters have been studied in literatures [45-67], such as boost converter, forward converter, half-bridge (HF) converter, full-bridge (FB) converter, and Dual active bridge (DAB) converter and so on. Their characteristics, performance, control, and loss and so on are also compared as well. In addition, the three different topologies, including the FB converter, the single active bridge (SAB) converter, and the resonant converter, are evaluated for the applications in the DC grid for offshore wind farms, regarding losses, contribution to energy production cost, design, and control and so on. However, the three topologies are all the two-level configurations, which may be not suitable for the medium-voltage and high-power application.

In this chapter, the possible DC/DC converters for wind turbine integrating into the DC grid are considered and compared, and an isolated full-bridge three-level (IFBTL) DC/DC converter is proposed to integrate the wind turbine into the DC grid. The corresponding modulation strategy and control are also studied. Finally, a down-scaled IFBTL DC/DC converter prototype was built and tested in the laboratory, and the results verified the theoretical analysis.

3.2 Wind Power Generator System

3.2.1 Aerodynamic System

According to [36], the extracted wind power of the wind turbine can be described as

$$P_w = \frac{1}{2}\rho\pi R_b{}^2 v^3 C_p(\theta,\lambda) \quad (3\text{-}1)$$

with

$$C_p = 0.73\left(\frac{151}{\lambda_i} - 0.58\theta - 0.002\theta^{2.14} - 13.2\right)e^{-18.4/\lambda_i} \quad (3\text{-}2)$$

$$\frac{1}{\lambda_i} = \frac{1}{(\lambda - 0.02\theta)} - \frac{0.003}{(\theta^3 + 1)} \quad (3\text{-}3)$$

where P_w is the extracted wind power, v is the wind speed, R_b is the blade radius, ρ is the air density, C_P is the power coefficient, θ is the pitch angle, $\lambda=\omega_w R/v$ is the tip speed ratio, ω_w is the wind turbine speed.

According to (3-1)~(3-3), Fig. 3.1 shows the wind turbine power curves under various wind speeds. There is a specific point in wind turbine power versus wind turbine speed curve for each wind speed, where the wind turbine power is maximized [74]. As a consequence, a variable-speed operation is used for the wind turbine, where the wind turbine will follow the optimal power for the wind below the rated wind speed. When the wind speed is high, the pitch angle control system will be activated to limit the wind turbine at the rated power.

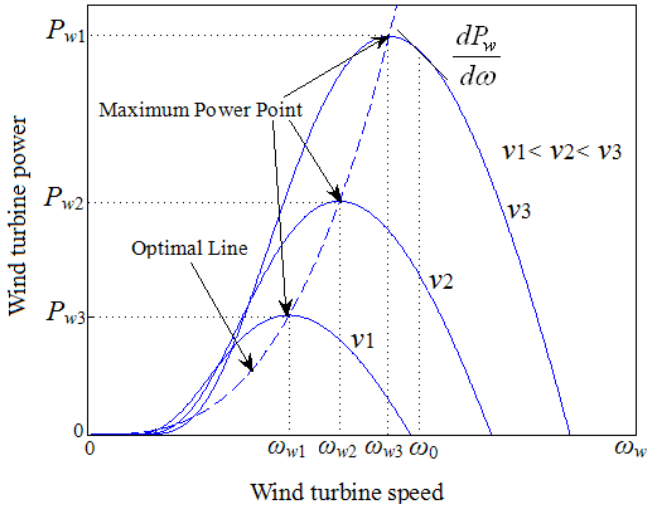

Fig. 3.1. Wind turbine power curves under different wind speeds.

Based on the aforementioned analysis, the optimal power captured from the wind can be expressed as

$$P_{w\_opt} = \frac{1}{2}\rho\pi R_b^{\,5}\frac{C_{p\_\max}}{\lambda_{opt}^3}\omega_w^3 \tag{3-4}$$

Fig. 3.2 shows the power versus rotor speed characteristic of the wind turbine that leads to optimal power capture from the wind based on the maximum power point tracking (MPPT) method [75]. The 5 MW wind turbine parameters are used here as shown in the Appendix A. The rotor speed of the wind turbine can be easily measured, and normally used as a controller input instead of the wind speed to get the reference power. A control curve AB is depicted in Fig. 3.2, because of the possible power fluctuations when the rotor speed changes near the minimum rotor speed [73].

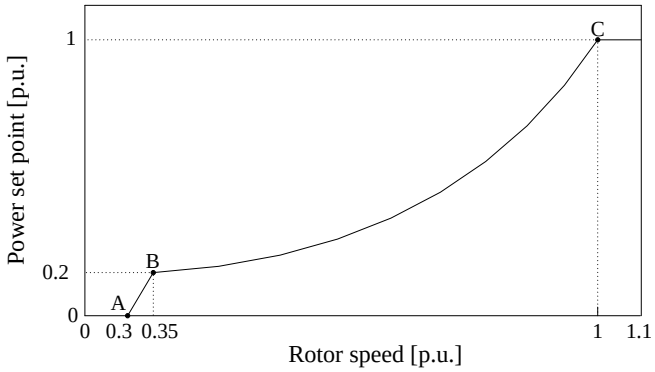

Fig. 3.2. Optimal power characteristic versus rotor speed.

3.2.2 Pitch Angle Control System

A pitch angle control system is normally needed to keep the turbine's speed constant without over-speed so as to limit the aerodynamic power of the wind turbine above the rated wind speed. Owing to the big inertia constant (3 to 9 s) for the MW-level wind turbine system, the pitch actuator angle in the MW-level wind turbine cannot be changed very quickly. The maximum change rate of the pitch angle in a MW-level wind turbine is normally between 3 and 10 degree per second [73].

Fig. 3.3 shows the pitch angle control system in the wind turbine, which is composed with a controller and a first-order actuator. If the generator rotor speed ω_e is below the reference value ω_{max}, the wind turbine power is controlled to track the optimal power. If the generator rotor speed ω_e is over the ω_{max}, the pitch angle control system will be activated to increase the pitch angle and drive the generator speed back to the maximum permitted value [76].

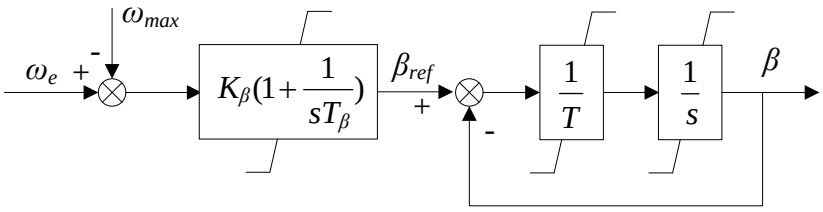

Fig. 3.3. Pitch angle control system.

3.2.3 Mechanical Drive Train

Fig. 3.4 shows the two-mass drive train, which has been proved to be suitable for transient stability analysis [77]. According to [78], the dynamic of the two-mass drive train can be described as

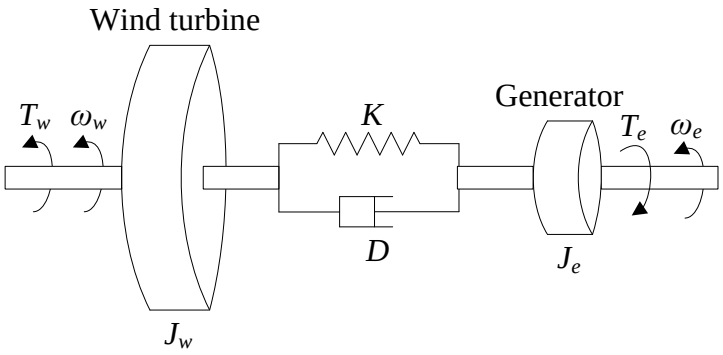

Fig. 3.4. Block diagram of the two-mass model.

$$\begin{cases} J_w \dfrac{d\omega_w}{dt} = T_w - K\theta_{we} - D(\omega_w - \omega_e) \\ J_e \dfrac{d\omega_e}{dt} = K\theta_{we} + D(\omega_w - \omega_e) - T_e \end{cases} \tag{3-5}$$

where T_w and T_e are the aerodynamic torque of the wind turbine and the generator torque, respectively. J_w and J_e are the equivalent wind turbine inertia and generator inertia, respectively. ω_w and ω_e are the wind turbine and generator rotor speed, respectively. θ_{we} is the angle between the turbine rotor and the generator rotor. K is the shaft stiffness. D is the shaft damping.

3.2.4 Permanent Magnet Synchronous Generator

The PMSG is chosen as the generator for the offshore wind farm in this study. In a PMSG, the rotor excitation is constant. According to [79], [84], the PMSG model under the synchronous reference frame can be described as

$$\begin{cases} \dfrac{di_{\mathrm{sd}}}{dt} = -\dfrac{R_s}{L_{\mathrm{sd}}} i_{\mathrm{sd}} + \omega_{\mathrm{e}} \dfrac{L_{\mathrm{sq}}}{L_{\mathrm{sd}}} i_{\mathrm{sq}} + \dfrac{1}{L_{\mathrm{sd}}} u_{\mathrm{sd}} \\ \dfrac{di_{\mathrm{sq}}}{dt} = -\dfrac{R_s}{L_{\mathrm{sq}}} i_{\mathrm{sq}} - \omega_{\mathrm{e}} \left(\dfrac{L_{\mathrm{sd}}}{L_{\mathrm{sq}}} i_{\mathrm{sd}} + \dfrac{1}{L_{\mathrm{sq}}} \psi_{\mathrm{r}} \right) + \dfrac{1}{L_{\mathrm{sq}}} u_{\mathrm{sq}} \end{cases} \tag{3-6}$$

The electromagnetic torque can be expressed as

$$T_e=1.5n_p((L_d-L_q)i_di_q+i_q\psi_f) \tag{3-7}$$

where R_s is the stator resistance. L_{sd} and L_{sq} are the generator inductances in the dq reference frame, respectively. u_{sd} and u_{sq} are the stator voltage in the dq reference frame, respectively. i_{sd} and i_{sq} are the stator current in the dq reference frame, respectively. ω_e is the electrical rotating speed of the generator. T_e is the electromagnetic torque. n_p is the number of pole pairs. ψ_r is the rotor magnetic flux.

3.2.5 Wind Turbine I

Fig. 3.5 shows the configuration of the wind turbine I, where the three-level NPC converter is used as the generator-side converter, and a DC/DC converter is used as the grid-side converter. The PMSG is controlled by the NPC converter for the optimal power capture, and the DC-link voltage V_{LV} in the wind turbine is kept constant by the DC/DC converter.

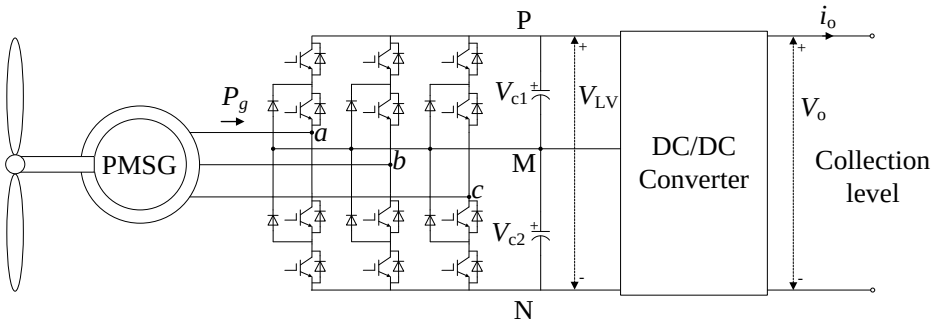

Fig. 3.5. Block diagram of the wind turbine I.

3.2.6 Wind Turbine II

The configuration of the wind turbine II is shown in Fig. 3.6, where the diode rectifier is used as the generator-side converter, and a DC/DC converter is used as the grid-side converter. The diode rectifier convert the AC output of the generator to DC, and the DC/DC converter boost the DC-link voltage to the collection voltage level. In wind turbine configuration II, the PMSG is controlled by the DC/DC converter.

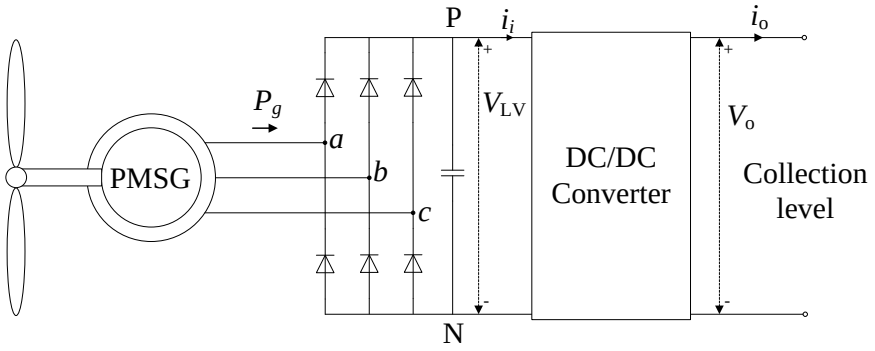

Fig. 3.6. Block diagram of the wind turbine II.

3.3 DC/DC Converter

In order to integrate the wind turbine into the DC grid, the high-efficiency DC/DC converter is inevitable. A number of DC/DC converters have been presented in the literatures [45-66]. In this thesis, the two-level and three-level configurations are mainly considered, because both of the two configurations have been widely used for wind turbines [66]. Among the existing DC/DC converters, a few possible candidates of the DC/DC converters to integrate the wind turbine into the DC grid are shown in Fig. 3.7, which mainly contains the basic FB two-level converter, the basic HF three-level converter, the basic FB three-level converter, and the FB three-level converter based on SMs. The four converter configurations for an example of a 2.5 MW wind turbine system are considered in Table 3.1. The system parameters are shown in the Appendix B. The rated input voltage V_i is 5.4 kV. The 1700V/600A IGBT (FZ600R17KE3) with the nominal device voltage V_{com} at 100 FIT as 900V is applied for the different converter configurations [80].

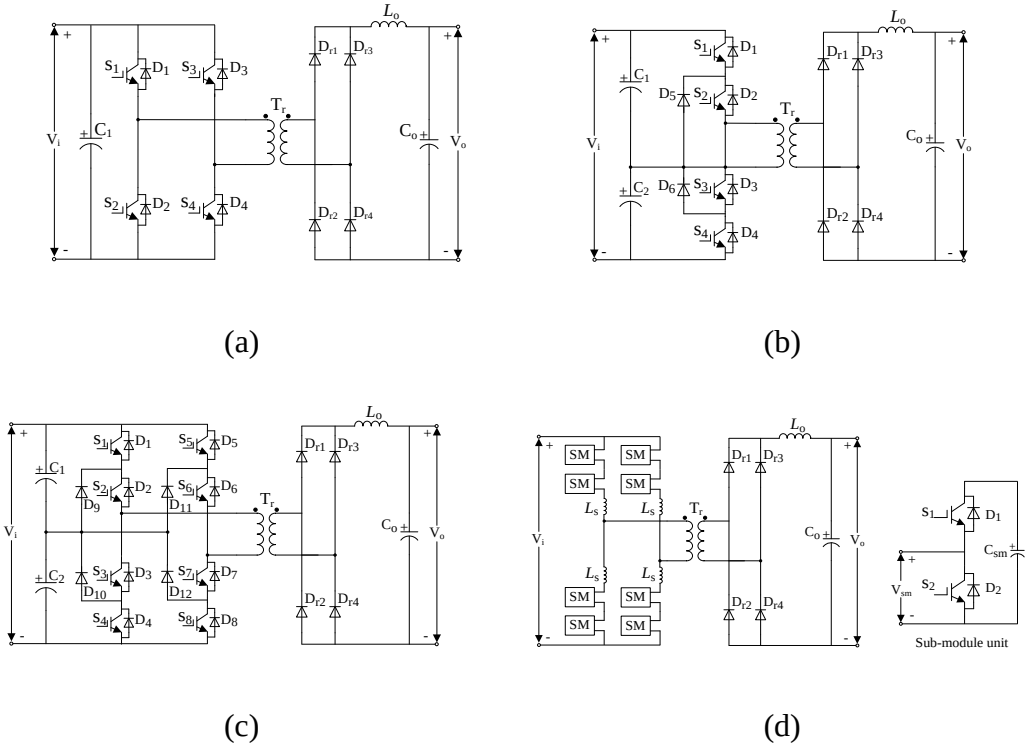

Fig. 3.7. (a) Basic FB two-level converter. (b) Basic half-bridge (HB) three-level converter. (c) Basic FB three-level converter. (d) Submodule (SMs) based FB Three-level converter.

TABLE 3.1
POSSIBLE DC/DC CONVERTER OPTIONS

Converter topology		Valve number	Switch number in each valve	Valve voltage	Produced voltage level	Voltage balance control complexity	Voltage sensor
2-level	Basic FB converter	4	6×1.7 kV IGBTs	DC link voltage	2	No	1
3-level	Basic HB converter	4	3×1.7 kV IGBTs	Half DC link voltage	3	Easy	2
3-level	Basic FB converter	8	3×1.7 kV IGBTs	Half DC link voltage	5	Easy	2
3-level	FB converter based on SMs	16	3 ×1.7 kV IGBTs	Half DC link voltage	5	Calculation is proportional to the SMs number	8

Two-Level Converter

Fig. 3.7(a) shows the basic FB two-level converter, which is composed with four IGBTs, a medium frequency transformer, a diode rectifier and an output inductor. In the basic FB two-level converter, the input bridge produces a high frequency square wave at the primary sides of the transformer. And then, the medium-frequency transformer (MFT)

transforms its second side voltage to a high level. Finally, the high voltage square wave at the second side of the transformer is rectified by the diode rectifier. Owing to the output inductor, the ripple of the current at the output side is effectively reduced.

From Fig. 3.7(a), it is easy to see that the required switches in the basic FB two-level converter are only four, which is the least number among the four possible configurations. However, as each switch in the basic FB two-level converter has to take the full DC link voltage, the voltage change rate dv/dt is high, therefore, may cause larger electromagnetic interference [55].

Three-Level Converter

Figs. 3.7(b)~(d) shows the possible three-level configurations for the DC/DC converter, including the basic HF three-level converter, the basic FB three-level converter, and the FB three-level converter based on SMs. The three-level converters have some advantages in the aspects of power quality, and Electromagnetic interference (EMI) for high power applications [55]. Furthermore, the switches in the basic HB three-level converter, FB three-level converter and the SMs-based FB three-level converter only take half of the DC link voltage, which effectively reduces the dv/dt in comparison with the FB two-level converter.

On the other hand, In order to realize the N-level configuration, 8(N-1) switches are needed for the SMs-based FB converter, whereas, the basic HB and FB converters only requires 2(N-1) and 4(N-1) switches, respectively [49], [60]. In addition, the complicate voltage balancing algorithm is required for the SMs-based FB converter [61].

The basic FBTL converter, with the advantage of the reduced voltage stress of the switches, reduced filter size, and improved dynamic response, is becoming highly suitable for medium-voltage and high-power conversion [49]. The basic FBTL and the SMs-based FBTL configurations can both produce five-level output voltage and reduces dv/dt in comparison with the basic HBTL configuration, particularly in the medium-voltage and high power application [60], [81], [82]. However, the basic FBTL converter has a simpler circuit structure and less number of switch devices than the SMs-based FBTL configuration, which results in high reliability of the basic FBTL converter.

3.4 IFBTL DC/DC Converter

The FB converter may be a suitable choice for wind farm application from the view of energy efficiency [25]. Hence, the isolated FBTL DC/DC converter is considered for high-power wind turbine systems. The chopping phase-shift (CPS) control and double

phase-shift (DPS) control are presented in [50] and [51], respectively, for the isolated FBTL converter, but they are not be suitable for the medium-voltage and high-power system because of the high voltage change rate dv/dt. An IFBTL DC/DC converter is presented for DC-grid wind turbine in this chapter, which may be used for high voltage and high power system.

3.4.1 Converter Configuration

The IFBTL DC/DC converter configuration is shown in Fig. 3.8, which is mainly composed with two divided capacitor, a three-level FB inverter, a passive filter, an MFT, a diode rectifier, an output inductor, and an output capacitor. A passive filter is inserted into the IFBTL DC/DC converter which can improve the performance of the DC/DC converter [83]. As a consequence, the harmonics and the voltage stress of the MFT is reduced, which is very significant for the power converter in the high-power application.

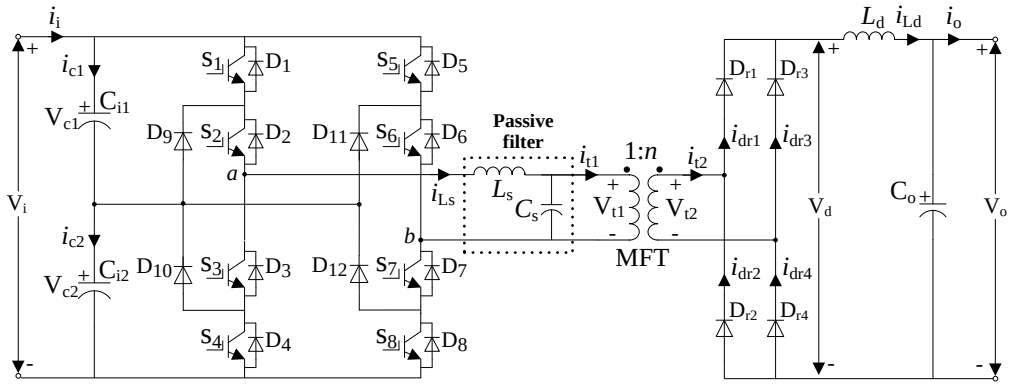

Fig. 3.8. Block diagram of the IFBTL DC/DC converter.

3.4.2 Modulation Strategy

In the IFBTL DC/DC converter, the switches S1~S8 are switched complementarily in pairs with a PWM (pair S1-S3, pair S4-S2, pair S5-S7, and pair S8-S6). The duty cycle for S1 is D. Through phase-shift the PWM for the other switch pairs, the different operation modes can be generated.

1) *Operation Mode I*: The operation mode I is shown in Fig. 3.9(a), where the PWM waveform for the pairs of S8-S6, S5-S7 and S4-S2 lags behind that for the pair S1-S3 by $(D\text{-}D_c)T_s/2$, $T_s/2$ and $(D\text{-}D_c\text{+}1)T_s/2$ respectively. T_s is the switching cycle. The overlap time between S1-S3 and S8-S6 and between S4-S2 and S5-S7 are both $D_cT_s/2$. D_c is defined as the overlap duty ratio.

2) Operation Mode II: The operation mode I is shown in Fig. 3.9(b), where the PWM waveform for the pair of S8-S6 leads before that for the pair S1-S3 by $(D-D_c)T_s/2$, and the PWM waveform for the pair S4-S2 and S5-S7 lags behind that for the pair S1-S3 by $(1-D+D_c)T_s/2$ and $T_s/2$ respectively. The overlap time between S1-S3 and S8-S6, and between S4-S2 and S5-S7 are also both $D_cT_s/2$.

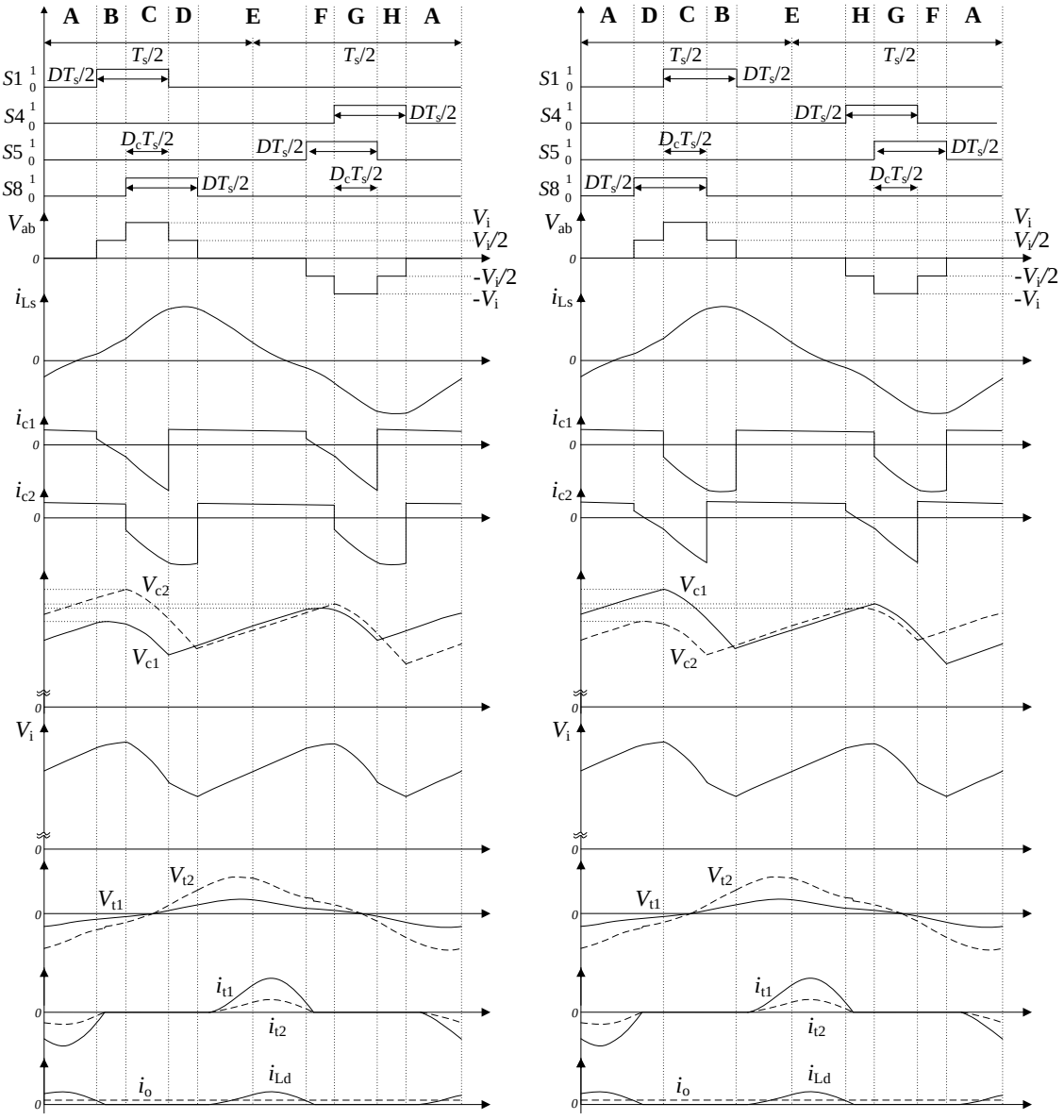

Fig. 3.9. Performance of IFBTL DC/DC converter during one cycle. (a) In operation mode I. (b) In operation mode II.

With the assumption C_{i1}=C_{i2}, the steady-state simulation results of the IFBTL DC/DC converter under the proposed modulation strategies are shown in Fig. 3.9 in one cycle T_s. The system parameters are given in Appendix C. The simulation results show that the voltage V_{ab}, V_{t1}, V_{t2} and the current i_{Ls}, i_{t1}, i_{t2} are all periodic waveforms with a period of T_s, and the current i_{c1}, i_{c2} and i_{Ld} are with a period of T_s/2. The performance of the converter including the voltage V_{t1}, V_{t2} and the current i_{t1}, i_{t2} are improved with the passive filter.

The main difference of the two operation modes is the capacitor charge and discharge situation in each half cycle as shown in Fig. 3.9. The capacitor C_{i2} discharge more energy than the capacitor C_{i1} in each half cycle in operation mode I, whereas the capacitor C_{i1} discharge more energy than the capacitor C_{i2} in each half cycle in operation mode II.

3.4.3 Voltage Balancing Control

A voltage balancing control strategy is proposed for the IFBTL DC/DC converter, which can be realized by using the operation mode I and II.

In Operation Mode I

The capacitor current i_{c1} and i_{c2} are both with the period of T_s/2 as shown in Fig. 3.9(a). According to Fig. 3.9(a), the charge or discharge situations for the capacitors C_{i1} and C_{i2} in stages A, C and E are the same in the first half cycle. The period of the stage B and D are the same. However, the current i_{c2} is more than i_{c1} in stage B, whereas the i_{c2} is far less than i_{c1} in stage D. Suppose $V_{c1} = V_{c2} = V_i/2$, the C_{i2} would provide more energy to the load than the C_{i1} in the first half cycle under the operation mode I. The analysis for the first half cycle is the same to that in the first half cycle, and the situation in the second half cycle is also the same to that in the first half cycles, which results in that the voltage V_{c1} would be increased and the voltage V_{c2} would be reduced in operation mode I. As a consequence, there will be the trend that the voltage V_{c1} would be more than the V_{c2} in operation mode I as shown in Fig. 3.9(a).

In Operation Mode II

Liking operation mode I, the charge or discharge situations for the capacitors C_{i1} and C_{i2} in stages A, C and E are the same in the first half cycle in operation mode II. The only difference is that the current i_{c2} is less than i_{c1} in stage D, while the i_{c2} is far more than i_{c1} in stage B in operation mode II. The period of the stage B and D are the same. In stage D, the current i_{c2} is less than i_{c1}, while the i_{c2} is far more than i_{c1} in stage B. Suppose $V_{c1} = V_{c2} = V_i/2$, the C_{i1} would provide more energy to the load than the C_{i2} in the first half

cycle under the operation mode II. The analysis for the second half cycle is the same to that in the first half cycle, and the situation in the second half cycle is also the same to that in the first half cycles, which results in that the voltage V_{c2} would be increased and the voltage V_{c1} would be reduced in operation mode II. As a consequence, there will be the trend that the voltage V_{c2} would be more than the V_{c1} in operation mode I as shown in Fig. 3.9(b).

Voltage Balancing Control Strategy

From aforementioned analysis that the V_{c1} would be more than V_{c2} in operation mode I, and V_{c1} would be less than V_{c2} in operation mode II, a capacitor voltage balancing control strategy is proposed as shown in Fig. 3.10. A comparator is used to compare the two capacitor voltage V_{c1} and V_{c2}. When V_{c1} is more than V_{c2}, the operation mode II will be selected in the next half cycle. When V_{c2} is more than V_{c1}, the operation mode I will be selected in the next half cycle.

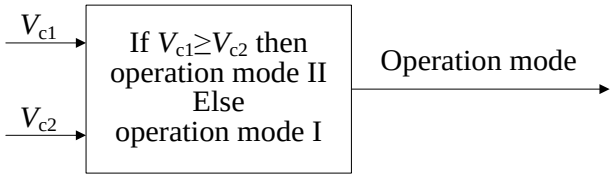

Fig. 3.10. Block diagram of the proposed voltage balancing control for IFBTL converter.

3.5 Control of Wind Turbine in DC Grid

3.5.1 Control of Wind Turbine I

Fig. 3.5 shows the wind turbine I, where the three-level NPC converter is used as the generator-side converter, and the IFBTL DC/DC converter is used as the grid-side converter. In wind turbine I, the PMSG is controlled by the NPC converter for the optimal power capture, and the DC-link voltage in the wind turbine is kept constant by the IFBTL DC/DC converter.

Generator-Side Converter Control

The control structure for the generator-side converter is shown in Fig. 3.11, which is based on the dynamic model of the PMSG in the synchronous rotating frame (3-6), with the *d*-axis is aligned with the rotor flux [84]. As the converter is directly connected to the PMSG, its *q*-axis current is proportional to the active power. The *d*-axis stator current is

proportional to the reactive power. The reactive power reference is set to zero to perform unity power factor operation.

The double control loops structure is adopted for the control of the wind turbine I as shown in Fig. 3.11. According to the measured generator speed ω_r, the optimal power command P_{g_ref} is calculated with the MPPT method based on the rotor speed versus power characteristic as shown in Fig. 3.2 [85]. In the outside loop, a PI controller is used to regulate the generator power P_g to track the reference P_{g_ref}, and produces corresponding reference current i_{qs_ref}. In inside loop, the PI controllers are used as the current regulators to regulate *d*- and *q*-axis stator current to track the reference values.

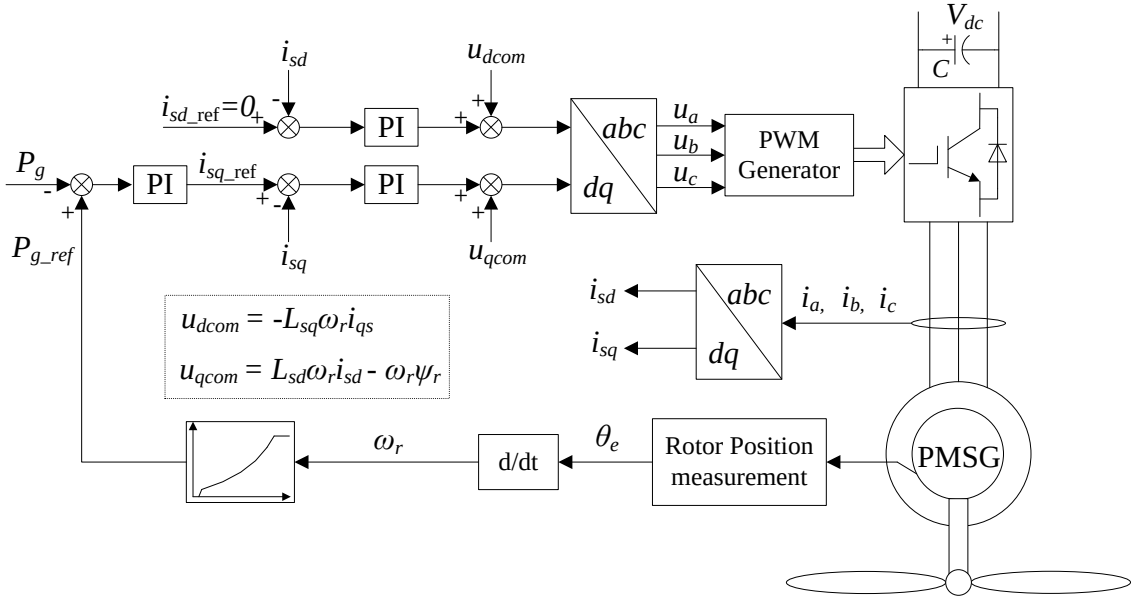

Fig. 3.11. Block diagram of the control for the generator-side converter.

Grid-Side Converter Control

The grid-side converter, IFBTL DC/DC converter, is used here to keep the DC-link voltage V_{dc} constant in the wind turbine. The control for the grid-side converter is shown in Fig. 3.12, which adopts double-loop control structure. A simple PI controller is used as the voltage regulator at the outside loop to generate the current reference i_{Ld_ref}, and the other PI controller used as the current regulator is adopted in the inside loop to track the current reference so as to follow the reference voltage V_{dc_ref}.

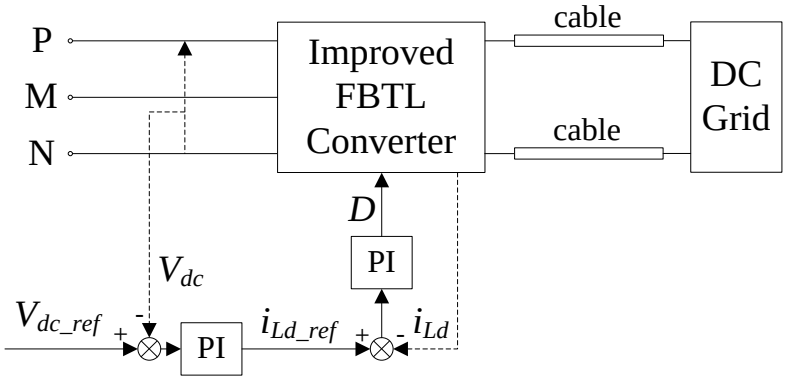

Fig. 3.12. Block diagram of the control for the grid-side converter.

3.5.2 Performance of Wind Turbine I

The simulation study is conducted for the DC-grid wind turbine as shown in Fig. 3.5 with the professional tool PSCAD/EMTDC. The wind turbine parameters are shown in the Appendix A.

The variable wind speed as shown in Fig. 3.13(a) is used to assess the performance of the DC-grid wind turbine. Figs. 3.13(b) and (c) show the wind turbine speed and power, respectively. With the proposed modulation strategy, voltage balancing control and wind turbine control, the voltage V_{dc} is kept constant and the capacitor voltage V_{c1} and V_{c2} is controlled balanced as shown in Fig. 3.13(d). Figs. 3.13 (e) and (f) show the output voltage V_o and current i_o of the DC-grid wind turbine, respectively.

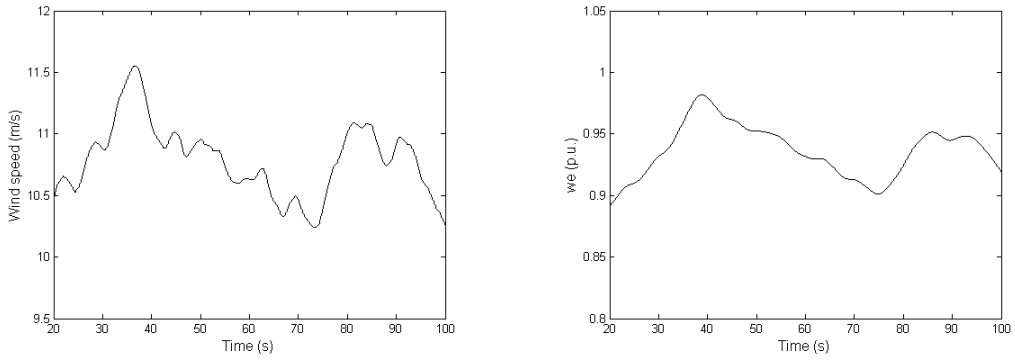

(a) (b)

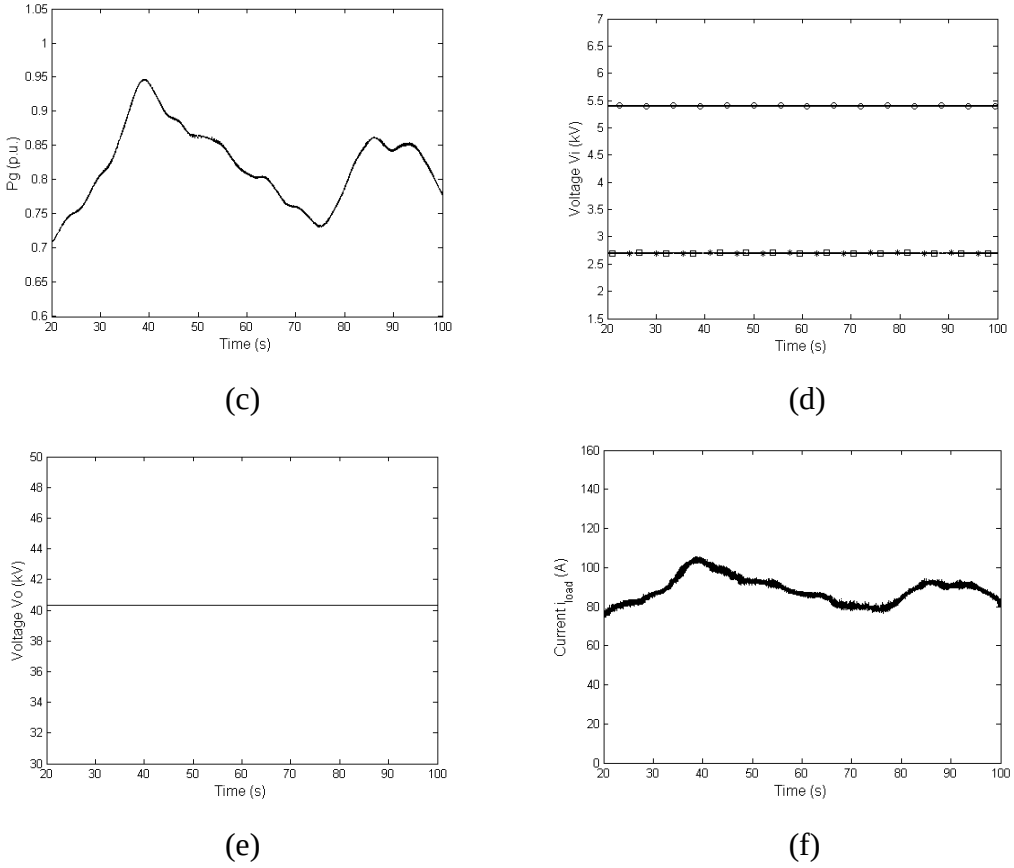

Fig. 3.13. (a) Wind speed. (b) Wind turbine speed. (c) Power P_g. (d) Voltage V_i, V_{c1} and V_{c2}. (e) Voltage V_o. (f) Current i_o.

In the wind turbine I, owing to the three-level configuration of the NPC PWM converter, there will be the problem about the mid-point voltage balancing in the NPC converter [45]. So far, a number of literatures have been reported about the control to keep the mid-point voltage balancing in the NPC converter, where these control algorithms are normally complicated [45]. As to the presented wind turbine I, an IFBTL DC/DC converter associated with the voltage balancing control method is proposed, which can effectively keep the mid-point voltage balancing in the NPC converter without the complicated algorithm for the NPC converter.

Fig. 3.14 and Fig. 3.15 illustrate the simulation results about the capacitor voltage in the different situations about wind turbine I, where a simple SPWM modulation control is adopted. Fig. 3.14 shows the performance of the 3L-NPC converter, while the mid-point *M* is not connected to the IFBTL DC/DC converter as shown in Fig. 3.5. In Fig. 3.14(a), the DC-link voltage V_{dc} is kept constant. However, the capacitor voltage is not balanced as shown in Fig. 3.14(b), because no voltage balancing control algorithm is used for the three-level NPC converter. Fig. 3.15 shows the performance of the three-level NPC

converter in wind turbine I, where the mid-point *M* is connected to the IFBTL DC/DC converter as shown in Fig. 3.5. Here, the DC-link voltage V_{dc} is kept constant as shown in Fig. 15(a). Although there is no voltage balancing control for the three-level NPC converter, a simple voltage balancing control algorithm is used for the IFBTL DC/DC converter, which ensures the capacitor voltage balancing as shown in Fig. 15(b).

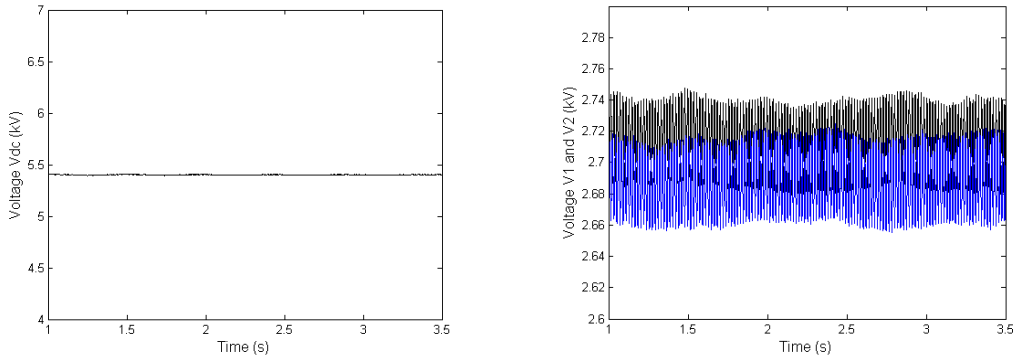

(a) (b)

Fig. 3.14. (a) DC-link voltage V_{dc}. (b) Capacitor voltage V_{c1} and V_{c2}.

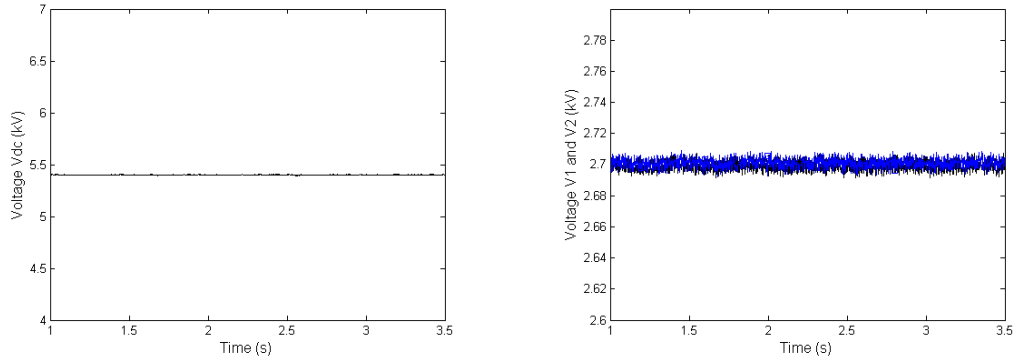

(a) (b)

Fig. 3.15. (a) DC-link voltage V_{dc}. (b) Capacitor voltage V_{c1} and V_{c2}.

3.5.3 Control of Wind Turbine II

Fig. 3.16 shows the configuration of the wind turbine II, where the uncontrollable diode rectifier is used as the generator-side converter and the IFBTL DC/DC converter is used as the grid side converter. In the wind turbine II, the PMSG is controlled by the IFBTL DC/DC converter to track the optimal power.

The control of the wind turbine II is shown in Fig. 3.16. The optimal power P_{g_ref} can be obtained with the MPPT method [36] based on the measured wind turbine speed ω_r. Neglecting the power electronics losses, the power relationship can be presented as

$$P_g = V_i\, i_i = V_o\, i_{Ld} \tag{3-8}$$

where P_g is the generator power, i_i is the input current of the IFBTL converter. A PI controller is used for the power regulation at the outside loop and produces the current reference i_{Ld_ref}. The other PI controller is used for the current regulation at the inside loop and produces the duty cycle D for the IFBTL converter to follow the optimal power.

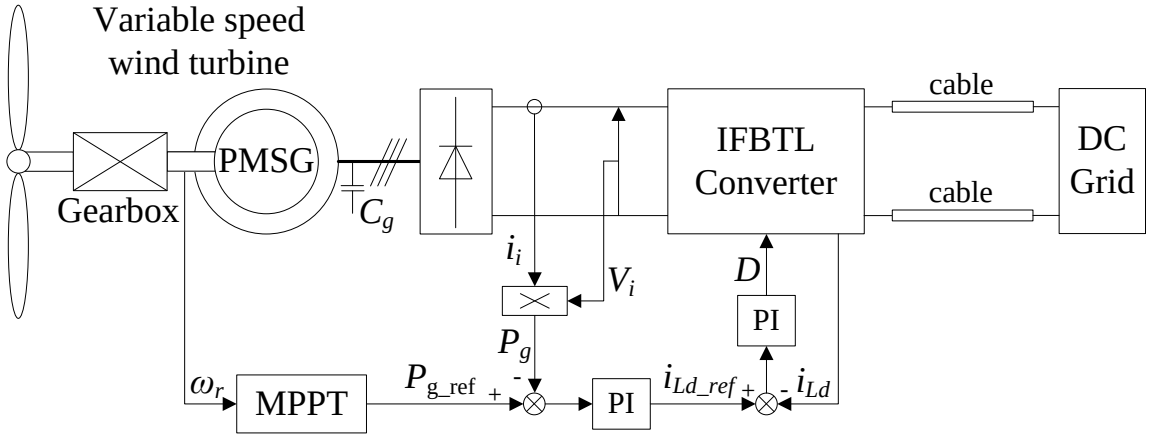

Fig. 3.16. Block diagram of the control for the wind turbine II.

3.5.4 Performance of Wind Turbine II

The simulation study for the wind turbine II is also conducted with the professional tool PSCAD/EMTDC. The wind turbine parameters are shown in the Appendix B. The variable wind speed is shown in Fig. 3.17(a), which is used to assess the performance of the wind turbine II. Fig. 3.17(b) shows the wind turbine speed. The wind turbine power is shown in Fig. 3.17(c). Figs. 3.17(d) and (e) shows the DC-link voltage V_i, V_{c1} and V_{c2} and

the input current i_i of the IFBTL converter, respectively, where the capacitor voltages are kept balanced with the proposed control strategy. The voltage V_o and DC-grid current i_o are shown in Figs. 3.17(f) and (g).

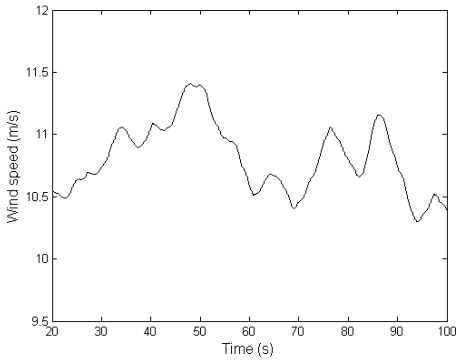

(a)

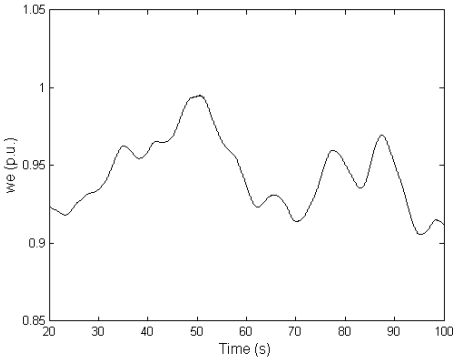

(b)

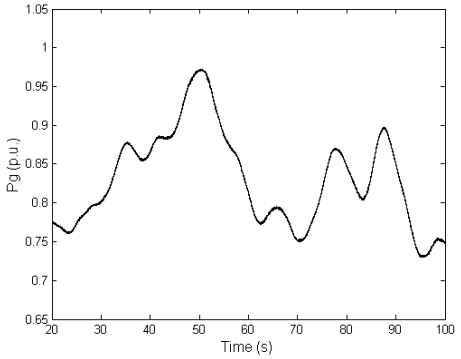

(c)

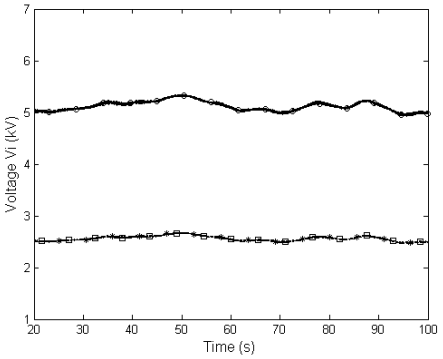

(d)

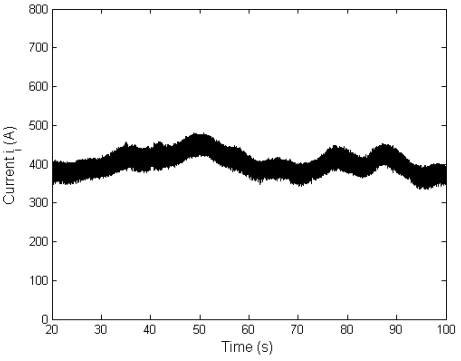

(e)

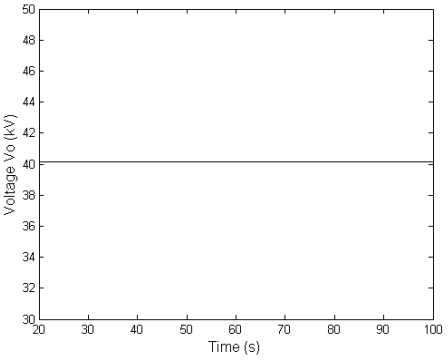

(f)

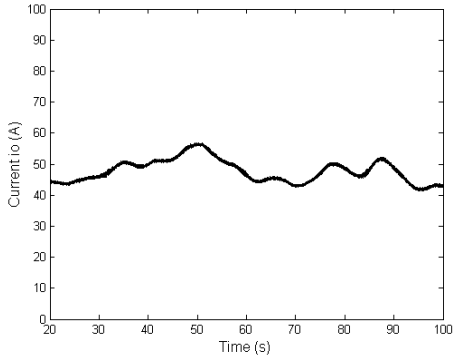

(g)

Fig. 3.17. (a) Wind speed. (b) Wind turbine speed. (c) Power P_g. (d) Voltage V_i, V_{c1} and V_{c2}. (e) Current i_i. (f) Voltage V_o. (g) Current i_o.

In order to realize the MPPT, the wind turbine speed should be varied in proportion to the wind speed so as that the DC-grid wind turbine can capture the optimal power from the wind. As a consequence, the generator power P_g and the DC-link voltage V_i should follow the optimal curves [86]. With the simulation study of the DC-grid wind turbine, the relationships between the optimal generator power P_g and the wind turbine speed ω_r, and between the optimal DC-link voltage V_i and the wind turbine speed ω_r are shown in Figs. 3.18(a) and (b), respectively.

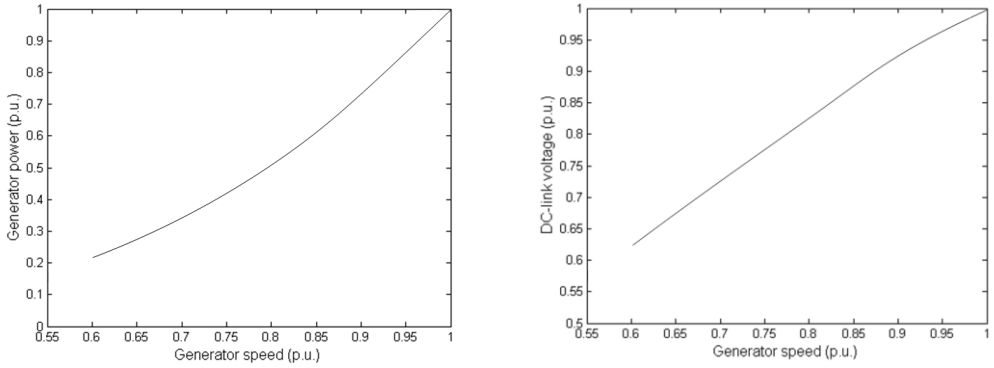

(a) (b)

Fig. 3.18. (a) Optimal generator power P_g under the different wind turbine speed ω_r. (b) Optimal DC-link voltage V_i under the different wind turbine speed ω_r.

3.6 Experimental Study

In the laboratory, a down-scale 1 kW IFBTL DC/DC converter prototype was built and tested to verify the presented function of the IFBTL DC/DC converter. The switching frequency is 5 kHz. The eight primary switches and diodes S1/D1-S8/D8 are the standard IXTH30N25 power MOSFET. The clamping diodes D9-D12 are STTH3006. The rectifier diodes D_{r1}-D_{r4} are STTH3010. The transformer turn ratio is 1:2.6. The transformer core is a PM87/70 ferrite core, and its leakage inductance is 10 μH. The filter inductor L_s and capacitor C_s are 0.44 mH and 3 uF respectively. The inductor L_d is 0.8 mH. The capacitor C_o is 1 mF. The input capacitors, both C_{i1} and $C_{i2,}$ are 400 V/330 μF. The dead-time is set as 1.5 μs.

Fig. 3.19 shows the experimental circuit, where an isolated transformer is used between the AC grid and the experiment system. A three-phase autotransformer followed by a three-phase diode rectifier is employed at the input side to produce the input voltage V_i. A DC power supply (SM300-10D) parallel with a resistor load R_{load} of 50 Ω at the output side to emulate the DC grid and support the constant output voltage V_o as 250V. An inductor with the value of 0.4 mH is inserted between the output of the converter and the DC power supply.

In the experiment, the dSPACE equipment is used as the control system. The dS2004 is the AC/DC board, which is used to capture the signals including the voltage V_i, V_1 and the current i_{Ld}. And then, these captured signals are sent to the main processor, where the voltage balancing control and the system control algorithms are conducted. Finally, the PWM pulse signals s_1~s_8 are generated with the PWM pulse board dS1105 based on the results from the processor.

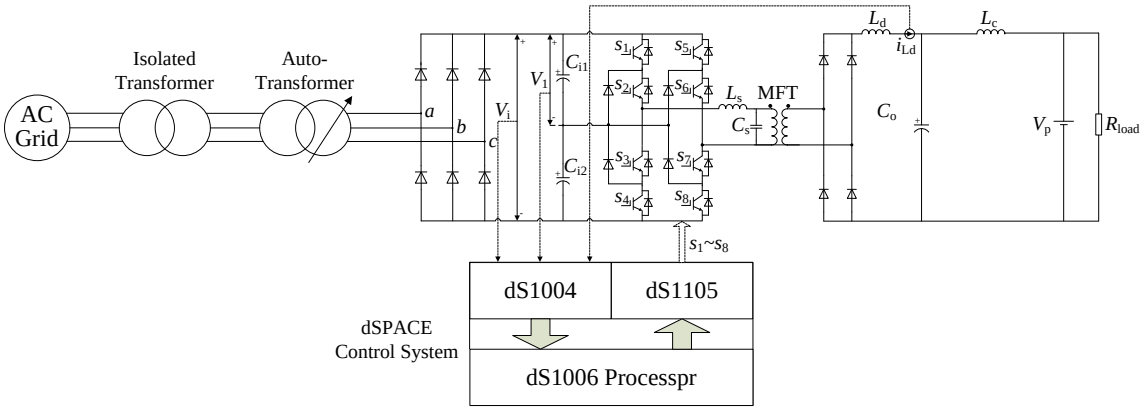

Fig. 3.19. Block diagram of the experimental circuit.

In order to verify the feasibility of the IFBTL DC/DC converter for wind turbines, the two curves of the optimal power versus wind turbine speed and the optimal DC-link voltage versus wind turbine speed as shown in Fig. 3.18 are used in the experiments, where the power base is 1 kW and the voltage base is 180 V.

Experiment Study 1

The experiment study 1 is conducted with the experiment circuit as shown in Fig. 3.19, where the system power is set as 200 W. Fig. 3.20~ Fig. 3.23 shows the waveforms of the system, where the (a) is with D_c/D=65%, and the (b) is with D_c/D=85%. Figs. 3.20(a) and (b) show the V_{ab}, V_{t1} and i_{Ls}, where the voltage V_{ab} is five-level configuration, which has symmetrical positive and negative segments. The V_{t1} and i_{Ls} are effectively improved by the passive filter as shown in Fig. 3.21. The voltage V_{t1}, V_{t2}, i_{t1}, i_{t2}, i_{Ld} and i_o under the different D_c/D are nearly the same as shown in Fig. 3.21 and Fig. 3.22. The capacitor voltage V_{c1} and V_{c2} are kept balanced with the proposed voltage balancing control strategy as shown in Fig. 3.23.

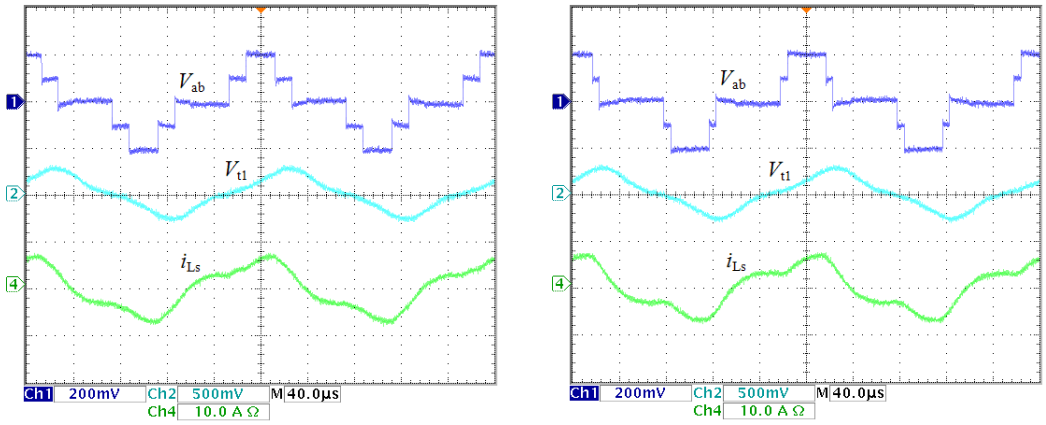

(a) (b)

Fig. 3.20. Measured converter waveforms including V_{ab} (100V/div), V_{t1} (250V/div), and i_{Ls} (10A/div). (a) D_c/D=65%. (b) D_c/D=85%. Time base is 40 µs/div.

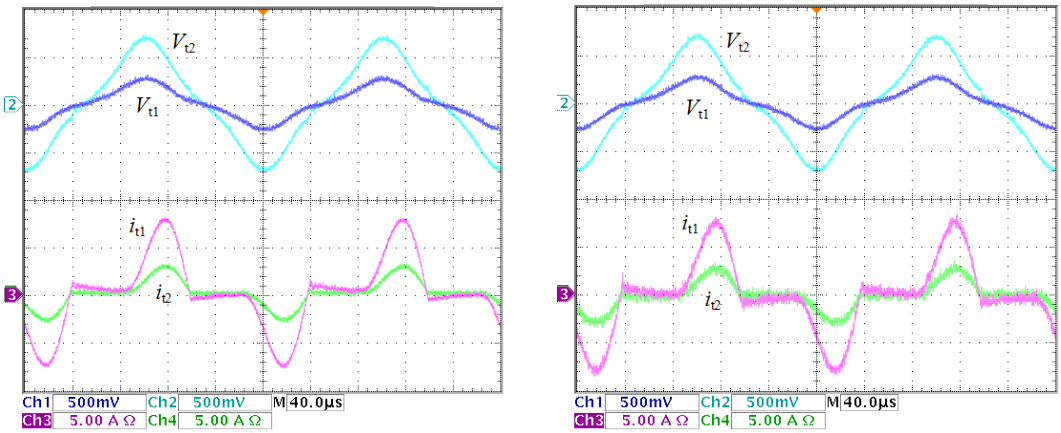

(a) (b)

Fig. 3.21. Measured converter waveforms including V_{t1} (250V/div), V_{t2} (250V/div), i_{t1} (5A/div), and i_{t2} (5A/div). (a) D_c/D=65%. (b) D_c/D=85%. Time base is 40 µs/div.

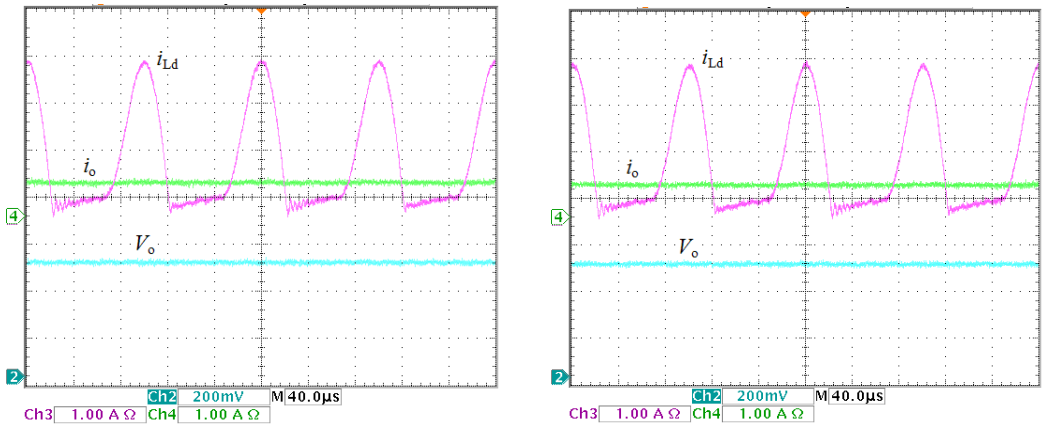

(a) (b)

Fig. 3.22. Measured converter waveforms including V_o (100V/div), i_{Ld} (1A/div), and i_o (1A/div). (a) D_c/D=65%. (b) D_c/D=85%. Time base is 40 µs/div.

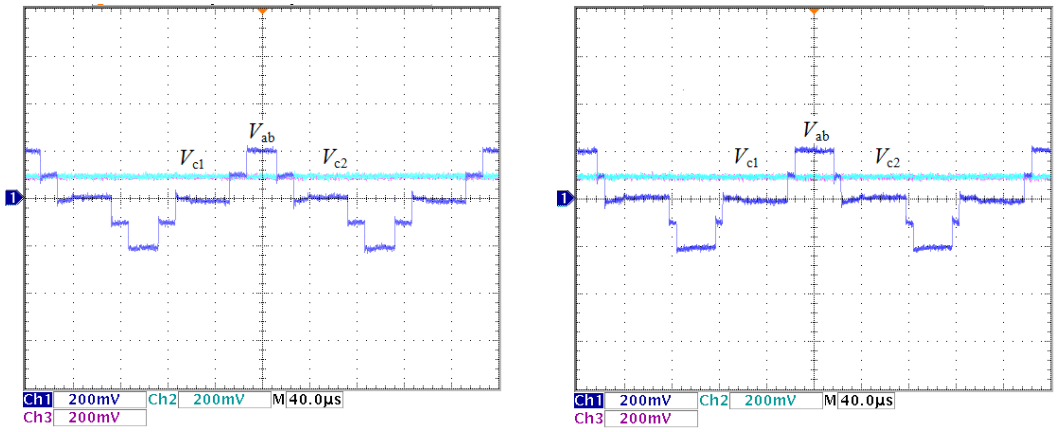

(a) (b)

Fig. 3.23. Measured converter waveforms including V_{ab} (100V/div), V_{c1} (100V/div), and V_{c2} (100V/div). (a) D_c/D=65%. (b) D_c/D=85%. Time base is 40 µs/div.

Experiment Study 2

The experiment study 2 is conducted with the experiment circuit as shown in Fig. 3.19, where the system power is 500 W. Fig. 3.24~Fig. 3.27 shows the experiment waveforms of the system with D_c/D being 65% and 85% respectively. The V_{t1} and i_{Ls} are improved with the passive filter in the DC/DC converter as shown in Fig. 3.24. Fig. 3.25 and Fig. 3.26 shows the voltage V_{t1}, V_{t2}, i_{t1}, i_{t2}, i_{Ld} and i_o under the different D_c/D, which are nearly the same. The capacitor voltage V_{c1} and V_{c2} are kept balanced with the proposed control strategy as shown in Fig. 3.27.

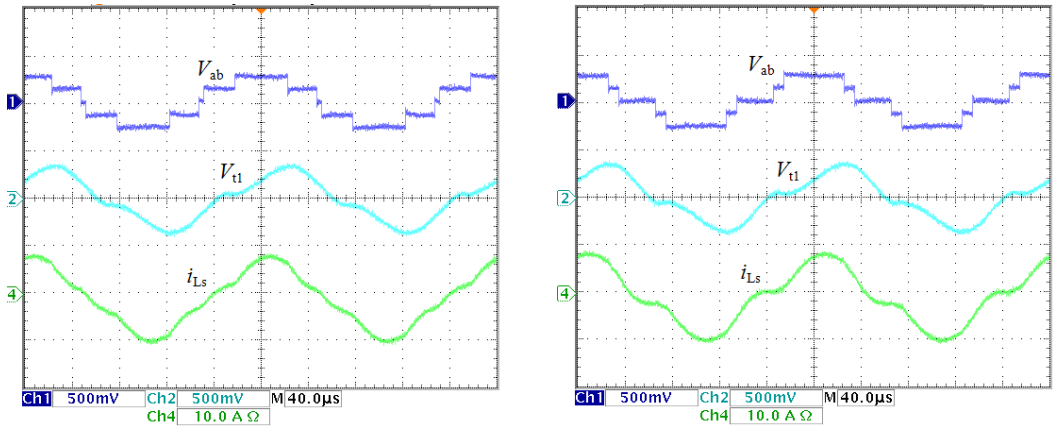

(a) (b)

Fig. 3.24. Measured converter waveforms including V_{ab} (250V/div), V_{t1} (250V/div), and i_{Ls} (10A/div). (a) D_c/D=65%. (b) D_c/D=85%. Time base is 40 µs/div.

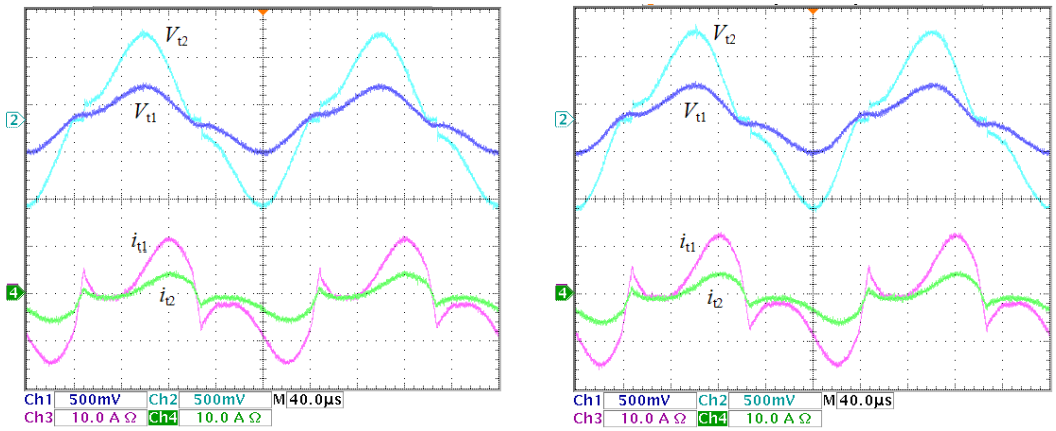

(a) (b)

Fig. 3.25. Measured converter waveforms including V_{t1} (250V/div), V_{t2} (250V/div), i_{t1} (10A/div), and i_{t2} (10A/div). (a) D_c/D=65%. (b) D_c/D=85%. Time base is 40 µs/div.

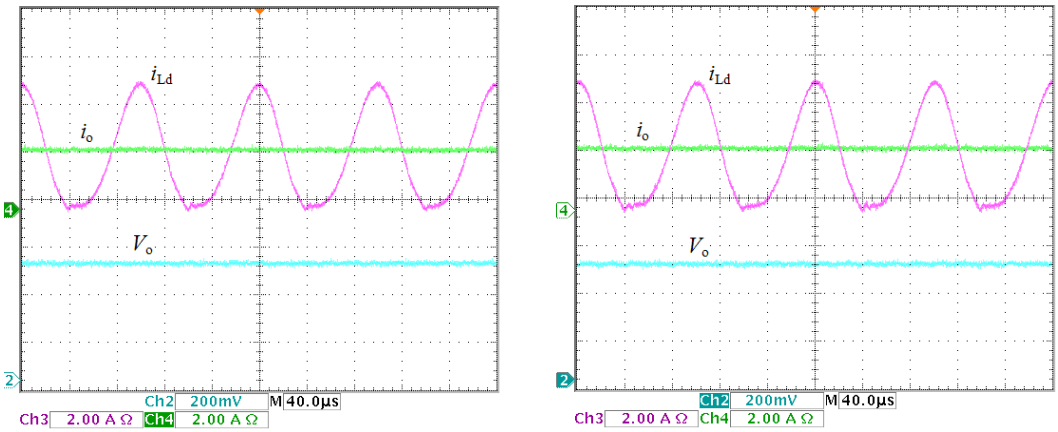

(a) (b)

Fig. 3.26. Measured converter waveforms including V_o (100V/div), i_{Ld} (2A/div), and i_o (2A/div). (a) D_c/D=65%. (b) D_c/D=85%. Time base is 40 µs/div.

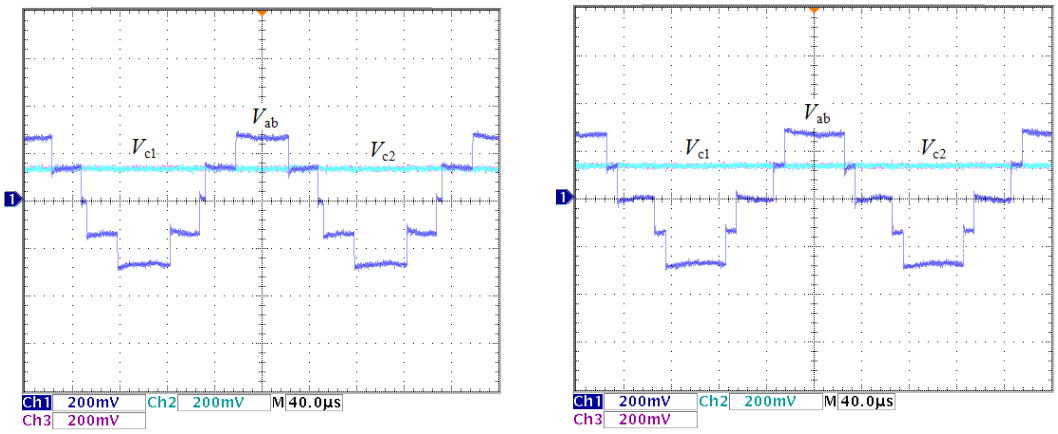

(a) (b)

Fig. 3.27. Measured converter waveforms including V_{ab} (100V/div), V_{c1} (100V/div), and V_{c2} (100V/div). (a) D_c/D=65%. (b) D_c/D=85%. Time base is 40 µs/div.

Experiment Study 3

The dynamic of the IFBTL DC/DC converter is studied as well with the control introduced in Fig. 3.16. According to the frequency-response design method [87], a simple current PI controller was designed with K_p and K_i as 0.15 and 120, respectively. In Fig. 28(a), the current i_o is stepped change from 0.4 A to 2.1 A in less than 4 ms. In Fig. 28(b), the current i_o is stepped change from 2.2 A to 0.5 A in less than 4 ms. Though the output current was changed, there is no significant deviation between the capacitor voltage V_{c1} and V_{c2} as shown in Fig. 3.28.

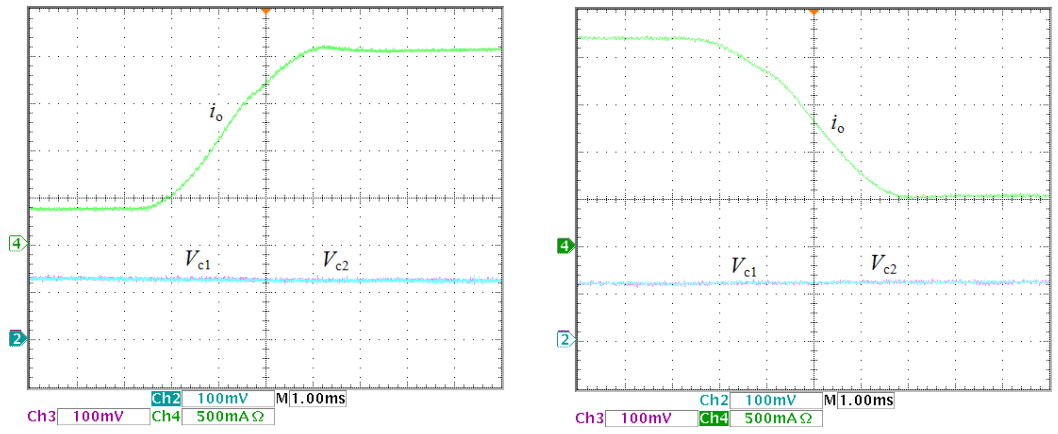

(a) (b)

Fig. 3.28. Measured converter waveforms including capacitor C_{i1} voltage V_{c1} (50V/div), capacitor C_{i2} voltage V_{c2} (50V/div), and inductor current i_o (0.5A/div) under D_c/D = 65%. (a) Inductor current i_o step up. (b) Inductor current i_o step down. Time base is 1 ms/div.

3.7 Summary

In this chapter, two DC-grid wind turbines are presented. One is with the three-level NPC converter as the generator-side converter and the DC/DC converter as the grid-side converter. The other one is with the diode rectifier as the generator-side converter and the DC/DC converter as the grid-side converter. The corresponding control for the two types of DC-grid wind turbines are introduced as well. The IFBTL DC/DC converter is presented for the DC-grid wind turbine. With the passive filter, the voltage stress for the medium frequency transformer can be reduced, which is significant for the high-voltage and high-power system. In addition, with the IFBTL DC/DC converter, the voltage balancing control for the generator-side converter (three-level NPC converter) can be omitted, which can be realized by the grid-side converter (IFBTL DC/DC converter). As a consequence, the system algorithm can be simplified. A down-scale IFBTL DC/DC converter prototype was established in the laboratory and tested, and the results verify the theoretical analysis.

Chapter 4

Control of DC Grids for Offshore Wind Farms

4.1 Introduction

The HVDC transmission technology is widely used in the electric power system, which is an efficient technology to transmit large amounts of electric power over long distance by overhead transmission lines or underground or submarine cables [1-8].

In the existing offshore wind farm, the collection system is AC system, and the offshore converter and onshore converter are both AC/DC converters. However, in the DC grid for offshore wind farms, the DC collection grid is used instead of the AC collection grid used in the existing offshore wind farm. The HVDC transmission technology in the DC grid would be different from that in the existing offshore wind farm. In the DC grid, the offshore converter is a DC/DC converter, which is used to step the collection voltage level to the transmission voltage level. As a consequence, the converter configurations associated with their control would be very important in the DC grid.

In this chapter, the HVDC transmission system in the DC grid is discussed in detail, and the corresponding control is presented as well. Furthermore, the fault ride-through control of the DC grid for offshore wind farms under AC grid faults is also introduced.

4.2 HVDC System Overview

According to the function and the location of the converter stations, various configurations of the HVDC transmission system can be arranged as follows [88].

1) Monopolar HVDC system

The monopolar HVDC system configuration is shown in Fig. 4.1, where two converters are used and separated by a single pole line, and a positive or a negative DC voltage is used. The Monopolar HVDC system is used for many cable transmissions with submarine connections, where there is only one insulated transmission conductor installed and the ground or sea provides the path for the return current [88].

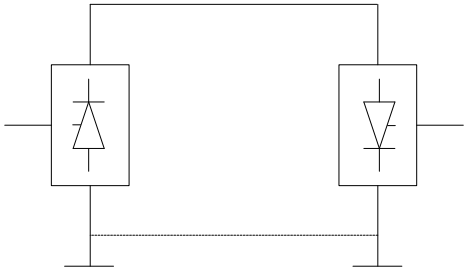

Fig. 4.1. Block diagram of the monopolar HVDC system.

2) Bipolar HVDC system

The bipolar HVDC system configuration is shown in Fig. 4.2, which increases the power transfer capacity and is the most commonly used. Two insulated conductors as positive and negative poles are used in the bipolar HVDC system, which can be operated independently. In case of failure of one pole, the power transmission in the bipolar HVDC system can continue in the other pole, which effectively increases the reliability [88].

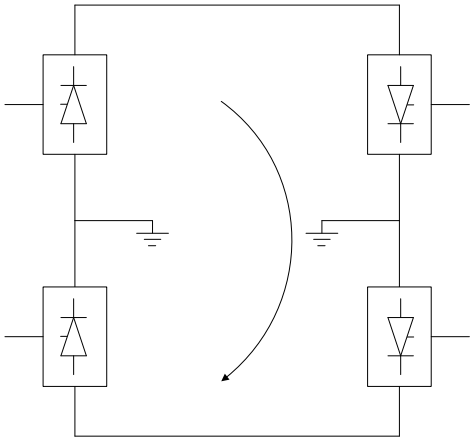

Fig. 4.2. Block diagram of the bipolar HVDC system.

3) Homopolar HVDC system

The homopolar HVDC system configuration is shown in Fig. 4.3, where two or more conductors have the negative polarity and the ground or a metallic is used for current return. The two poles operation in parallel in the homopolar HVDC system can effectively reduce the insulation costs [88].

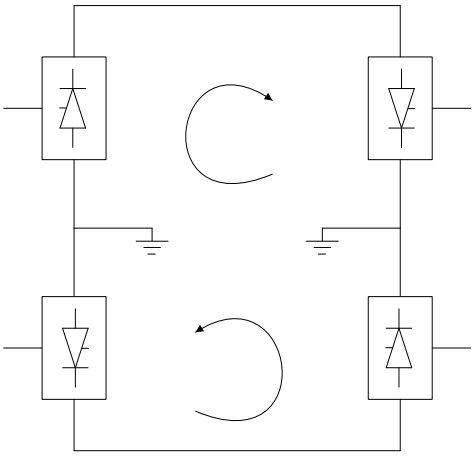

Fig. 4.3. Block diagram of the homopolar HVDC system.

4) Back-to-back HVDC system

The back-to-back HVDC system configuration is shown in Fig. 4.4, which is commonly used to connect two AC systems [88].

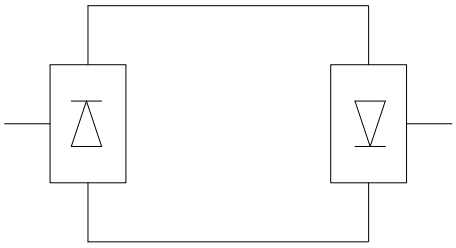

Fig. 4.4. Block diagram of the back-to-back HVDC system.

5) Multiterminal HVDC system

The multiterminal HVDC system configuration is shown in Fig. 4.5, where a number of HVDC converter stations are geographically separated and connected through transmission lines or cables. In the multiterminal HVDC system, these converters can be connected in parallel or in series [88].

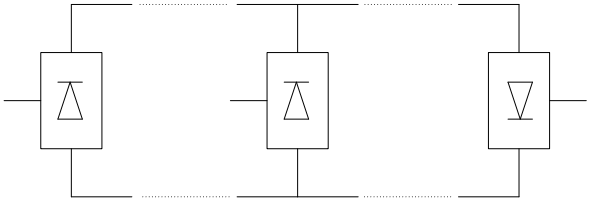

(a)

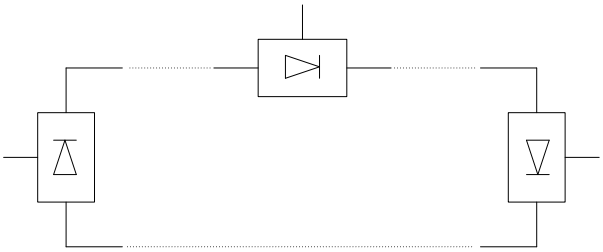

(b)

Fig. 4.5. Block diagram of the multiterminal HVDC system. (a) Parallel configuration. (b) Series configuration.

4.3 DC Grid System

The studied DC grid system for the offshore wind farm is shown in Fig. 4.6. The DC-grid wind turbine I is considered in the DC grid, where the power generator is a PMSG, the generator-side converter is a three-level NPC converter, and the grid-side converter is an IFBTL DC/DC converter. The DC-grid wind turbines in the wind farm are collected with the DC distribution system. Owing to the high voltage of the collection system, the cable losses at the collection system can be effectively reduced. The DC voltage in the collection level is stepped up to the transmission voltage level by the offshore converter. And then, the wind farm power is sent to the land with the HVDC technology and injected into the grid through the transformer.

In Fig. 4.6, the HVDC transmission system contains the offshore station, transmission cables, and onshore station. The offshore converter and the onshore converter are composed with positive onshore converter (PONC), negative onshore converter (NONC), positive offshore converter (POFC), and negative offshore converter (NOFC) respectively. The offshore converter is used to collect the DC clusters and convert the DC voltage level from the collection voltage level to the transmission voltage level. The onshore converter is used to convert the DC voltage into AC and sends the wind farm power to the AC grid. Therefore, the HVDC transmission system in the DC grid is different from the existing HVDC transmission system, where the existing HVDC transmission system is used for AC/DC or DC/AC power conversion at each point of the HVDC transmission system. As a consequence, a novel HVDC transmission system configuration is required for the DC grid.

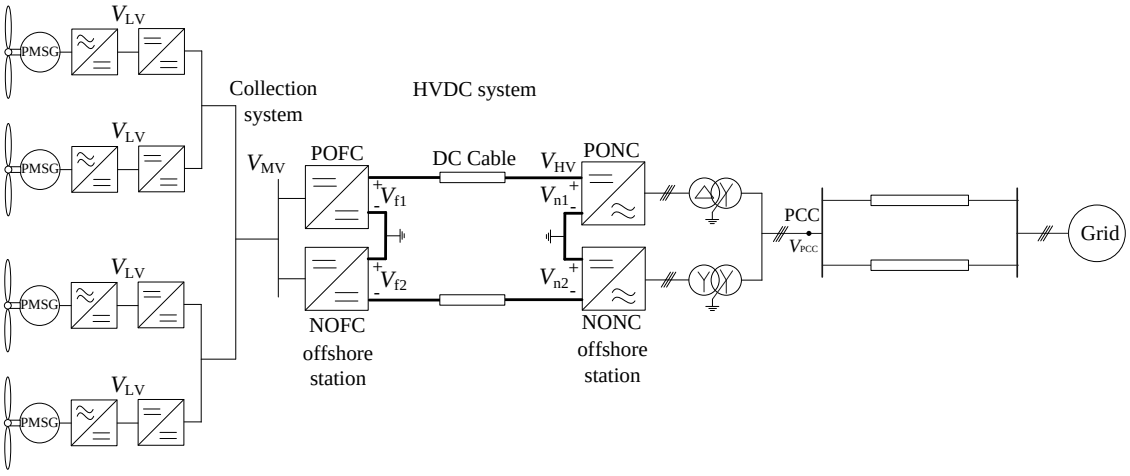

Fig. 4.6. Block diagram of the DC grid for the offshore wind farm.

4.4 Onshore Converter

MMC is an emerging and highly attractive topology for medium- or high-voltage applications based on the features of modularity and scalability, particularly for HVDC transmission system, with the advantages of small harmonics and small filter in comparison with the two-level VSC topology [89].

The MMC was developed in the early 2000s, which is based on cascaded modular cells. The MMC consist of a number of SMs, which is composed of half-bridge converter cells fed by floating DC capacitors. There is no need for high-voltage DC-link capacitors (or series connected capacitor) because the intrinsic capacitors of the cells perform these tasks, which reduces the costs of the converter and increases its reliability. Besides, the high number of levels enables a great reduction in the device average switching frequency without compromise of power quality [90-94]. Furthermore, an inductor is in series with the distributed energy storage capacitors in each arm, so the effects of faults arising inside or outside the converter can be reduced substantially by the arm inductors [95]. Owing to the aforementioned advantages, the MMC may be selected as the onshore converter.

To date, the MMC has been reported in some literatures. The capacitor voltage-balancing control is introduced in [96], where the PWM scheme is applied to MMC based on the combination of averaging and balancing control without any external circuit, and the results are verified by simulation and experiment. The dynamic performance of an MMC-based, back-to-back HVDC system under balanced and unbalanced grid condition is investigated in [61], where a phase-disposition (PD) sinusoidal pulse width modulation (SPWM) strategy, including a voltage balancing method, for the operation of an MMC is also presented. The performance of MMC operated with various multicarrier SPWM techniques is evaluated in [97]. A new PWM modulation scheme is introduced for MMC, and the semiconductor losses and loss distribution is investigated in [98]. An efficient modeling method of MMC for electromagnetic transient simulation is proposed in [99]. A reduced switching-frequency voltage balancing algorithms is developed for MMC, and a circulating current suppressing controller is proposed for the three-phase MMC in [100]. The impact of sampling frequency on harmonic distortion for MMC is investigated in [101]. The inner energy control is discussed in [102].

4.4.1 Modular Multilevel Converter

The diagram of a three-phase MMC for onshore converter is shown in Fig. 4.7(a), which is composed with six arms. Each arm consists of *n* SMs in series, and an arm inductor L_s. The SM is depicted in Fig. 4.7(b), which contains an IGBT half bridge as switching element and a DC storage capacitor with corresponding voltage as V_c. The switches S1 and S2 in SM are controlled with complementary signals and produce two active switching states that can connect or bypass its respective capacitor to the converter leg. As a consequence, the output voltage V_{sm} of the SM can be decided depending on the switching states, which is shown in Table 4.1. One thing mentioned is that, the SM state is defined as switched-on if S1 is switch on and S2 is switch off. Here, the output voltage V_{sm} equals to V_c. In contrast, the SM state is defined as switched-off if S1 is switched off and S2 is switched on. In this situation, the V_{sm} is zero.

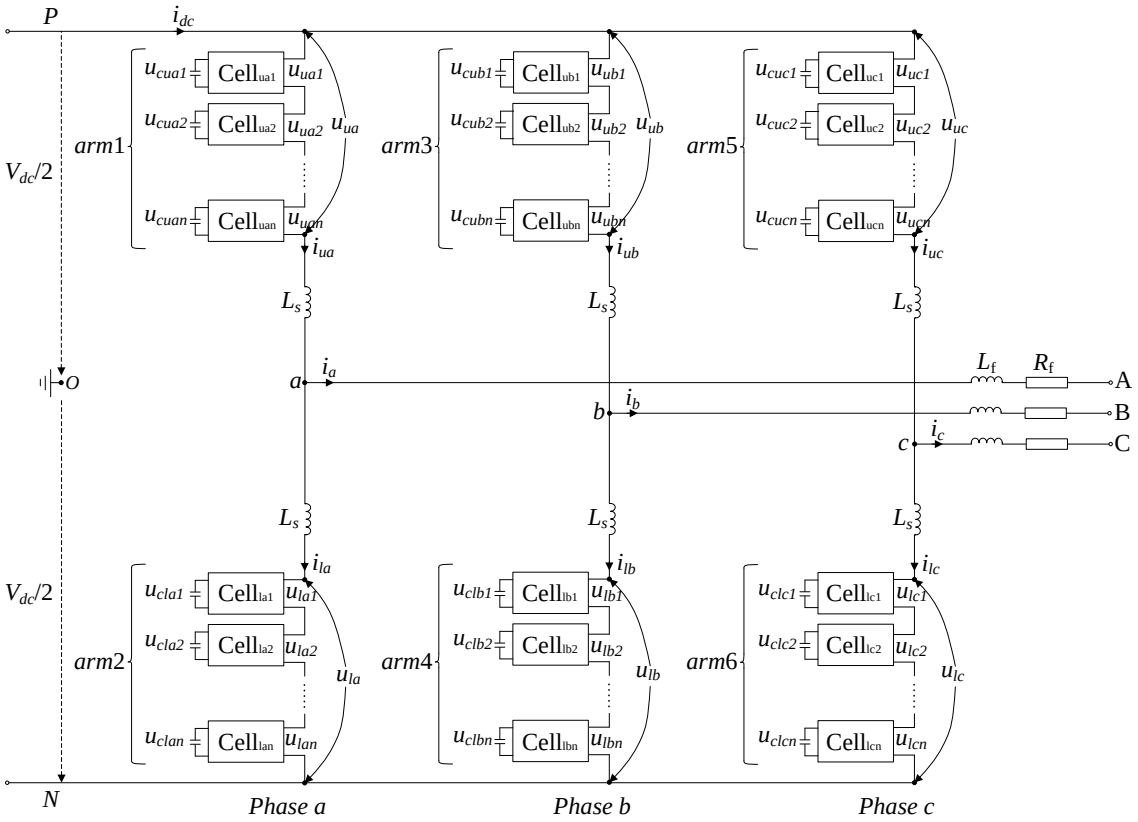

(a)

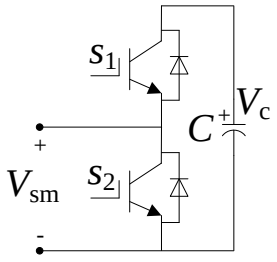

(b)

Fig. 4.7. (a) Diagram of three-phase MMC. (b) SM unit.

Table 4.1
SM state.

SM state	S1	S2	V_{sm}
On	On	Off	V_c
Off	Off	On	0

According to [99], the arm current in Fig. 4.7 can be expressed as

$$\begin{cases} i_{uj} = \dfrac{i_j}{2} + i_{diff\_j} \\ i_{lj} = -\dfrac{i_j}{2} + i_{diff\_j} \end{cases}, \quad j = a,b,c \tag{4-1}$$

where i_{uj} and i_{lj} are the upper arm current and the lower arm current of phase j (j=a, b, c), respectively. i_j is the AC current of phase j (j=a, b, c). i_{diff_j} is the inner difference current of phase j (j=a, b, c), respectively, which contains two parts as (4-2). One part is the DC component, which is one-third of the DC-link current as i_{dc}/3. The other part is the circulating current i_{2f_j} of phase j (j=a, b, c).

$$i_{diff\_j} = \frac{i_{dc}}{3} + i_{2f\_j}, \qquad j = a,b,c \tag{4-2}$$

and

$$i_{2f\_a} + i_{2f\_b} + i_{2f\_c} = 0 \tag{4-3}$$

Although the circulating currents i_{2f_j} (j=a, b, c) flow through the three phases of the MMC and have no effect on the AC side and the DC-link, it increases the rating values of the MMC devices, the converter power losses, and the SM capacitor voltage ripple [99].

According to [99], the voltage relationship of the MMC in Fig. 1 can be described as

$$V_{dc} = (u_{uj} + u_{lj}) + L_s(\frac{di_{uj}}{dt} + \frac{di_{lj}}{dt}) + R_s(i_{uj} + i_{lj}), \quad j = a,b,c \tag{4-4}$$

where V_{dc} is the DC bus voltage. u_{uj} and u_{lj} are the total output voltage of the up and the low series-connected SMs of phase j (j=a, b, c) respectively. Considering the point "o" as shown in Fig. 4.7 as the fictitious DC-link mid-point, the AC side can be described as [61], [99]

$$u_{jo} = e_j - \frac{R_s}{2} i_j - \frac{L_s}{2} \frac{di_j}{dt}, \ j = a,b,c \tag{4-5}$$

where u_{jo} is the output voltage of phase j (j=a, b, c), e_j=(u_{lj}-u_{lj})/2 is the inner Electric and magnetic field (EMF) generated in phase j (j=a, b, c).

4.4.2 Modulation Strategy

The modulation strategies for the MMC are mainly focused on the PD-SPWM modulation strategy and the PSC-SPWM modulation strategy as follows.

1) PD-SPWM modulation strategy

Suppose that the capacitor voltage in each SM is the same with V_c=V_{dc}/n, in the MMC with n SMs in each arm, the PD-SPWM modulation strategy can be used to synthesize an (n+1)-level waveform at the AC-side of the MMC, where n in-phase carrier waves displaced symmetrically with respect to the zero-axis. The output voltage level at the AC-side of the MMC can be determined by comparing a sinusoidal reference wave with the n carrier waves [61].

In each phase of the MMC, the total number of the SMs to be turned on at each instant is n/2, which means that the summation of the number n_u of the SMs turned on in the upper arm and the number n_l of the SMs turned on in the lower arm is n/2. The numbers n_u and n_l can be determined by the desired voltage level of the phase from the PD-SPWM modulation strategy.

Suppose that there are 4 SMs in each arm, and the capacitor voltage in each SM is the same, an example of 5-level waveform at the AC side of the phase with respect to the mid-point "*o*" can be synthesized as shown in Fig. 4.8.

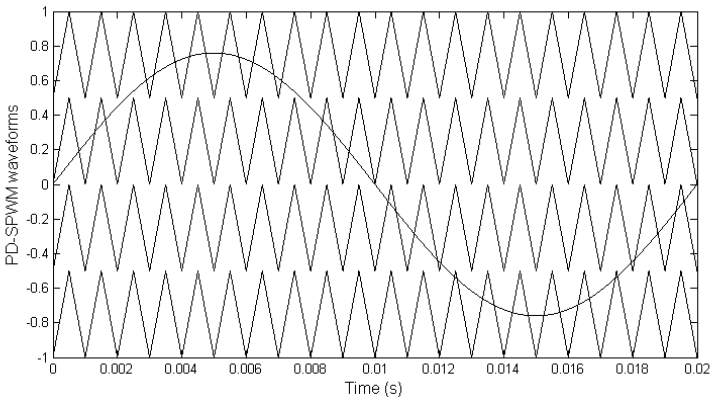

(a)

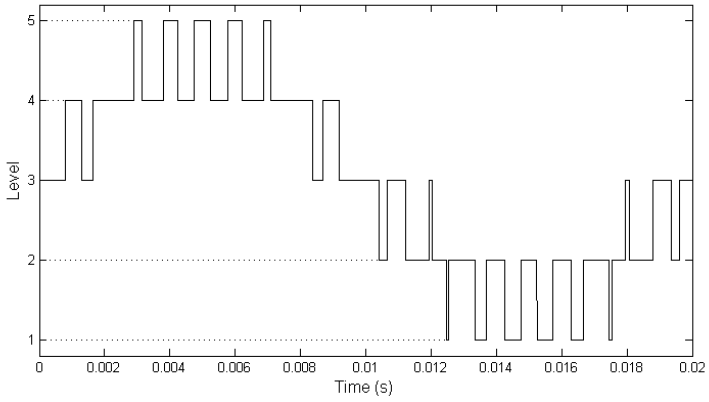

(b)

Fig. 4.8. PD-SPWM modulation strategy. (a) Reference and carrier waves. (b) Produced voltage level.

(1) Level 1: the output voltage u_{jo}=-V_{dc}/2 (j=a, b, c). In this situation, 4 SMs in the upper arm are turned on, and 4 SMs in the lower arm are turned off. In this situation, n_u=4, n_l=0.

(2) Level 2: the output voltage u_{jo}=-V_{dc}/4 (j=a, b, c). Here, there are 3 SMs turned on in the upper arm, and only 1 SM turned on in the lower arm. Here, n_u=3, n_l=1.

(3) Level 3: the output voltage u_{jo}=0 (j=a, b, c). Here, 2 SMs in the upper arm are turned on, and 2 SMs in the lower arm is turned on. In this situation, n_u=2, n_l=2.

(4) Level 4: the output voltage u_{jo}= V_{dc}/4 (j=a, b, c). Here, 1 SM in the upper arm is turned on, and 3 SMs in the lower arm are turned on. Here, n_u=1, n_l=3.

(5) Level 5: the output voltage u_{jo}= V_{dc}/2 (j=a, b, c). In this situation, 4 SMs in the upper arm are turned off, and all the SMs in the lower arm are turned on. Here, n_u=0, n_l=4.

2) PSC-SPWM modulation strategy

The phase-shifted carrier-based SPWM modulation can also be used for the MMC with the advantage that it can suppress some harmonics for multilevel converters, decrease the switching frequency, and reduce the losses [99].

The PSC-SPWM modulation strategy is shown in Fig. 4.9(a), where each arm with n SMs requires n carrier waves, and these carriers are phase shifted by $360^o/n$. By comparing the reference wave and the n carrier waves, the total number n_{on} of SMs that are needed to be switched on simultaneously in each arm can be decided as shown in Fig. 4.9(b), which would be used in the voltage balancing control described later.

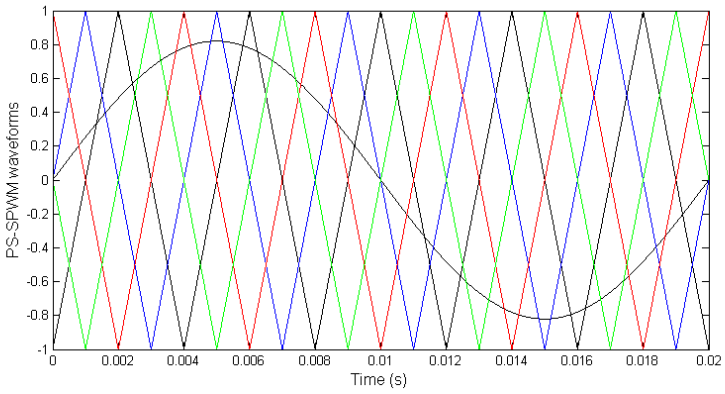

(a)

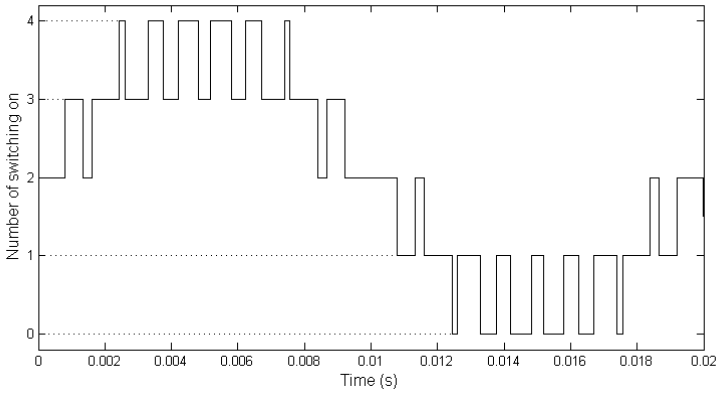

(b)

Fig. 4.9 PS-SPWM modulation strategy. (a) Reference and carrier waveforms. (b) Number of switching on.

The above description introduces the number of the SM in the upper and the lower arms to be switched on with PD-SPWM and PSC-SPWM, respectively. As to the specific SM to be turned on, it will be introduced later in the voltage balancing control.

4.4.3 Voltage Balancing Control

The capacitor voltage control is an important issue, which should be monitored in real time and kept balanced. In the aforementioned two modulation strategies, the number of the SMs to be turned on at a time in the upper arm and the lower arm has been decided. The capacitor voltage values and the direction of the arm current are used to select the specific SMs to be switched on.

The capacitor voltage in each SM is related to its switch stage and the direction of arm current as shown in Table 4.2. Normally, when the arm current is positive as shown in Fig. 4.7, and the SM is turned on, the corresponding capacitor in the SM will be charged and its voltage will be increased. When the arm current is negative and the SM in the arm is turned on, the corresponding capacitor in the SM will be discharged and its voltage will be decreased. No matter of the direction of the arm current, if the SM is turned off, which means that the corresponding capacitor in the SM will be bypassed, and the capacitor voltage will be unchanged.

In order to realize the capacitor voltage balancing control, the capacitor voltage of the SMs in each arm are measured and sorted in descending order. The specific voltage balancing control for SM can be presented as follows [61].

1) If the arm current is positive, the n_{on} SMs in the arm with the lowest voltage are switched on.

2) If the arm current is negative, the n_{on} SMs in the arm with the highest voltage are switched on.

TABLE 4.2
CAPACITOR STATE

Arm current (i_u or i_l)	SM state	Capacitor state	Capacitor voltage V_c
Positive	On	Charge	Increased
	Off	Bypass	Unchanged
Negative	On	Discharge	Decreased
	Off	Bypass	Unchanged

4.4.4 Circulating Current Elimination

According to the analysis before, a circulating current would flow through the three phases of the MMC, which increases the rating values of the MMC devices, the converter power losses, and the SM capacitor voltage ripple. The circulating current is caused by the inner voltage differences, and they are in the form of negative sequence with the frequency as twice the fundamental wave. In the normal operation of the MMC, the circulating current should be eliminated.

According to (4-2), the second harmonic circulating current can be described as

$$\begin{cases} i_{2f\_a} = I_{2fm}\sin(2\omega_o t + \varphi) \\ i_{2f\_b} = I_{2fm}\sin(2\omega_o t + \varphi + \dfrac{2\pi}{3}) \\ i_{2f\_c} = I_{2fm}\sin(2\omega_o t + \varphi - \dfrac{2\pi}{3}) \end{cases} \tag{4-6}$$

where I_{2fm} is the peak value of the second harmonic circulating current. ω_o is the fundamental frequency. φ is the initial phase angle.

Based on Fig. 4.7, the inner dynamic of the MMC with the circulating current can be defined as

$$\begin{cases} u_{2f\_a} = L_s \dfrac{di_{2f\_a}}{dt} + R_s i_{2f\_a} \\ u_{2f\_b} = L_s \dfrac{di_{2f\_b}}{dt} + R_s i_{2f\_b} \\ u_{2f\_c} = L_s \dfrac{di_{2f\_c}}{dt} + R_s i_{2f\_c} \end{cases} \tag{4-7}$$

where u_{2f_j} is the inner voltage of phase j (j=a, b, c). The (4-7) can be transferred into the dq reference frame with the transformation matrix below

$$T_{abc/dq} = \frac{2}{3}\begin{bmatrix} \cos\theta_o & \cos(\theta_o - \frac{2\pi}{3}) & \cos(\theta_o + \frac{2\pi}{3}) \\ -\sin\theta_o & -\sin(\theta_o - \frac{2\pi}{3}) & -\sin(\theta_o + \frac{2\pi}{3}) \end{bmatrix} \tag{4-8}$$

$$\begin{bmatrix} u_{2f\_d} \\ u_{2f\_q} \end{bmatrix} = L_s \frac{d}{dt}\begin{bmatrix} i_{2f\_d} \\ i_{2f\_q} \end{bmatrix} + \begin{bmatrix} 0 & -2\omega_o L_s \\ 2\omega_o L_s & 0 \end{bmatrix}\begin{bmatrix} i_{2f\_d} \\ i_{2f\_q} \end{bmatrix} + R_s \begin{bmatrix} i_{2f\_d} \\ i_{2f\_q} \end{bmatrix} \tag{4-9}$$

where u_{2f_d} and u_{2f_q} are the inner voltage in the dq reference frame, respectively. i_{2f_d} and i_{2f_q} are the second harmonic circulating current in the dq reference frame, respectively. θ_o=$\omega_o t$.

A control structure is presented to eliminate the circulating current as shown in Fig. 4.10. According to (4-2), the difference current can be obtained by the summation of the upper arm current i_{uj} and the lower arm current i_{lj} of phase j (j=a, b, c). And then, the three-phase circulating current can be transformed to the dq reference frame as i_{2f_d} and i_{2f_q}. In Fig. 4.10, the reference values are set as zero, and the simple PI controllers are used here to eliminate the current i_{2f_d} and i_{2f_q}. Finally, the three reference values u_{a_2f}, u_{b_2f} and u_{c_2f} are generated. Here, $T_{dq/abc}$= $T_{abc/dq}^{-1}$.

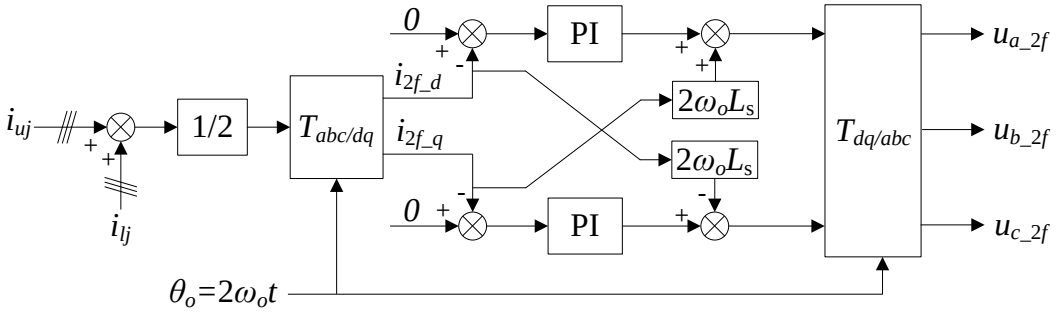

Fig. 4.10 Block diagram of the control for second circulating current elimination.

4.4.5 Onshore Converter Control

According to (4-5) and [99], the three-phase MMC can be decoupled into *dq* reference frame as

$$\begin{cases} \dfrac{di_{md}}{dt} = -\dfrac{R_o}{L_o} i_d + \omega_o i_q - \dfrac{1}{L_o} u_{gd} + \dfrac{1}{L_o} e_d \\ \dfrac{di_{mq}}{dt} = -\dfrac{R_o}{L_o} i_q - \omega_o i_d - \dfrac{1}{L_o} u_{gq} + \dfrac{1}{L_o} e_q \end{cases} \tag{4-10}$$

$$\begin{cases} P = \dfrac{3}{2}(e_d i_{md} + e_q i_{mq}) \\ Q = \dfrac{3}{2}(e_q i_{mp} - e_d i_{mq}) \end{cases} \tag{4-11}$$

where u_{gd} and u_{gq} are the grid positive sequence voltage in the *dq* reference frame respectively. e_d, e_q, and i_{md}, i_{mq} are the inner voltage and grid current in the *dq* reference frame respectively. L_o=L_f+L_s/2 and R_o=R_f+R_s/2 as shown in Fig. 4.7(a).

The onshore converter is used to maintain the HVDC link voltage close to the reference by adjusting the active power transmitted to the onshore AC network to match the power received from the offshore HVDC converter. The vector control technique has been developed for the onshore current regulation. It is illustrated in Fig. 4.11, where the subscripts *d* and *q* refer to the *d*, *q*-axis quantities. The MMC is controlled in a synchronous rotating *d*, *q*-axis frame with the *d*-axis oriented along the grid voltage vector position, which ensures the decoupling control of active and reactive powers into the AC grid. The double control loops are used for the onshore converter. The grid current is controlled in the inside loop. The outside loop is used to maintain the transmission level DC voltage V_{dc}. The system reactive power can also be regulated with the outside loop. One thing to be mentioned is that, the circulating current elimination control signals u_{a_2f}, u_{b_2f} and u_{c_2f} are inserted into the onshore converter control, which can effectively suppress the circulating current in the three phases of the MMC.

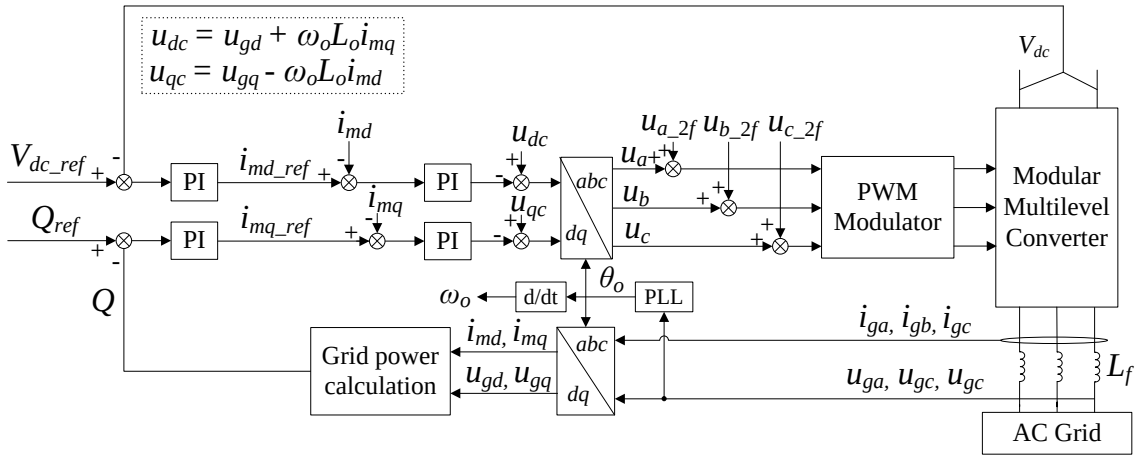

Fig. 4.11. Block diagram of the control for the three-phase MMC.

4.5 Offshore Converter

4.5.1 Offshore Converter Configuration

The offshore converter is a key component in the DC-grid offshore wind farm, which is a DC/DC converter to boost the collection level voltage to the transmission level voltage. Fig. 4.12 shows the offshore converter. Owing to the advantages of small harmonics, the three-phase MMC is used. The output of the DC/DC converter will take a high voltage level. Hence, the diode rectifier is used at the output side. The three-phase MMC at the input side converts the DC voltage into AC voltage. The frequency of the AC voltage is higher than 50 Hz used in the normal AC system, which can significantly reduce the size and the weight of the transformer. Afterwards, the AC voltage is stepped up by the transformer and rectified into DC at the output side.

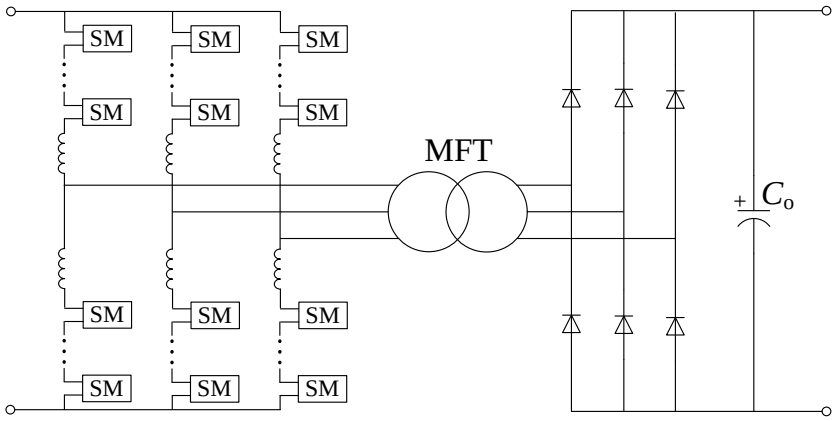

Fig. 4.12. Block diagram of the offshore converter.

4.5.2 Offshore Converter Control

The modulation strategy and the voltage balancing control strategy for the three-phase MMC in the offshore converter is the same to that in the onshore converter, which is not repeated here.

The offshore converter is composed with POFC and NOFC, which are connected in series. The NOFC is used to maintain the collection level voltage close to the specified reference level, and the POFC is used to track the power of the NOFC.

The proposed offshore converter control is shown in Fig. 4.13. Fig. 4.13 (a) is used for NOFC to keep the collection level voltage constant. A simple PI controller is used as the DC-link voltage controller to generate the required modulation *m*. And then, the PWM generator will produce the corresponding pulses to drive the MMC so as to ensure that the collection level voltage V_{MV} tracks the reference voltage V_{MV_ref}. A power control loop is used here to limit the NOFC power. If the NOFC power P_{off2} is over the limit value P_{off2_lim} of 1.1 p.u., the power control loop will limit the NOFC power.

Fig. 4.13(b) is used for the POFC to make its power P_{off1} follow the NOFC power P_{off2}, which is similar to Fig. 4.13(a). A PI controller is used as the power controller to generate the required modulation ratio *m*. And then, the PWM generator will produce the corresponding pulses to drive the MMC. Finally, the POFC power P_{off1} follows the NOFC power P_{off2}.

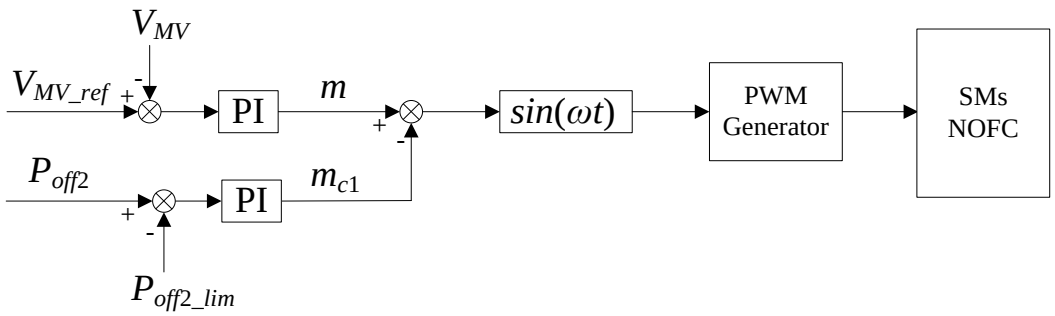

(a)

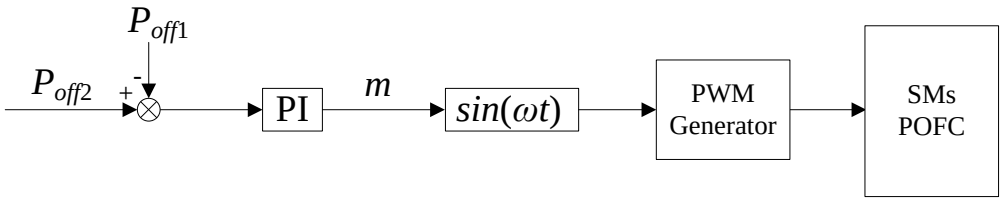

(b)

Fig. 4.13. Block diagram of (a) The control for NOFC. (b) The control for POFC.

4.6 AC Grid Faults Ride Through

4.6.1 AC Grid Faults

Owing to the continuous increase in wind power penetration level, the operation of existing utility networks may be affected, especially the stability of the power system. The grid codes are now being revised to reflect new requirements for wind turbine integration into the network. According to the grid code, at a short-circuit fault in the external AC grid, wind turbines should keep connection to the grid and restore their normal operation after the fault is cleared [103], [104]. The reason is that, when the wind power penetration level is high, the protective disconnection of a large amount of wind power will be an unacceptable consequence that may threaten the power system stability [105], [106]. The wind turbine must thus be equipped with fault ride-through capability required in the grid codes. The American Wind Energy Association (AWEA) has proposed low-voltage ride-through requirements for the interconnection of large wind generators [16]. The proposed voltage requirement are described by Fig. 4.14, which shows the grid voltage drop area where the wind generators must remain connected to the grid.

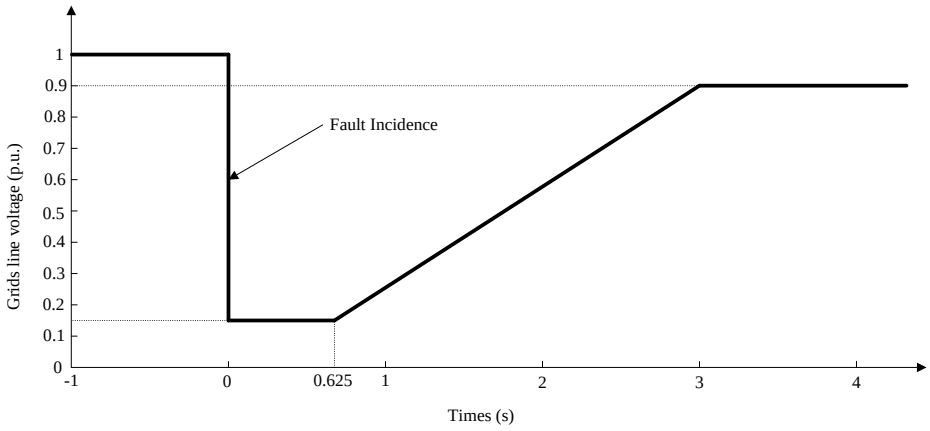

Fig. 4.14. Low voltage ride-through requirement by AWEA.

The DC grid is shown in Fig. 4.6, where the power flow can be described as shown in Fig. 4.15. Neglecting the power electronics loss, the relationship of the power in the DC grid can be expressed as

$$P_w = P_k + P_g \tag{4-12}$$

$$P_g = P_c + P_{ca1} \tag{4-13}$$

$$P_c = P_{off} + P_{ca2} \tag{4-14}$$

$$P_{off} = P_{on} + P_{ca3} \tag{4-15}$$

where P_w is the captured power from the wind. P_k is the kinetic energy in the wind turbine. P_g is the generator power. P_{ca1} is the capacitor power in the wind turbine's power converter. P_c is the output power of the wind turbine. P_{ca2} is the capacitor power in the collection system. P_{off} is the offshore converter power, which is the summation of P_{off1} and P_{off2}. P_{ca3} is the capacitor power in the HVDC transmission system. P_{on} is the onshore converter power. The generator controlled by generator-side converter captures the power P_g from the wind power P_w, the power P_k is stored as the kinetic energy. And then, the grid-side converter transmits the power P_c from the generator to the collection level, while power P_{ca1} is stored in the capacitor between the generator-side converter and the grid-side converter. Afterwards, the collection level power is sent to the transmission level as P_{off} by the offshore converter, except that some is stored in the collection level capacitors as P_{ca2}. Finally, the AC grid extracts the power P_{on} from the onshore converter with some power stored in the transmission level capacitors as P_{ca3}.

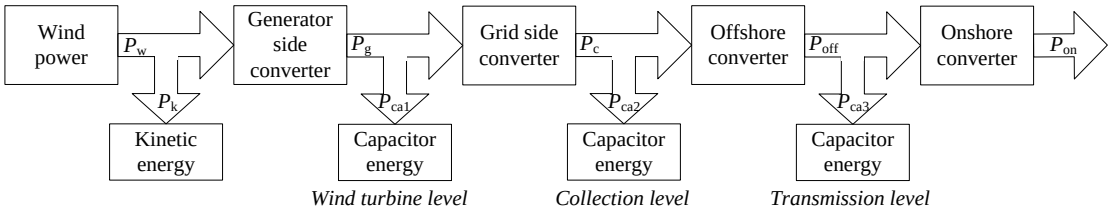

Fig. 4.15. Power flow in the DC grid for offshore wind farms.

When a disturbance occurs in the external on shore AC grid, a voltage dip occurs at the AC output terminal of the DC grid. The maximum active power that the DC grid can send to the AC grid is decreased with the dip of the terminal voltage. At this time, the output power of the onshore converter is quickly reduced. However, the input power of the onshore converter is nearly not changed. Therefore, there is a power imbalance in the transmission level under the grid disturbance, which results in the increase of the transmission level voltage, and may damage the HVDC transmission system.

The low voltage ride-through of the DC grid as shown in Fig. 4.6 is studied here. The configurations and the control strategies for the wind turbine, the offshore converter, and the onshore converter in normal situation have been introduced in detailed before. The response of the DC grid under AC grid disturbance is analyzed here, which mainly focuses on the voltage dip situation at the point of common coupling (PCC). An effective control strategy is presented to improve the faults ride-through capability of the DC grid, which is significant to limit the DC-link voltage fluctuation in a small range, and avoid the system damage. The presented control for faults ride-through mainly includes onshore converter control, offshore converter control, and the wind turbine control, which will be discussed below.

4.6.2 Offshore Converter Control under Faults

In order to improve the performance of the offshore converter under faults and avoid overvoltage situation in the HVDC transmission system, the control for the offshore converter is improved with the dotted box area as shown in Fig. 4.16, which is based on Fig. 4.13. In Fig. 4.16, a voltage limit loop is inserted into the controller, which can effectively limit the overvoltage in the HVDC transmission level under grid faults.

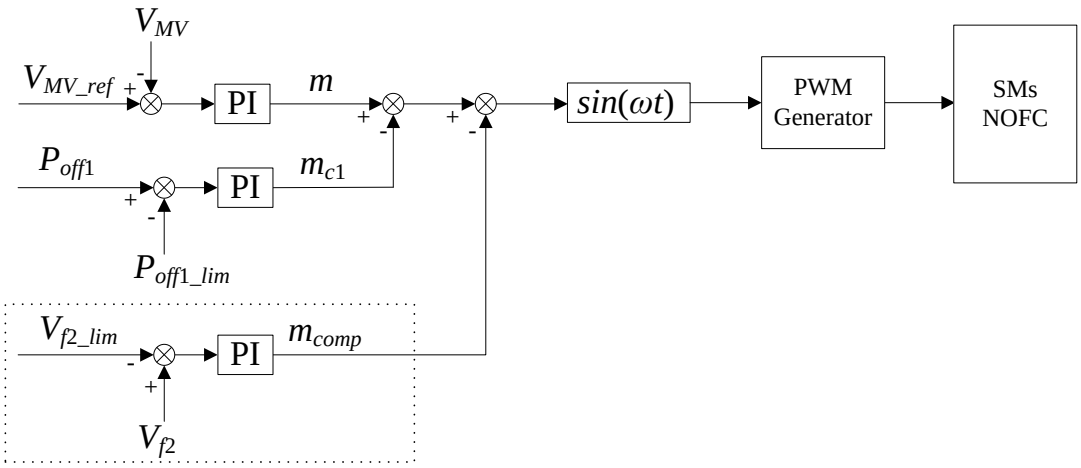

(a)

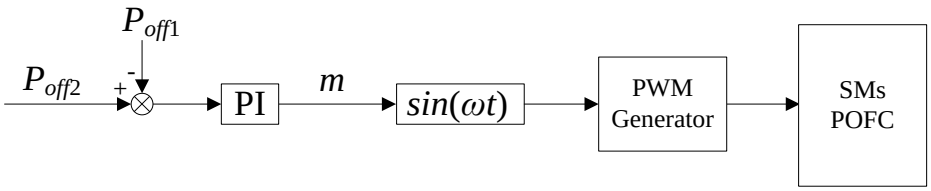

(b)

Fig. 4.16. Block diagram of (a) The control for NOFC under grid faults. (b) The control for POFC under grid faults.

In Fig. 4.16, when the output voltage V_{f2} of the NOFC, as shown in Fig. 4.6, is increased and over the limit value V_{f2_lim}, which is set as 1.1 p.u. under grid faults, the voltage limit loop starts to be active to produce a modulation ratio compensation component m_{comp}, which is embedded into the voltage control loop to reduce the modulation ratio. As a consequence, the NOFC power P_{off2} transmitted to the transmission level is effectively reduced. According to (4-15), although the AC grid power P_{on} is reduced owing to the voltage dip at PCC, the offshore converter power P_{off} is also fast reduced, which could effectively reduce the capacitor power P_{ca3} and limits the increase of the capacitor voltage in the transmission level.

On the other hand, based on (4-14), the decrease of the power P_{off} sent to the transmission level by the offshore converter could result in the increase of power P_{ca2}. Consequently, the overvoltage may appear in the collection level. The following wind turbine control could effectively handle this problem.

4.6.3 Wind Turbine Control under Faults

The wind turbine I associated with its control is used in the DC grid, which is composed with the grid-side converter control and the generator-side converter control.

Grid-Side Converter Control

As the aforementioned introduction, the control for the offshore converter results in that more power is stored in the collection level, which could make the DC-link voltage in the collection level increased. Here, an improved control is presented for the grid-side converter in the wind turbine, which can effectively avoid the overvoltage in the collection system.

According to the control for the grid-side converter in normal situation in Chapter 3, the control for the grid-side converter is improved with the dotted box area as shown in Fig. 4.17. The output voltage of the wind turbine V_{wt} is measured by the control system and compared with the limit value V_{wt_lim}, which is set as 1.1 p.u. in this study. Once the wind turbine output voltage V_{wt} is over the value V_{wt_lim}, the reference current is reduced by the voltage limit loop, which indirectly results in the decrease of the output power P_c of the wind turbine. Consequently, according to (4-14), the capacitor energy in collection level could not be increase so much, and the voltage in the collection level is effectively limited.

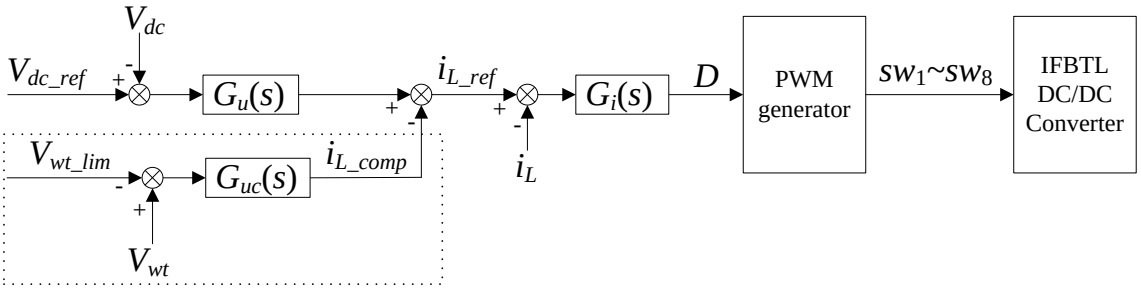

Fig. 4.17. Block diagram of the improved control for the grid-side converter.

Generator-Side Converter Control

According to (4-13), owing to the reduction of the wind turbine output power P_c by the improved control for the grid-side converter, more power would be stored in the DC-link capacitor in the wind turbine power converter, which may result in that the capacitor voltage is increased in the wind turbine. Here, an improved control is presented for the generator-side converter so as to prevent the overvoltage.

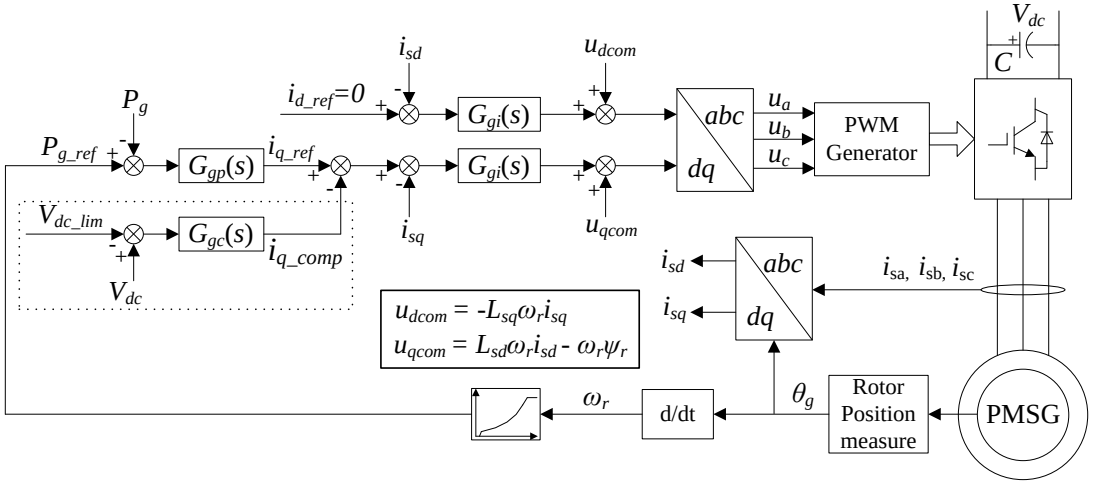

Fig. 4.18. Block diagram of the improved control for the generator-side converter.

The generator-side converter control is improved with the dotted box area, as shown in Fig. 4.18. When the DC-link voltage V_{dc} in the wind turbine is higher than the reference value V_{dc_lim} as 1.1 p.u., the compensation is active in the power control loop, which is used to reduce the active power P_g of the generator. According to (4-13), it can be seen that with the decrease of the generator power P_g, the capacitor power in the wind turbine is effectively limited. Hence, the overvoltage in the DC link of the wind turbine converter is avoided. According to (4-12), it can be realized that more power is transferred to kinetic energy because of the decrease of the generator power. As a consequence, the kinetic energy is increased with the increase of the wind turbine speed. However, the inertia constant for the MW-level wind turbine is big and within the range of 2-9 s. As a consequence, the wind turbine speed is only increased a little during the short fault period. On the other hand, if the wind turbine speed is over the rated value, the pitch angle control system will be active to limit the wind turbine speed.

4.6.4 DC Grid Performance under Faults

The performance of the DC grid under AC grid faults is studied with the professional tool PSCAD/EMTDC. A 400 MW DC grid for offshore wind farm is modeled as shown in Fig. 4.6, where four aggregated variable speed wind turbines with 100 MW each respectively are used in the wind turbine system. It is assumed that each aggregated model has twenty of 5 MW wind turbines lumped together. The three-phase short-circuit fault happened on one of the 110 kV double circuit transmission lines, and result in that the voltage V_{pcc} at the PCC is dipped to 15% of the rated value. After 150 ms, the fault is cleared from the power system and the voltage of PCC is recovered. The wind turbine parameters, cable parameters, and the HVDC system parameters are shown in the Appendix A, D, and E, respectively. The aforementioned control is applied for the DC grid, and the DC grid performance is shown in Fig 4.19~Fig. 4.21.

Fig. 4.19(a) shows the wind speeds for the wind turbines in the wind farm. A grid fault happened at 7 s causes AC grid voltage V_{pcc} dip to 15% of the rated value and lasting for 150 ms as shown in Fig. 4.19(b).

Fig. 4.20 shows the performance of the DC grid only with the normal control and not with the improved control under faults. In normal situation, these wind turbines in the wind farm are controlled to capture the optimal power from the wind by the generator-side converter associated with the pitch angle control system. The grid-side converter keeps the DC-link capacitor voltage constant as 5.4kV in the wind turbine for the normal operation of the generator-side converter. The collection level voltage is kept by the offshore converter as 40 kV and the transmission level voltage is maintained as 150 kV by the onshore converter before grid faults.

Once the grid fault happened at 7 s, and the AC grid voltage V_{pcc} dipped to 15% of the rated value, the power sent into the grid is reduced in proportional to the decrease of the AC grid voltage shown in Fig. 4.20(i). At this time, the onshore converter loses its controllability, and could only send little power to the AC grid. However, the power transferred from the offshore converter is nearly unchanged. Consequently, more energy is stored on the transmission level, which results in the increase of the transmission level voltage. It can be seen that the transmission level voltage is nearly increased more than four times as shown in Fig. 4.20(h). Figs. 19(a)~(g) shows the performances of the wind turbines and the collection system.

Fig. 4.21 shows the DC grid performance with the improved control under faults. During the grid faults, if the transmission level voltage is measured to be over the limit value as 1.1 p.u., the offshore converter starts to reduce its input power so as to limit the

increase of transmission level voltage. Fig. 4.21(h) shows that the transmission level voltage, which is only increased to 1.2 p.u.. Because of the decrease of the input power for the offshore converter, the imbalance appears in the collection level, which causes the increase of the collection level voltage. With the improved control under faults, the grid-side converter in the wind turbine reduces its output power as shown in Fig. 4.21(e) if its output voltage is over the reference value as 1.1 p.u.. Hence, the collection level voltage is effectively limited with the maximum value as 1.2 p.u. shown in Fig. 4.21(f). Also, the DC-link voltage in the wind turbine converter is increased because of the decrease of its output power. With the improved control under faults, the generator-side converter starts to reduce its output power shown in Fig. 4.21(c) to keep the DC-link voltage in the wind turbine if the DC-link voltage is over the set point as 1.1 p.u. as shown in Fig. 4.21(d). Finally, the decrease of the generator power causes the increase of the kinetic energy. As a consequence, the wind turbine speeds are increased, as shown in Fig. 4.21(a). Nevertheless, owing to the action of pitch angle control system as shown in Fig. 4.21(b) and the big inertia of the wind turbine, the wind turbine speed could not have a big change during the short time period. As a consequence, the DC grid for the offshore wind farm could have a good performance with the improved control under faults.

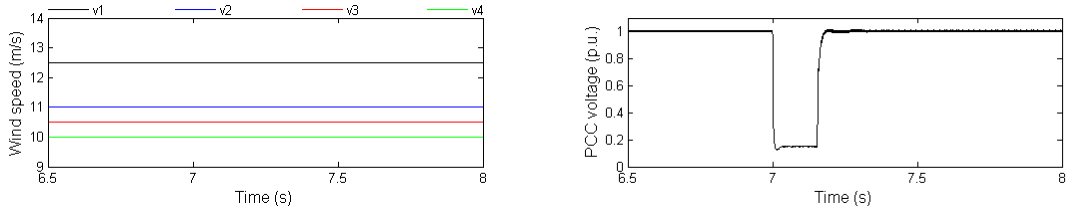

(a) (b)

Fig. 4.19. (a) Wind speed. (b) PCC voltage.

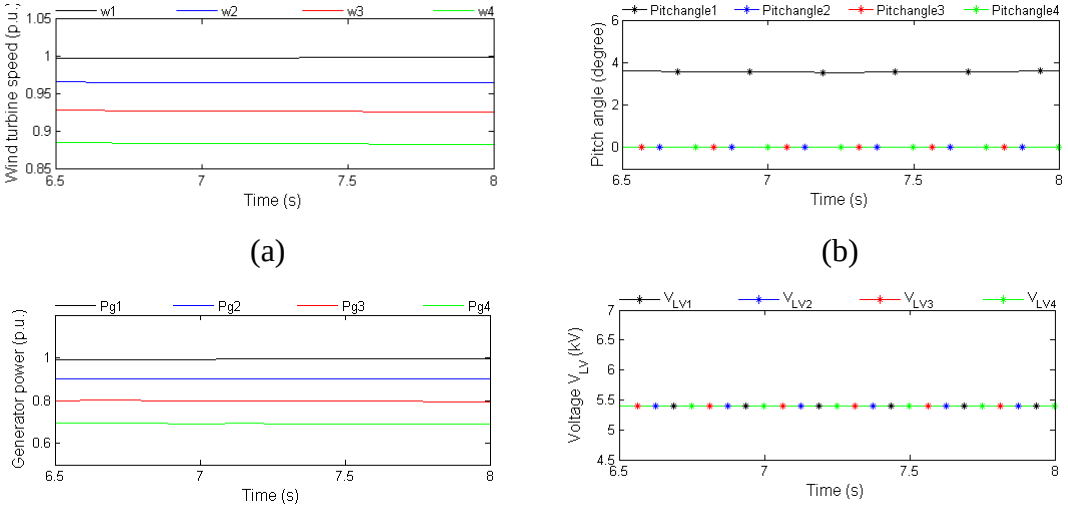

(a) (b)

(c) (d)

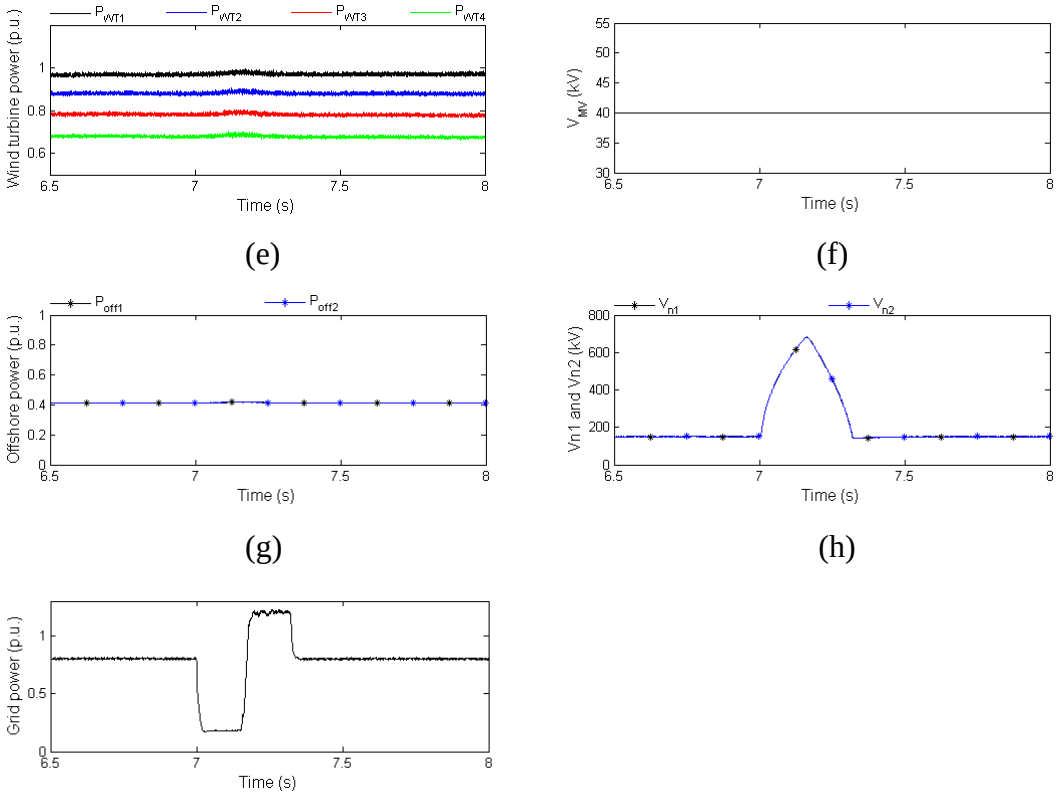

Fig. 4.20. Performance of the DC-grid offshore wind farm without the improved control. (a) Wind turbine speed. (b) Pitch angle. (c) Generator power. (d) DC-link voltage in the wind turbine. (e) Wind turbine output power. (f) Collection level voltage. (g) Offshore converter power. (h) Transmission level voltage. (i) Grid power.

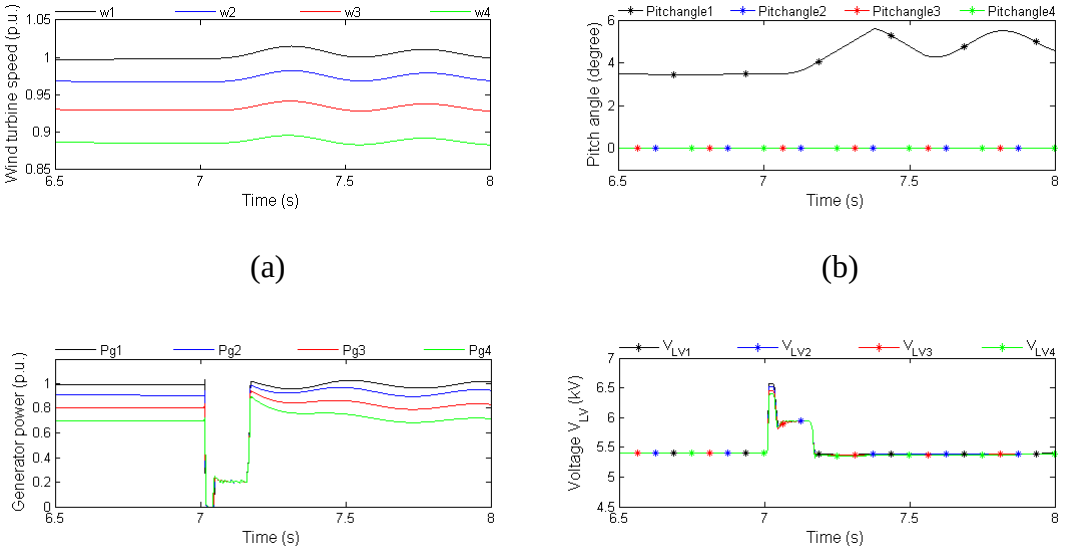

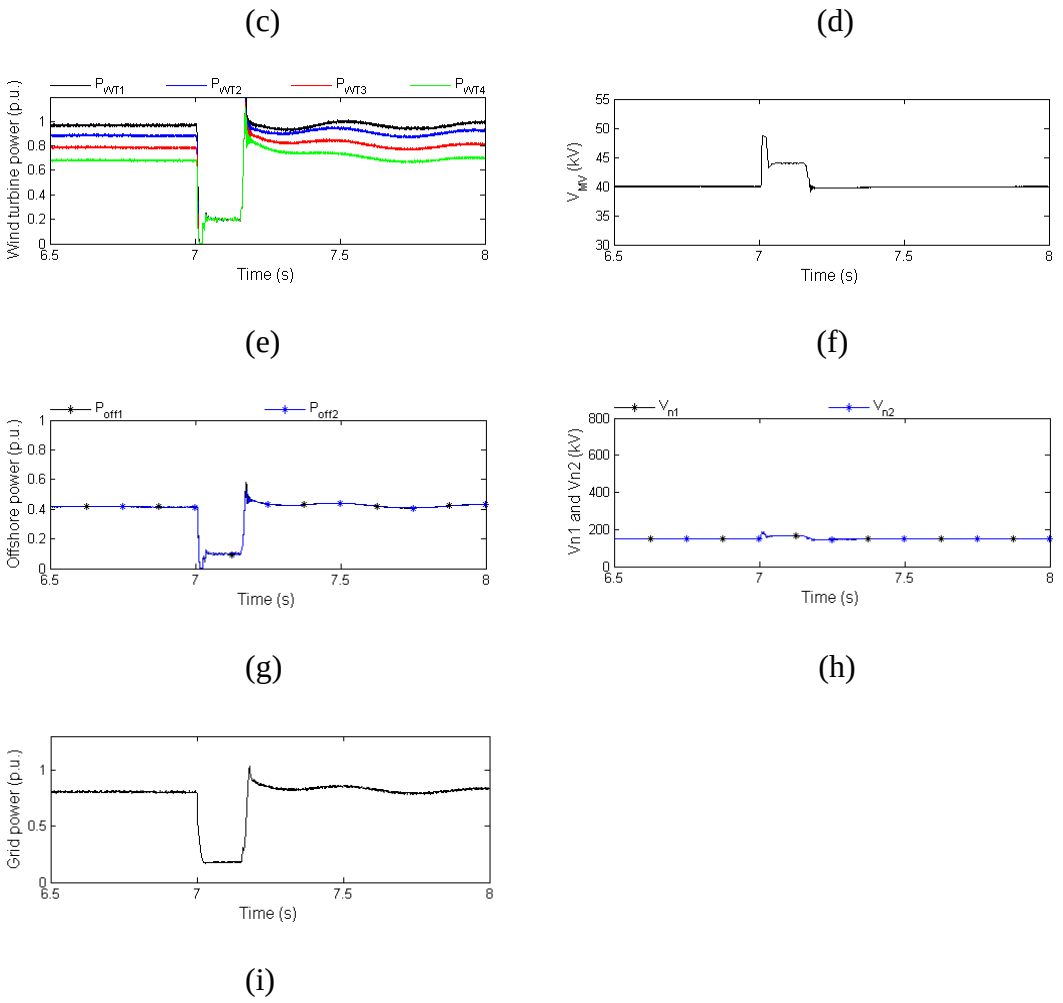

Fig. 4.21. Performance of the DC-grid offshore wind farm with the improved control. (a) Wind turbine speed. (b) Pitch angle. (c) Generator power. (d) DC-link voltage in the wind turbine. (e) Wind turbine output power. (f) Collection level voltage. (g) Offshore converter power. (h) Transmission level voltage. (i) Grid power.

4.7 Summary

In this chapter, the HVDC transmission system in the DC grid is introduced. The MMC-based VSC configuration associated with its control is presented for the onshore converter. Owing to the special requirement for the offshore converter in the DC grid, a MMC-based DC/DC converter is presented, and the corresponding control is introduced. A medium frequency transformer is used in the offshore converter, which may reduce the size and weight of the offshore converter. The ride-through control for the AC grid fault is presented. Through the improvement of the offshore converter control and the wind turbine control, the performance of the DC grid under AC grid faults can be effectively improved.

Chapter 5

Protection and Redundancy under HVDC System Faults

5.1 Introduction

At present, the collection system in all existing offshore wind farms is an AC system. Through the high voltage AC or DC transmission technology, the collected AC power is transmitted to the onshore AC grid. As a consequence, the existing grid codes for wind turbines and the investigation on low voltage ride through capabilities are mainly focused on the AC systems.

As to the DC grid for offshore wind farm, a promising wind farm system in future, where the DC collection system is used instead of the AC collection system [1-10], it also requires the corresponding grid codes for its development. Unfortunately, there are rarely grid codes for DC transmission and collection systems of the wind farm. Therefore, the behaviors, protection, redundancy, and control and so on are needed to be studied for the offshore wind farm with DC grid.

In the DC grid for the offshore wind farm, the fishing activities, anchors, ageing phenomena and so on, would cause the cable faults with the possibility as approximate 1 fault/100 km/year [107], which may result in the HVDC transmission system fault and may damage the DC grid. The repair for the damaged system in the offshore wind farm is costly, and often takes considerable time, even several months, which results in that the possible loss of income is enormous [108]. Normally, the overvoltage and overcurrent situations may be caused in the HVDC transmission system because of the DC cable fault, which is very harmful to the HVDC transmission system and may damage the onshore

converter and the offshore converter and should be avoided. As a consequence, the protection for the DC grid is very important to enhance its reliability and save the costs.

To date, a few protective devices have been developed such as AC CBs, DC CBs, and DC switches and so on. The DC CB based on ETO thyristor has been introduced in some literatures [26], [29]. Although the DC CB has fast switch speed in less than 10 us, and can be used in series with capacitor to limit and interrupt the capacitor discharge current during a fault, this kind of DC CB based on ETO may not be used in this high voltage DC system because of its low voltage capacity. The references [27] and [28] presents the new type of active DC CB based on standard SF_6 AC circuit breakers with auxiliary circuits, which normally needs tens of milliseconds to interrupt the DC circuit, but this active DC CB may also not be fast enough to protect the transmission system since the capacitor in the onshore or offshore converters discharges very fast under DC faults.

In this chapter, the cables short-circuit fault of the HVDC transmission system is studied in the DC grid for offshore wind farms. The dynamic performance of the DC grid under faults is analyzed, and the corresponding protection is presented. In addition, the protection design is also introduced, which can effectively protect the DC grid and avoid the damage, and significantly enhances the reliability of the HVDC transmission system. On the other hand, the redundancy of the HVDC system under DC cable faults is presented. Through the corresponding operation of switchgears and the related control, the DC grid can effectively ride-through the HVDC system fault. The DC grid for offshore wind farms is modeled and simulated, and the results validate the feasibility of the presented protection, redundancy, operation, and control.

5.2 DC Cable Faults

The DC grid for the offshore wind farm is shown in Fig. 4.6, which is composed with the wind turbines, DC-grid collection system and HVDC transmission system and so on. Fig. 5.1 shows the HVDC transmission system in detail, which consists of the PONC, NONC, POFC, NOFC, and transmission cables. In case of breakdown of anyone converter, the transmission system can still be operated with the other healthy converters. As a consequence, this type configuration as shown in Fig. 5.1 can provide a high degree of reliability for the HVDC transmission system. Although the MMC-based HVDC system maybe evaluated to be attractive in the wind power industry, such as the Trans Bay Cable project [67], the two-level and three-level voltage source converters have been widely used for the HVDC transmission system. As a consequence, the two- and three-level VSC are considered here for the onshore converter in the HVDC transmission system.

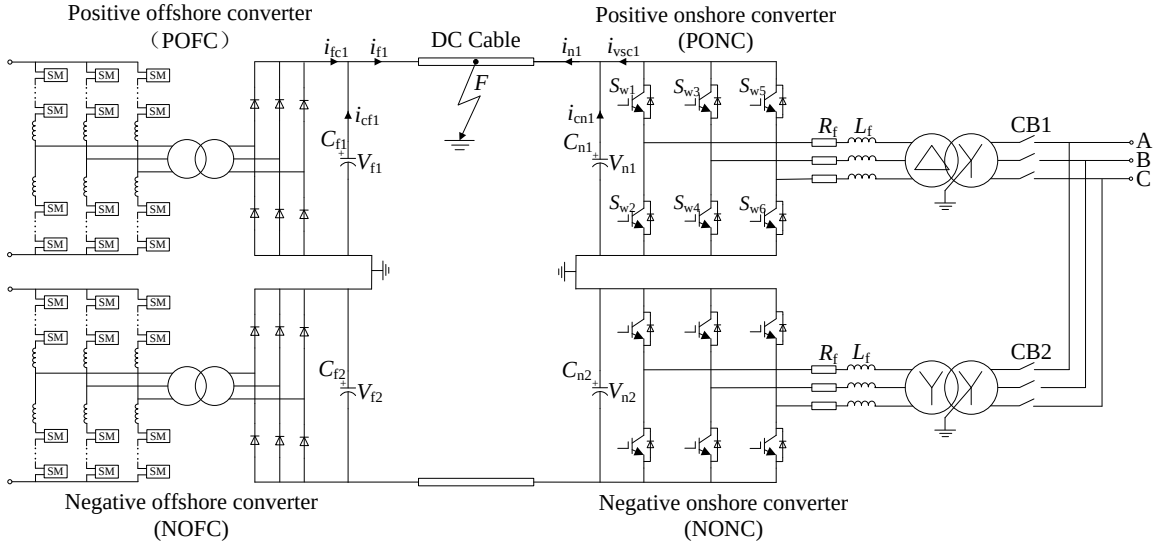

Fig. 5.1. HVDC transmission system with positive pole cable-to-ground fault.

In this chapter, the positive pole cable-to-ground fault on the HVDC transmission is considered and studied as shown in Fig. 5.1. The possible impacts of the fault on the onshore converter and offshore converter are analyzed and discussed. Furthermore, the corresponding protection is presented and designed. The negative pole cable-to-ground fault can also be treated with the same method.

5.3 HVDC System Performance under Faults

5.3.1 Dynamic Performance of Onshore Converter

Fig. 5.2 shows the equivalent circuit of the onshore converter under faults. During the fault, the IGBTs are all switched off. The e_a, e_b and e_c are equivalent transformer voltage. L_f and R_f are the filter inductance and resistance. L_{eq} and R_{eq} are the equivalent inductance and resistance. The cable-to-ground fault happened at the point F. l_n is the cable length between the PONC and the fault point F.

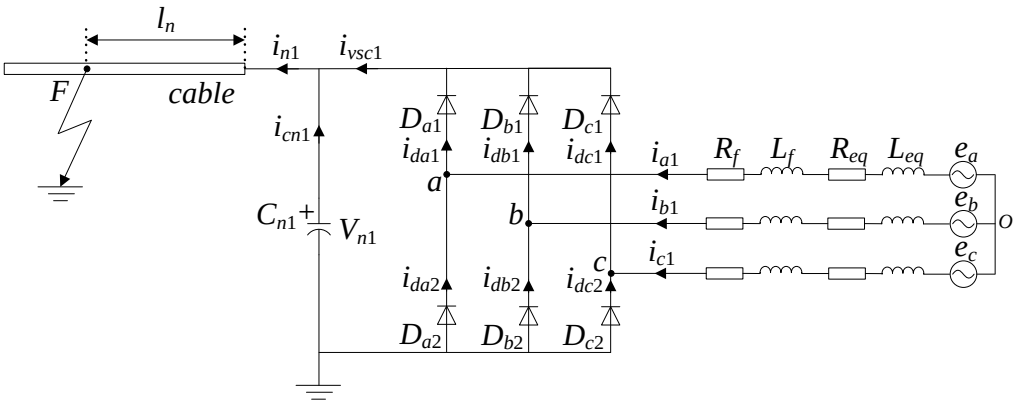

Fig. 5.2. Equivalent circuit for the onshore converter under faults.

Once the cable-to-ground fault happens as shown in Fig. 5.2, the cable current at the receiving end, $-i_{n1}$, reduces to 0 firstly, and then reverses the current direction while the capacitors C_{n1} at the terminal starts to discharge into the fault point F, which may result in a high short circuit current in the system, even that the PONC IGBTs are blocked for protection purpose during the fault.

The capacitor C_{n1} will be bypassed by the diodes when the capacitor voltage V_{n1} collapses and is reduced to 0. Afterwards, the cable inductance starts to discharge and the cable current circulates in the freewheel diodes with an initial value. Each phase-leg carries a third of the cable current. As a consequence, a huge current suddenly appears in the diodes when the capacitor is bypassed by the diodes, which may damage the diodes.

On the other hand, the short circuit fault causes a transient performance at the AC side, where the AC current i_{a1}, i_{b1}, and i_{c1} are fed into the DC-link via diodes. After the capacitor voltage collapses within a very short time and the capacitor is bypassed by the diodes, the AC side is short circuit at the points a, b, and c. Suppose that the AC grid phase a voltage after the short circuit occurs is expressed as

$$e_a = U_m \sin(\omega t+\alpha) \tag{5-1}$$

where U_m is the amplitude of transformer phase voltage. ω is the synchronous angular frequency. α is the phase angle. The phase a current under the AC grid three-phase short circuit can be obtained as (5-2) [26].

$$i_{a1}(t) = I_m \sin(\omega t+\alpha-\varphi) + [I_{m0} \sin(\alpha-\varphi_0) - I_m \sin(\alpha-\varphi)]e^{-t/\tau} \tag{5-2}$$

with $I_m^2=U_m^2/(R^2+\omega^2L^2)$, φ=arctan($\omega L/R$), $L=L_f+L_{eq}$, $R=R_f+R_{eq}$, $\tau=L/R$, I_{m0} and φ_0 are the grid current amplitude and phase angle at the beginning of the AC grid three-phase short circuit. The phase b current $i_{b1}(t)$ and the phase c current $i_{c1}(t)$ can be obtained with the same method, which are not repeated here.

According to the parameters in the Appendix E, suppose the initial values of I_{m0} is 0, the most serious transient current i_{a1} at the AC side with the maximum value of approximate 11.1 kA is plotted as shown in Fig. 5.3 under the condition that the grid voltage phase angle is zero at the short circuit initiation [26]. Although the AC CB is equipped at the AC side as shown in Fig. 5.1, it may not be fast enough to avoid the large current because approximate tens of milliseconds is required for the AC CB to interrupt the circuit [16].

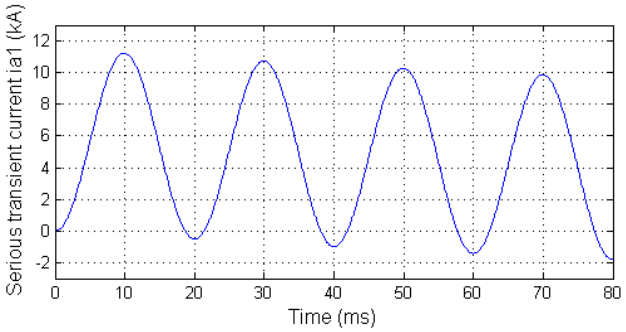

Fig. 5.3. The most serious transient current i_{a1} at AC grid under faults.

The performance of the onshore converter under faults is analyzed with Fig. 4.6. The positive pole cable-to-ground fault is considered as shown in Fig. 5.1. The fault resistance is very small, and considered as zero in this study. The different fault distances l_n including 0.1 km, 1 km and 10 km are conducted respectively. Suppose the positive onshore converter is initially operated with the rated power P_{rated} as 200 MW, the cable initial current is the rated value as $I_{n10}=P_{rated}\div V_{n1}$ =200MW ÷150kV=1.33kA.

The simulation results are shown in Fig. 5.4~Fig. 5.5. Under faults, the DC-link voltage V_{n1} collapses fast in less than 1 ms. Along with the reduction of the fault distance l_n, the voltage V_{n1} collapses faster, and the peak value of the cable current would be

higher. The maximum cable current nearly reaches 68 kA when l_n=0.1 km. When the voltage V_{n1} is reduced to 0, the capacitor is bypassed by the diodes. As a consequence, the huge cable current abruptly flows through the freewheel diodes, which may damage the diodes. The most serious AC grid transient current i_{a1} under l_n=0.1 km is shown in Fig. 5.4(d) with the maximum value of approximate 11 kA, which is quite close to the value as shown in Fig. 5.3.

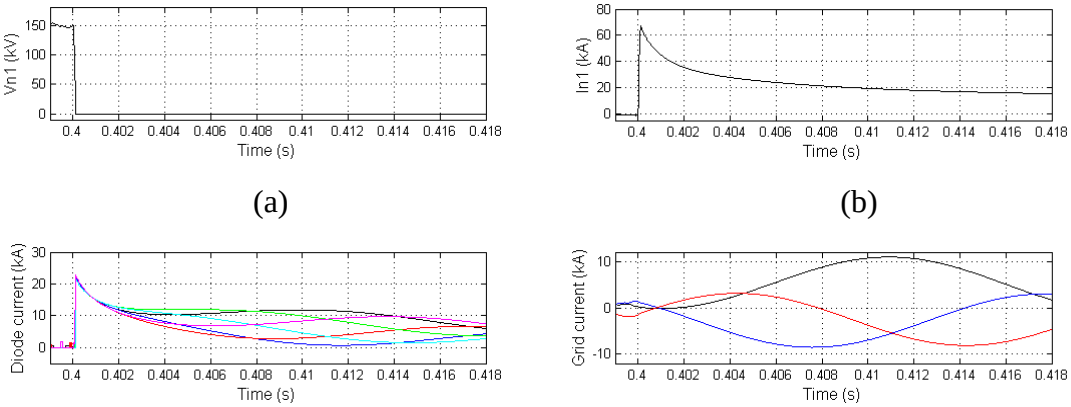

Fig. 5.4. Onshore converter performance under the fault distances l_n as 0.1 km. (a) Voltage V_{n1}. (b) Cable current i_{n1}. (d) Diode current. (g) Grid current.

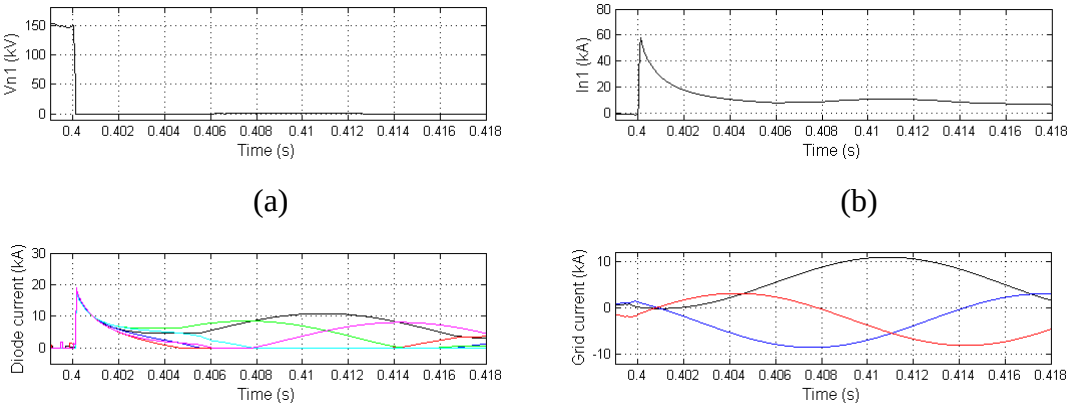

Fig. 5.5. Onshore converter performance under the fault distances l_n as 1 km. (a) Voltage V_{n1}. (b) Cable current i_{n1}. (d) Diode current. (g) Grid current.

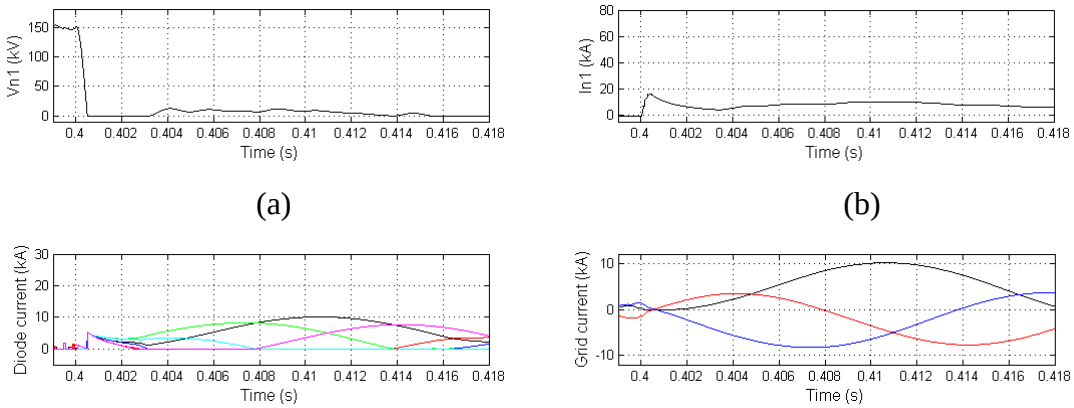

Fig. 5.6. Onshore converter performance under the fault distances l_n as 10 km. (a) Voltage V_{n1}. (b) Cable current i_{n1}. (d) Diode current. (g) Grid current.

5.3.2 Dynamic Performance of Offshore Converter

Fig. 5.7 shows the equivalent circuit of the offshore converter, where the cable-to-ground fault happened at the point *F*. The l_f is the distance between the POFC and the fault point *F*. During the fault, the IGBTs of the POFC are blocked if the cable current i_{f1} is over the IGBT protection value, and the wind farm power will be blocked by the POFC and cannot be sent to the grid with the positive-pole cable. As a consequence, only the diode rectifier at the output side of the offshore converter reacts to the cable-to-ground fault under faults, and the equivalent circuit of the offshore converter under faults would be a diode rectifier.

During the cable-to-ground fault, the offshore converter performance only contains capacitor discharge phenomenon and diode freewheel phenomenon. Once the cable-to-ground fault happens, the capacitor at the offshore converter discharges very fast. When the capacitor voltage V_{f1} is reduced to 0 and the capacitor is bypassed by the diodes, the cable current starts to circulate in the freewheel diodes. Owing to three diode phase-legs in the offshore converter, each phase-leg takes one third of the cable current.

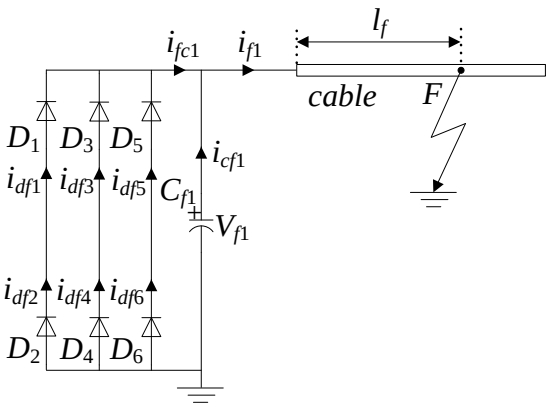

Fig. 5.7. Equivalent circuit for the offshore converter under faults.

Fig. 5.8~Fig. 5.10 shows the offshore converter performance under faults, where the different fault distances l_f including 0.1 km, 1 km and 10 km are conducted respectively. Suppose the POFC is initially operated with the rated power P_{rated} as 200 MW, the capacitor initial voltage is approximately $V_{f10}=V_{n1}+I_{f10}\times R_c \times L_{cable}$=150kV+1.33kA×0.0151 Ω/km×100km =152kV, where R_c is the cable resistor (Ω/km), and L_{cable} is the cable length (km). The cable initial current I_{f10} is the rated value as 1.33kA.

According to the simulation results, the DC voltage V_{f1} collapses in less than 1 ms under faults. Along with the increase of the fault distance l_f, the DC voltage collapses slower and the maximum value of the capacitor discharge current i_{cf1} and cable current i_{f1} becomes smaller. After the voltage V_{f1} is reduced to 0 and the capacitor C_{f1} is bypassed by diodes, the cable current starts to circulate in the diodes with a big initial value. In this situation, each diode phase-leg takes one third of the cable current, which is still very huge and may damage the diodes.

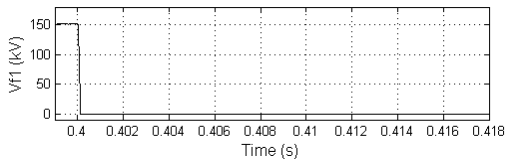

(a)

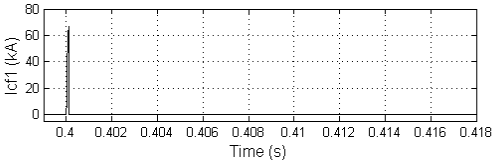

(b)

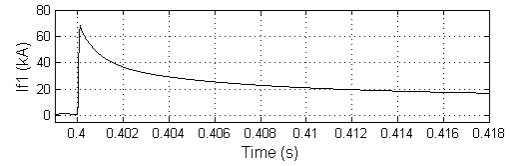

(c)

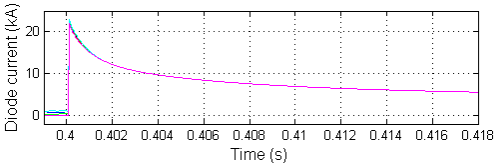

(d)

Fig. 5.8. Offshore converter performance under the fault distances l_f as 0.1 km. (a) Voltage V_{f1}. (b) Capacitor discharge current i_{cf1}. (c) Cable current i_{f1}. (d) Diode current.

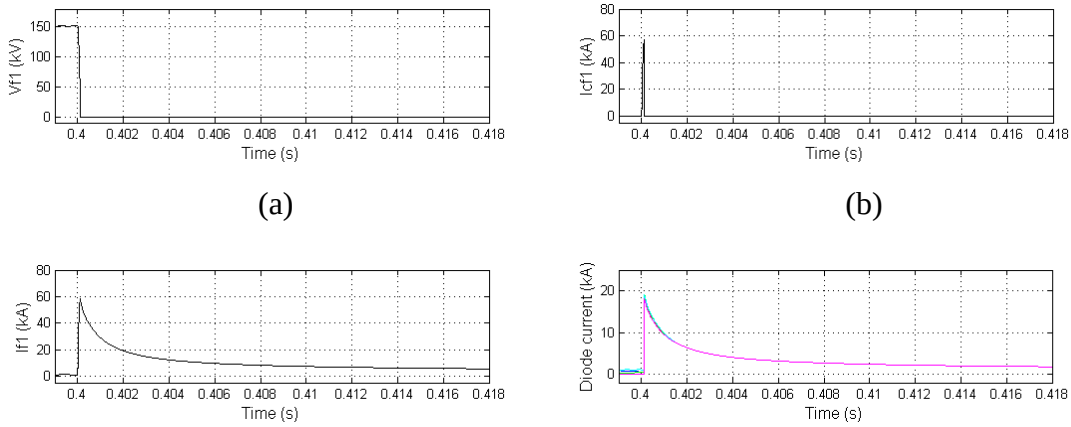

Fig. 5.9. Offshore converter performance under the fault distances l_f as 1 km. (a) Voltage V_{f1}. (b) Capacitor discharge current i_{cf1}. (c) Cable current i_{f1}. (d) Diode current.

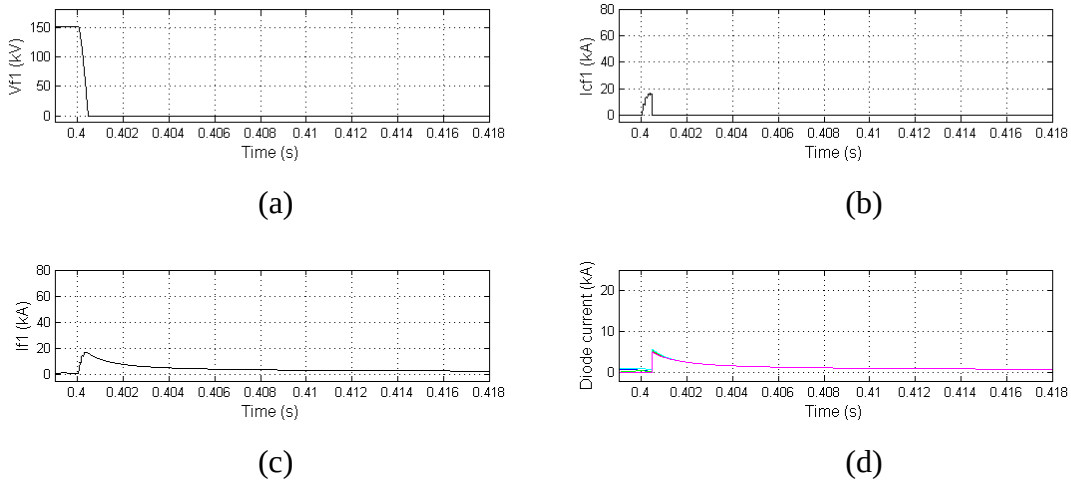

Fig. 5.10. Offshore converter performance under the fault distances l_f as 10 km. (a) Voltage V_{f1}. (b) Capacitor discharge current i_{cf1}. (c) Cable current i_{f1}. (d) Diode current.

5.4 Protection for HVDC System

5.4.1 Protective Inductor for Onshore Converter

Normally, the IGBTs of the onshore converter will be switched off under faults, and only diodes in the onshore converter may carry current. In this situation, there will be two situations for each phase-leg in Fig. 5.2. One situation is that both of the diodes in the phase-leg are conducted, the other situation is that only one diode in the phase-leg is conducted.

1) Both diodes in one leg in conduction

In Fig. 5.2, if the two diodes in phase x ($x\in$ (a, b, c)) are both conducted, the diodes current in this phase-leg can be expressed as

$$\begin{cases} i_{dx1}(t) = (i_{dx1}(t) + i_{dx2}(t))/2 + i_{x1}(t)/2 \\ i_{dx2}(t) = (i_{dx1}(t) + i_{dx2}(t))/2 - i_{x1}(t)/2 \end{cases} \tag{5-3}$$

If both of the two diodes in the phase-leg are conducted, there will be the following relationship

$$(i_{dx1}(t) + i_{dx2}(t))/2 > |i_{x1}(t)|/2 \tag{5-4}$$

The maximum diode current i_{d1_max} in this situation can be presented as

$$i_{d1\_max} = \text{Max}[(i_{da1}(t)+i_{da2}(t))/2+|i_{a1}(t)|/2, (i_{db1}(t)+i_{db2}(t))/2+| i_{b1}(t)|/2,$$
$$(i_{dc1}(t)+i_{dc2}(t))/2+|i_{c1}(t)|/2] \tag{5-5}$$

If the diodes in any two different phases α and β ($\alpha, \beta\in$ (a, b, c)) are all conducted in Fig. 5.2, there will be the relationship as

$$(i_{d\alpha1}(t) + i_{d\alpha2}(t))/2 = (i_{d\beta1}(t) + i_{d\beta2}(t))/2 \tag{5-6}$$

Based on (5-3) and (5-6), the $(i_{dx1}(t) + i_{dx2}(t))/2$ possibly gets its maximum value when the diodes in the three phase-legs are all conducted, which is a third of the cable current and can be expressed as

$$(i_{dx1}(t) + i_{dx2}(t))/2 \le i_{n1}(t)/3 \tag{5-7}$$

Substituting (5-7) into (5-5), the possible maximum diode current in this situation can be obtained as

$$i_{\text{d1\_max}} = \text{Max}[i_{n1}(t)/3+\text{Max}[|i_{a1}(t)|, |i_{b1}(t)|, |i_{c1}(t)|]/2]$$

$$\leq \text{Max}[i_{n1}(t)]/3+\text{Max}[|i_{a1}(t)|, |i_{b1}(t)|, |i_{c1}(t)|]/2 \quad (5\text{-}8)$$

The Max[$i_{n1}(t)$] may be reached when the capacitor voltage V_{n1} is reduced to zero under faults, which can be expressed as i_{n1m} and discussed later. The Max[$|i_{a1}(t)|$, $|i_{b1}(t)|$, $|i_{c1}(t)|$] can be derived from (5-2) and Fig. 5.3 under the most serious transient situation, which can be presented as

$$\text{Max}[|i_{a1}(t)|, |i_{b1}(t)|, |i_{c1}(t)|] = I_m\,[1+e^{-1/(2f\tau)}] \quad (5\text{-}9)$$

where f is AC grid frequency. Substituting (5-9) into (5-8), the possible maximum diode current in this situation can be obtained as

$$i_{d1\_max} \leq i_{n1m}/3+ I_m\,[1+e^{-1/(2f\tau)}]/2 \quad (5\text{-}10)$$

2) One of diodes in one leg in conduction

If (5-4) is not true and $(i_{dx1}(t) + i_{dx2}(t))/2=|i_{x1}(t)|/2$, one of the two diodes in the phase x would be blocked, and the other one takes the current $|i_{x1}(t)|$ in Fig. 5.2. As a consequence, the possible maximum diode current i_{d2_max} in this situation can be obtained when the most serious transient situation occurs, and i_{d2_max} can be expressed as

$$i_{d2\_max} = \text{Max}[|i_{a1}(t)|, |i_{b1}(t)|, |i_{c1}(t)|] = I_m\,[1+e^{-1/(2f\tau)}] \quad (5\text{-}11)$$

To reduce the diode current and protect converters under faults, it should be

$$i_{d1\_max} \leq i_{d2\_max} \quad (5\text{-}12)$$

The i_{d2_max} is considered as the possible maximum fault current under faults.

In order to protect the system under faults, a protective inductor, L_{pn}, is designed as shown in Fig. 5. 11. The protective inductor is installed at the terminal of the onshore converter to prevent overcurrent and makes (5-12) satisfied under faults, therefore, the diodes in the converters can be protected.

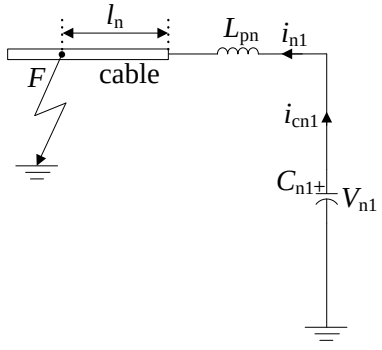

Fig. 5.11. Protection design for the onshore converter.

Suppose that the initial capacitor current I_{cn10} is 0 in Fig. 5.11, if the fault distance l_n is 0, the possible maximum cable current i_{n1m} can be obtained as (5-13) when the capacitor voltage is reduced to zero.

$$i_{n1m} = V_{n10}\sqrt{C_{n1}/L_{pn}} \tag{5-13}$$

To get the relationship between the current i_{n1m} and the inductor L_{pn}, the initial capacitor voltage V_{n10} is set as 165 kV with a margin of 1.1 for the 150 kV transmission system because of the possible voltage variation. Along with the increase of the inductance value L_{pn}, the possible maximum cable current i_{n1m} is reduced as shown in Fig. 5.12. As a consequence, the diode freewheel current is also decreased.

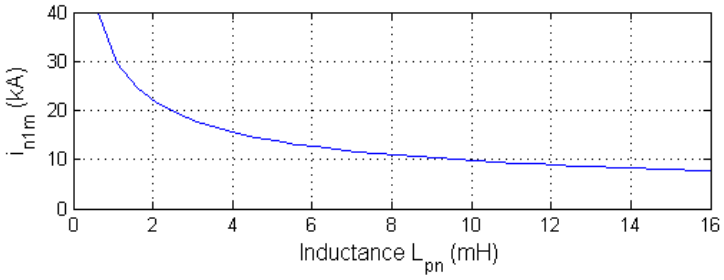

Fig. 5.12. The possible maximum values for capacitor C_{n1} discharge current i_{cn1} under different inductance L_{pn}.

In order to protect the diode, limit the cable current and satisfy (5-12), the protective inductor L_{pn} can be designed. According to (5-13), a 6.5 mH inductor L_{pn} is selected. With the protective inductor, (5-12) is satisfied, and the maximum capacitor discharge current is limited as 12.2 kA as shown in Fig. 5.12. According to (5-2) and Fig. 5.3, the possible maximum diode current is approximate 11.1 kA. As a consequence, the capacity of the diodes in the onshore converters can be designed as 12.2 kA with a margin of 1.1.

5.4.2 Dynamic Performance of Onshore Converter under Protection

The DC grid for the offshore wind farms has been modeled with the professional tool PSCAD/EMTDC as shown in Fig. 4.6. The positive pole cable-to-ground fault is considered in the simulation as shown in Fig. 5.1. The fault resistance is very small, and considered as zero in this study.

With the proposed protection, a 6.5 mH protective inductor is equipped in the onshore side, and Fig. 5.13~Fig. 5.16 shows the simulation results. In Fig. 5.1, the positive pole cable-to-ground fault happened at 0.4 s, and the different fault distances are studied including 0 km, 0.1 km, 1 km and 10 km.

With the protective inductor, the voltage V_{n1} collapses slowly, and the peak value of the cable current i_{n1} is limited in a small range, which effectively reduce the diode current and protect the diodes in the onshore converter. The AC currents under different fault distances are similar.

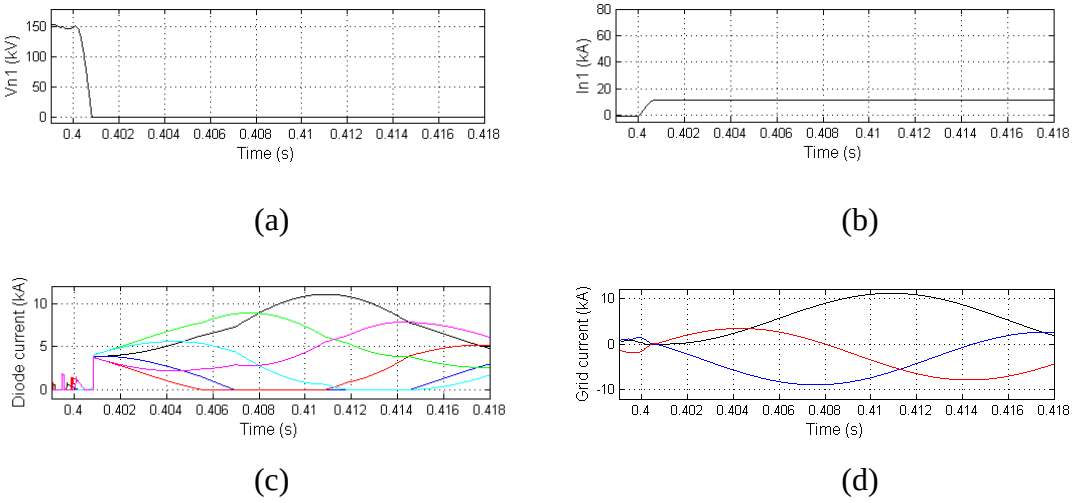

Fig. 5.13. Onshore converter performance under the fault distances l_n as 0 km. (a) Voltage V_{n1}. (b) Cable current i_{n1}. (c) Diode current. (h) AC grid current.

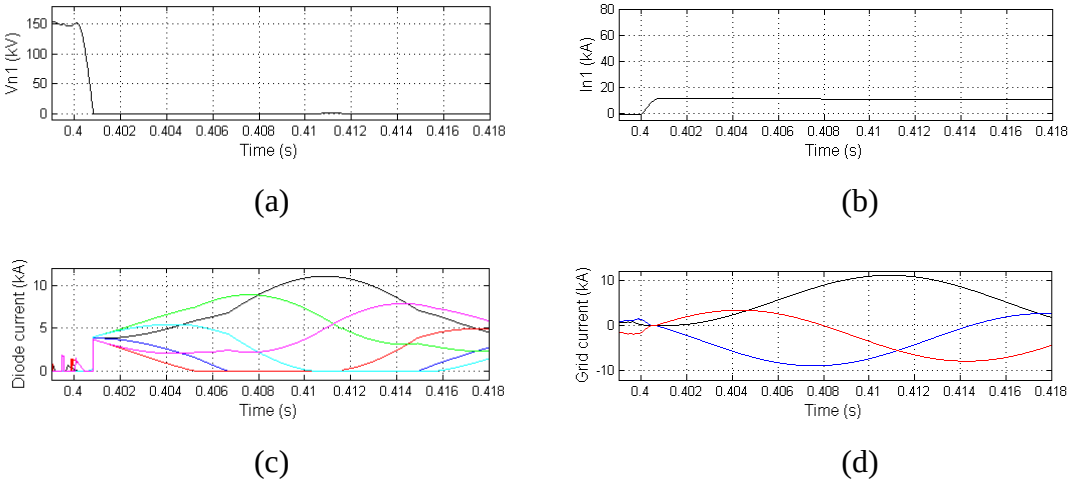

Fig. 5.14. Onshore converter performance under the fault distances l_n as 0.1 km. (a) Voltage V_{n1}. (b) Cable current i_{n1}. (c) Diode current. (h) AC grid current.

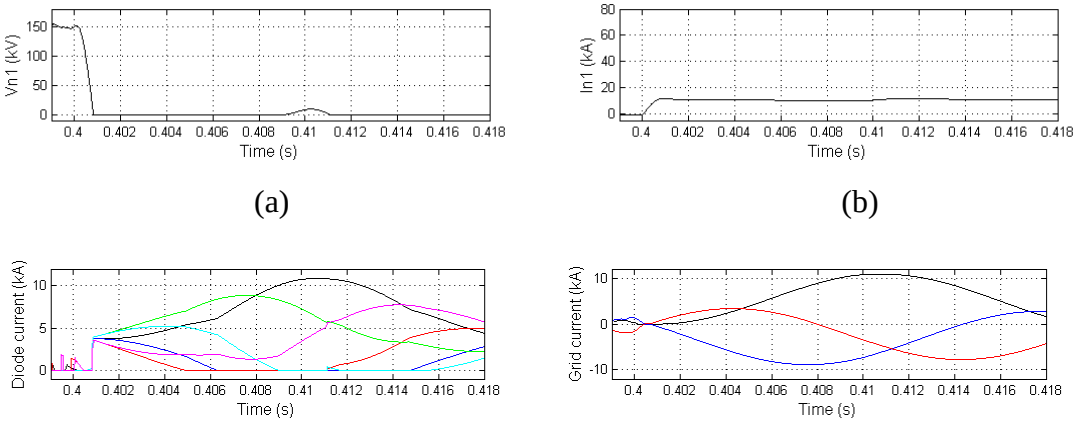

Fig. 5.15. Onshore converter performance under the fault distances l_n as 1 km. (a) Voltage V_{n1}. (b) Cable current i_{n1}. (c) Diode current. (h) AC grid current.

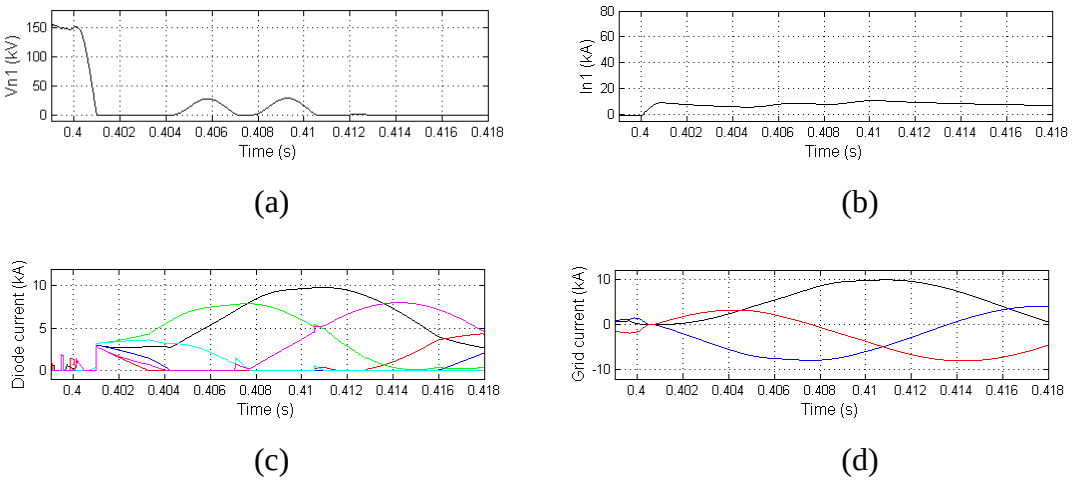

Fig. 5.16. Onshore converter performance under the fault distances l_n as 10 km. (a) Voltage V_{n1}. (b) Cable current i_{n1}. (c) Diode current. (h) AC grid current.

The current components under the fault distance l_n = 0 km is shown in Fig. 5.13(d) and Fig. 5.17(a). There is the relationship $-i_{b1}(t)/2=\text{Max}[|i_{a1}(t)|, |i_{b1}(t)|, |i_{c1}(t)|]/2>i_{n1}(t)/3$ between 0.4057 s and 0.408 s. During this short time, 0.4057 s to 0.408 s, the $D3$ is blocked and the $D4$ takes the maximum diode current $|i_{b1}(t)|$. From 0.408 s to 0.4145 s, there is $i_{a1}(t)/2=\text{Max}[|i_{a1}(t)|, |i_{b1}(t)|, |i_{c1}(t)|]/2>i_{n1}(t)/3$, which makes the diode $D2$ blocked and the diode $D1$ flow through the maximum diode current i_{a1}. The $i_{a1}/2$ appears as the maximum value of 5.5 kA at 0.411 s as shown in Fig. 5.18(a), and the maximum diode current of 11 kA is caused, which could be tolerated by the selected onshore diodes before. Figs. 5.17(b)~(d) shows the diode current in a short time under faults, when the

diodes in the three phase-legs are all conducted. In Figs. 5.17(b)~(d), the simulation results are the same as the calculation results based on (5-3) and (5-6).

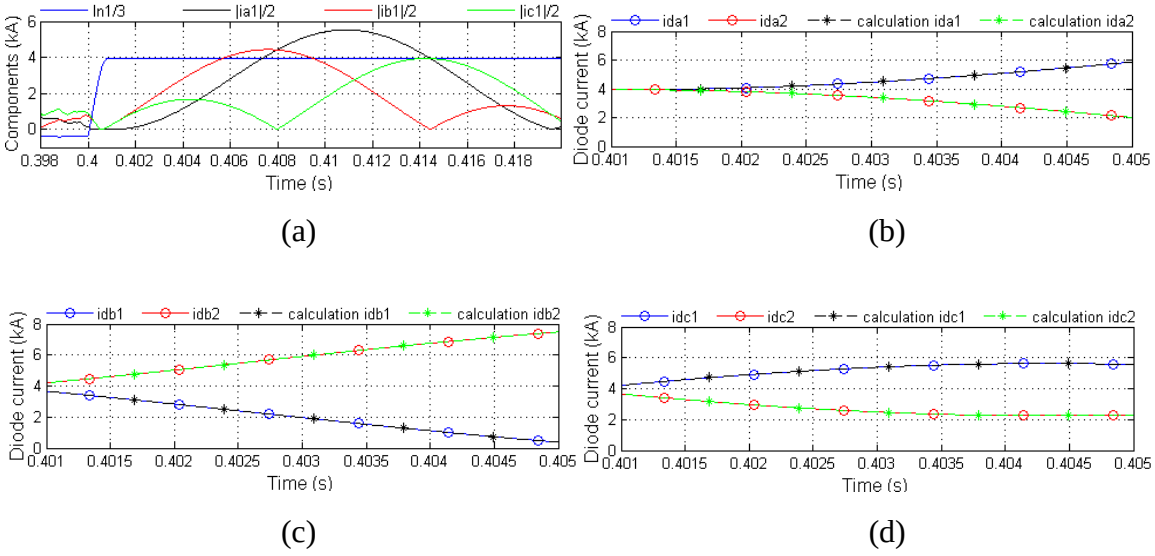

Fig. 5.17. (a) Current components under l_n as 0 km. (b) Diode current i_{da1} and i_{da2} under l_n as 0 km. (c) Diode current i_{db1} and i_{db2} under l_n as 0 km. (d) Diode current i_{dc1} and i_{dc2} under l_n as 0 km.

5.4.3 Protection Inductor for Offshore Converter

Similar to the onshore converter, an inductor L_{pf} is designed and installed at the terminal of the offshore converter as shown in Fig. 5.19, which is used to prevent overcurrent and protect the diodes in the offshore converters.

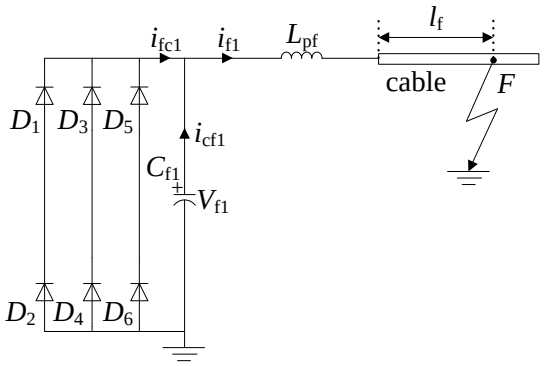

Fig. 5.18. Protection design for the offshore converter.

Suppose that the fault distance l_f is 0, the current i_{cf1} as shown in Fig. 5.18 can be expressed as

$$i_{cf1}(t) = \sqrt{V_{f10}^2 \frac{C_{f1}}{L_{pf}} + I_{f10}^2} \sin\left(\sqrt{\frac{1}{L_{pf} C_{f1}}} t + tg^{-1} \frac{I_{f10}}{V_{f10}} \sqrt{\frac{L_{fp}}{C_{f1}}}\right) \tag{5-14}$$

The POFC is supposed to be operated with the rated power of 200 MW, the cable initial current I_{f10} is the rated value as 1.33 kA. Because of the voltage variation in the transmission system, the capacitor initial voltage V_{f10} is set with 1.1 margin as $1.1 \times (V_{n1} + P_{rated} \div V_{n1} \times R_c \times L_{cable}) = 167.2$ kV. According to (5-14), Fig. 5.19 shows the possible maximum capacitor discharge current values under different protective inductance. In Fig. 5.19, the bigger of the selected protective inductance value, the smaller of the possible maximum capacitor discharge current, and the diode freewheel current can be limited in a small range.

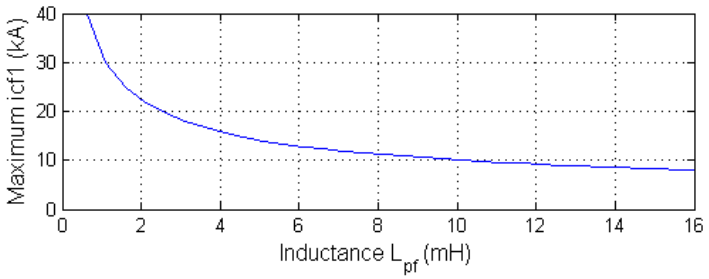

Fig. 5.19 The possible maximum value for capacitor C_{f1} discharge current i_{cf1} under different inductance $L_{pf.}$

In order to limit the capacitor discharge current and diode current, the offshore protective inductor L_{pf} can be designed. According to (5-14), the L_{pf} is selected as 6.5 mH, which can limit the maximum capacitor discharge current approximately to 12.4 kA as shown in Fig. 5.19, and the possible maximum diode current is approximately 4.1 kA. As a consequence, the capacity for the offshore diodes can be designed as 4.5 kA with a margin of 1.1.

5.4.4 Dynamic Performance of Offshore Converter under Protection

Fig. 5.20~Fig. 5.23 show the offshore converter performance, where the 6.5 mH protective inductor is equipped at the offshore converter. The positive pole cable-to-ground fault happened at 0.4 s. The different fault distances such as 0 km, 0.1 km, 1 km and 10 km are conducted.

With the protective inductor, the maximum capacitor discharge current i_{cf1} and cable

current i_{f1} is effectively limited. The maximum cable current is approximately 11.2 kA under l_f = 0 km as shown in Fig. 5.20(c). As a consequence, the diode currents under different fault distances are also decreased, which is within the offshore diode capacity selected before. Therefore, the offshore converter can be protected.

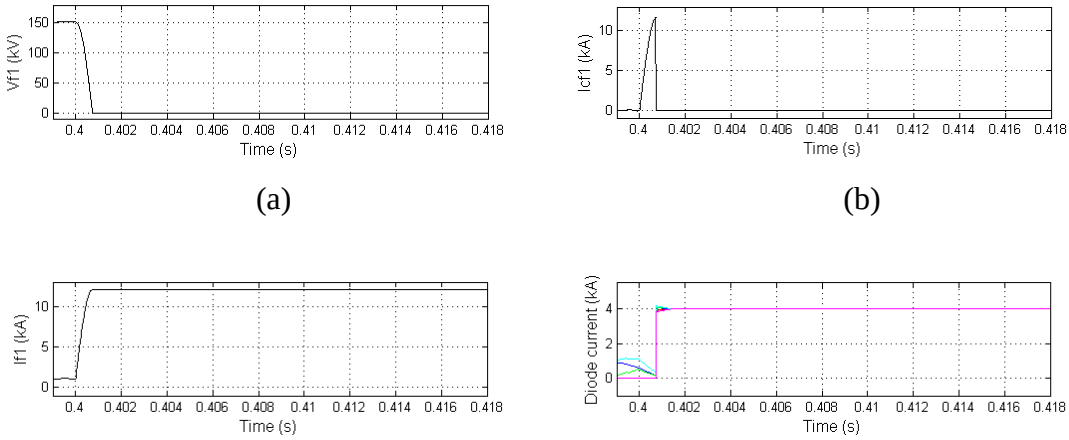

Fig. 5.20. Offshore converter performance under the fault distances l_f as 0 km. (a) Voltage V_{f1}. (b) Capacitor discharge current i_{cf1}. (c) Cable current i_{f1}. (d) Diode current.

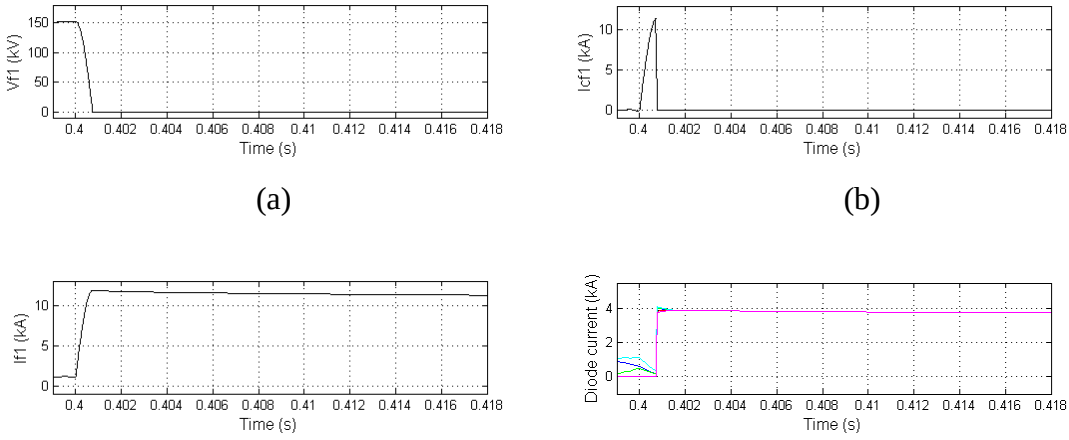

Fig. 5.21. Offshore converter performance under the fault distances l_f as 0.1 km. (a) Voltage V_{f1}. (b) Capacitor discharge current i_{cf1}. (c) Cable current i_{f1}. (d) Diode current.

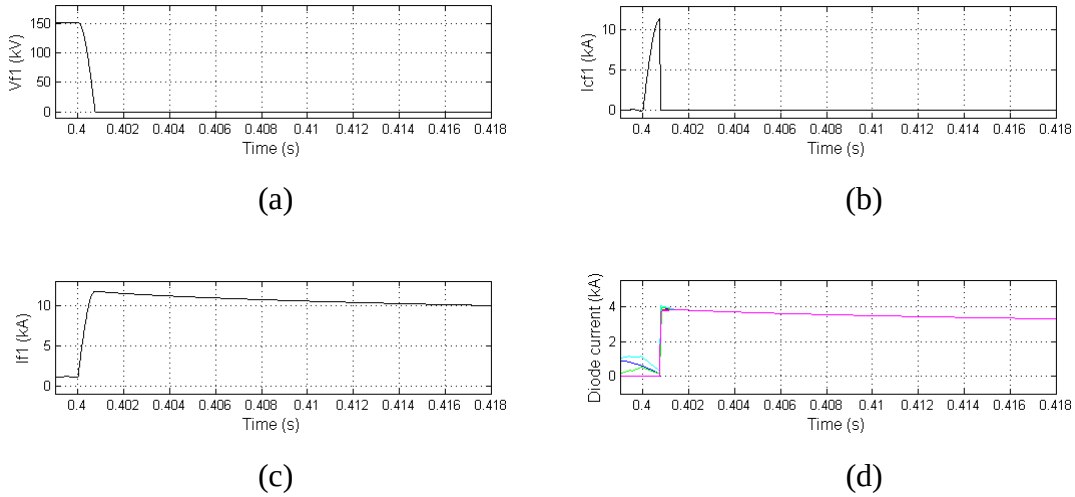

Fig. 5.22. Offshore converter performance under the fault distances l_f as 1 km. (a) Voltage V_{f1}. (b) Capacitor discharge current i_{cf1}. (c) Cable current i_{f1}. (d) Diode current.

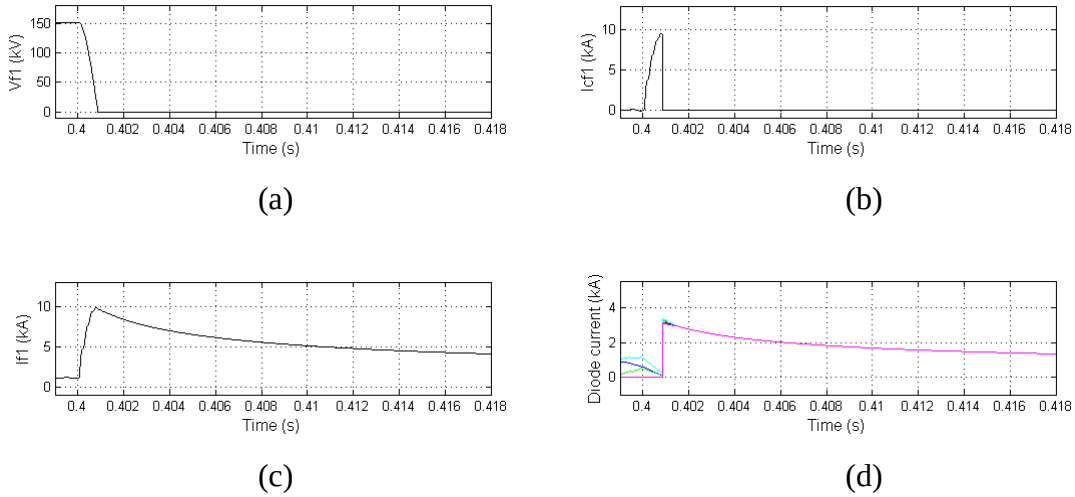

Fig. 5.23. Offshore converter performance under the fault distances l_f as 10 km. (a) Voltage V_{f1}. (b) Capacitor discharge current i_{cf1}. (c) Cable current i_{f1}. (d) Diode current.

5.5 Redundancy of HVDC System

In order to enhance the system reliability, the redundancy of the HVDC transmission system under DC cable faults is an important issue, which can be realized by operating the switches (DC switches S1-S12 and the AC circuit breakers CB1 and CB2), the chopper resistors as shown in Fig. 5.24, and the corresponding control. In the normal situation, the DC switches S1-S12, AC circuit breakers CB1 and CB2 are all closed so as to ensure the normal operation of the system.

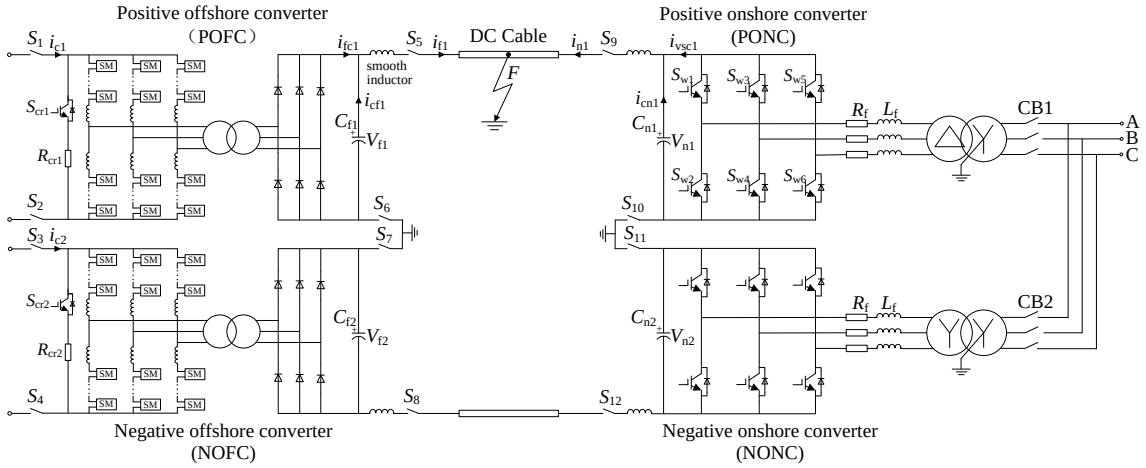

Fig. 5.24. Block diagram of the HVDC transmission system with detailed switchgears in DC grid.

5.5.1 Onshore Converter Operation

Fig. 5.25 shows the operations for the onshore station. When the cable current i_{n1} is increased under faults, all the IGBTs of the PONC may be blocked for protection purpose at t_{n1}. At the same time, the CB1 is opened, which can interrupt the AC current after a short interval at t_{n2} [72]. As a consequence, the i_{n1} is reduced to 0 at t_{n3}. And then, the S9 and S10 are opened to isolate the faulted cable.

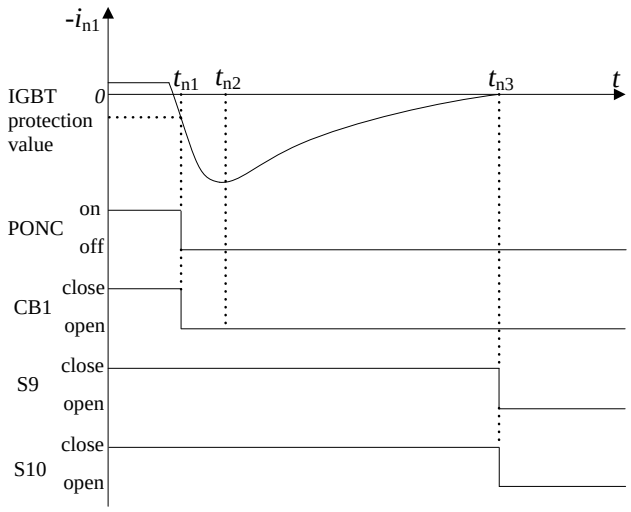

Fig. 5.25. DC transmission link fault current (onshore converter side) and components' operation sequence of the onshore station.

5.5.2 Offshore Converter Operation

The offshore station operations are shown in Fig. 5.26. Once the cable current i_{f1} is measured over IGBT protection value under faults, all the IGBTs of the POFC are blocked at t_{f1}, which prevents the corresponding wind farm power from flowing into the DC transmission link. When the i_{f1} is reduced to 0 at t_{f2}, the switches S5 and S6 are opened to isolate the faulted positive pole cable. On the other hand, the POFC will be isolated by the switches S1 and S2 when the current i_{c1} is reduced to 0.

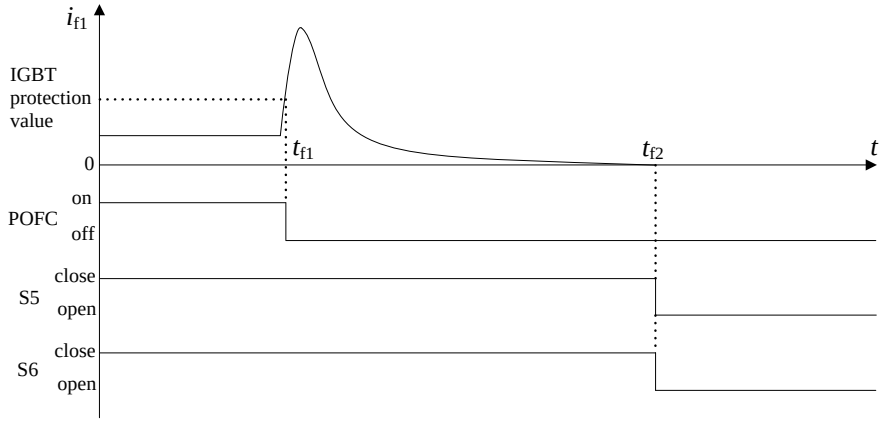

Fig. 5.26. DC transmission link fault current (onshore converter side) and components' operation sequence of the onshore station.

5.6 Fault Ride-Through Control for HVDC System

The DC cable short-circuit fault is one of the most serious disturbances of the HVDC transmission system, which may paralyze the DC grid. Therefore, the DC grid must have the capability of the fault ride-through under the DC cable fault. To date, only a few literatures report the DC cable faults in the DC grid. The basic control and design of the DC grid for offshore wind farms are presented in [10], where the different DC wind farm topologies are compared and the corresponding control is introduced. The handshaking method is proposed in [30], which can locate and isolate the faulted DC line and restore the DC system without telecommunication. The protection for the low voltage DC system is discussed in [29], where the modern voltage-source converters are considered as fast-acting current-limiting circuit breakers. The fault characteristic for the DC grid is analyzed and some possible protection methods are given in [26]. A DC overvoltage control during loss of converter in the multi-terminal VSC-HVDC system is presented in [31]. However, the fault ride-through issue in the DC grid for offshore wind farms under a DC transmission cable fault has not been mentioned in relevant grid codes and literatures.

The fault ride-through control strategy in the DC grid for offshore wind farms is considered here, which contains the onshore converter control, offshore converter control, chopper resistor control, and the wind turbine control. The proposed fault ride-through control can ensure the normal operation of the DC grid and send as much as possible power to the grid under DC cable faults.

5.6.1 Onshore Converter Control

The onshore converters are used to keep the transmission level voltage constant, whose control has been introduced in Chapter 4 and is not described in detail here. In normal situation, the DC-link voltage V_{n1} and V_{n2} are regulated by the PONC and NONC to be constant, respectively. The reactive power is controlled to be zero which means a unity power factor. During the positive-pole cable fault, the NONC still keeps the DC-link voltage V_{n2} constant, while all the IGBTs of the PONC are blocked from t_{n1} as shown in Fig. 5.25.

5.6.2 Offshore Converter Control

The NOFC is used to keep the collection level voltage V_{MV} constant, and the POFC would track the NOFC power, whose control has been presented in Chapter 4 in detail.

When the positive-pole cable-to-ground fault happened, all the IGBTs of the POFC are blocked at t_{f1} as shown in Fig. 5.26, so as to prevent the wind farm power from flowing to the faulted cable. As a consequence, only the NOFC is operated to keep the HVDC system operation.

5.6.3 Chopper Resistor Control

If the IGBTs of the POFC are switched off at t_{f1} as shown in Fig. 5.26 under faults, the wind farm power will be sent to the grid only with the NOFC. In this situation, when the wind farm power is less than the capacity of the NOFC, the collection level voltage V_{MV} can be kept constant without overvoltage when the fault happened. On the contrary, if the wind farm power is more than the capacity of the NOFC, the collection level voltage V_{MV} cannot be controlled. Here, the voltage V_{MV} may be increased under faults, and the overvoltage may be caused in the collection level when the fault happened.

The chopper resistor is equipped at the NOFC as shown in Fig. 5.24 to avoid the overvoltage at the collection system. The control for the chopper resistor system is shown in Fig. 5.27. If the V_{MV} is out of control and increased over the limit value V_{MV_lim}, set as 1.1 p.u., the chopper resistor system will cost some power and ensure the voltage V_{MV} no more than the V_{MV_lim}.

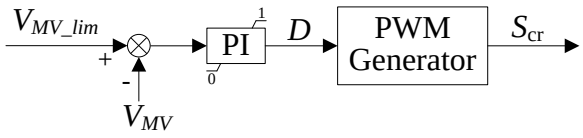

Fig. 5.27. Control for the chopper resistor.

5.6.4 Wind Turbine Control

Wind turbine control is an important issue for the fault ride-through. The grid-side converter of the wind turbine is used to keep the DC-link voltage V_{LV} constant, which has been introduced in Chapter 3. The generator-side converter control under faults is shown in Fig. 5.28(a), which is based on the dynamic model of the PMSG in the synchronous rotating frame, with the *d*-axis being aligned with the rotor flux. The reactive power reference is set to zero to perform unity power factor operation.

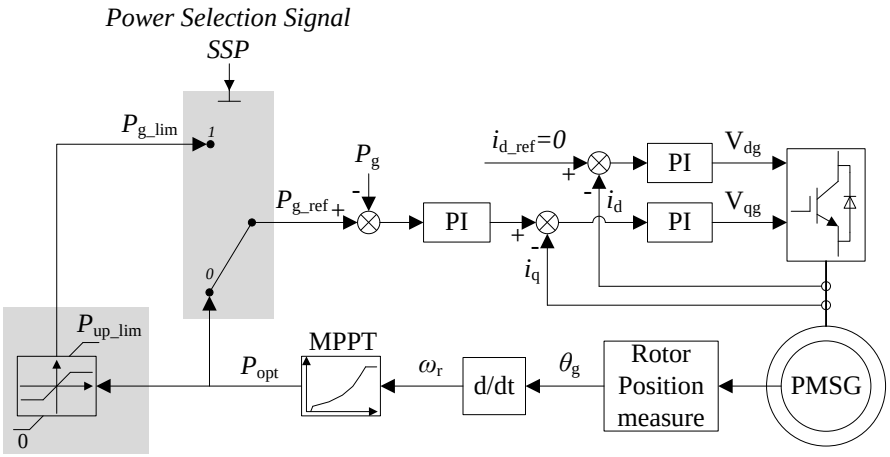

(a)

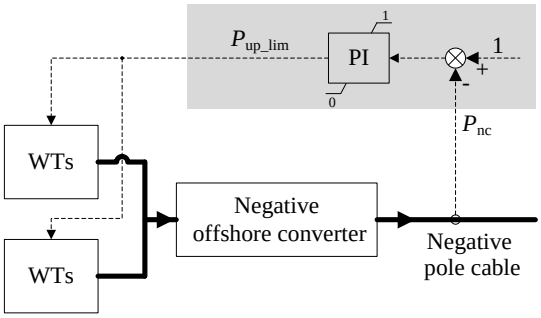

(b)

Fig. 5.28. (b) Control for the generator. (c) Centralized power control for the offshore wind farm.

Before t_{f1} in Fig. 5.26, the generator power control selection signal *SSP* is switched to 0 as shown in Fig. 5.28(a), where the wind turbine captures its optimal power P_{opt} based on the maximum power point tracking (MPPT) method [36].

From t_{f1} in Fig. 5.26, the selection signal *SSP* is switched to 1. A limiter is inserted into the generator controller as shown in Fig. 5.28(a). The assignment of the upper limit P_{up_lim} is accomplished by a centralized control as shown in Fig. 5.28(b), where the negative pole cable power is P_{nc} p.u.. If P_{nc} is less then 1 p.u., the centralized power controller will increase P_{up_lim} to increase the wind farm power. In contrast, if P_{nc} is more then 1 p.u., the centralized power controller will reduce P_{up_lim} to reduce the wind farm power. Through the centralized power control, the power P_{nc} can be sent to the onshore as much as possible within the cable's capacity and the converter's capacity. The offshore

wind farm performance may be described with the following two situations.

1) $P_{nc} = 1$ *under condition* $\sum P_{opt\_i} \geq 1$

When the summation of each wind turbine optimal power P_{opt_i} in the wind farm is more than or equal to the negative pole cable's capacity of 1 p.u., the centralized controller will regulate P_{up_lim} to limit the power reference for the wind turbines, so as to make the P_{nc} equal to the cable's capacity.

As to some wind turbine, if the P_{up_lim} is more than its P_{opt_i}, the wind turbine is operated to track the optimal power with $P_g = P_{opt\_i} < P_{up\_lim}$. If the P_{up_lim} is less than or equal to its P_{opt_i}, the P_g will follow P_{up_lim} with $P_g = P_{up\_lim} \leq P_{opt\_i}$.

2) $P_{nc} = \sum P_{opt\_i}$ *under condition* $\sum P_{opt\_i} < 1$

If the summation $\sum P_{opt\_i}$ of each wind turbine optimal power is less than 1, each wind turbine would be controlled to follow its optimal power P_{opt_i} by the centralized power controller. Hence, the power P_{nc} is equal to $\sum P_{opt\_i}$.

5.7 System Performance under HVDC System Faults

The DC grid for offshore wind farms, as shown in Fig. 4.6, has been modeled using the simulation tool PSCAD/EMTDC. The positive pole cable-to-ground fault occurs at 10 s, at 10 km away from the offshore station. The fault resistance is small and considered as zero. The wind farm power is approximately 0.52 p.u. at the beginning of the fault. The presented redundancy and the proposed control strategy are applied to the DC grid and tested by simulation results.

Fig. 5.29 shows the simulation results. The variable wind speeds as shown in Fig. 5.29(a) are used to evaluate the performance of the DC grid. Owing to the fault at 10 s, the offshore converter voltage V_{f1} and the onshore converter voltage V_{n1} are reduced to zero as shown in Figs. 5.29(g) and (i), and the huge cable current i_{f1} and i_{n1} are caused. During the faults, the IGBTs at the POFC are blocked, which results in that the cable current i_{f1} and i_{n1} are reduced to zero as shown in Figs. 5. 29(h) and (j). And then the fault cable is isolated by the switches S5 and S9. As a consequence, the POFC power and PONC power are reduced to zero under faults as shown in Figs. 5.29(k) and (l).

When the fault happened at 10 s, a communication delay about 20 ms is set for the wind turbines to get the signal to be operated with the proposed control under faults. At this time, the wind farm power may be more than the NOFC capacity. Hence, the more energy will be stored at the collection, which would increase the collection level voltage. Based on the chopper resistor control before, if the collection voltage is over 1.1 p.u., the

chopper resistor will work to limit the collection level voltage as shown in Fig. 5.29(f).

After the wind turbines are controlled with the proposed control as shown in Fig. 5.28, the wind turbines power would be reduced to decrease the wind farm power as shown in Fig. 5.29(d). The reduction of the wind turbines power results in that the wind turbines speeds are increased as shown in Fig. 5.29(b). Because the wind turbine speeds are not over the rated value, the pitch angles are still zero as shown in Fig. 5.29(c).

In the proposed wind turbine control under faults as shown in Fig. 5.28, the upper limit P_{up_lim} is regulated by the central controller and sent to each wind turbine in the offshore wind farm, so that the wind farm can produce the power as much as possible but no more than the cable and converter's capacity. Consequently, the P_{off2} is quickly regulated to 0.5 p.u. as shown in Fig. 5.29(k).

In Fig. 5.29(d), between 10 s and 16.1 s, the P_{opt1} is less than P_{up_lim}, the P_{opt2}, P_{opt3}, and P_{opt4} are more than P_{up_lim}, which makes WT 1 follow its optimal power and WTs 2~3 follow the P_{up_lim} so as to keep the P_{off} as 0.5 p.u.. From 16.1 s to 17 s, P_{opt1} ~ P_{opt4} are all more than P_{up_lim}, and all the wind turbines follow the P_{up_lim} to make the P_{off} as 0.5 p.u.. From 17 s, the P_{opt1} is less than P_{up_lim}. Here, the WT 1 tracks the P_{opt1}, and the P_{up_lim} is increased to make the other three wind turbines produce more power to keep the P_{off} as 0.5 p. u.. After 19.4 s, P_{opt2} is also less than P_{up_lim}, and the WT 2 follows the P_{opt3}. In order to produce more power, the P_{up_lim} is re-set by the central controller. Hence, more power is produced by the WT 3 and WT 4. From 20.3 s, the P_{opt3} is less than P_{up_lim} as well. Only WT 4 is left to follow the increased P_{up_lim} so as to produce more power. At 25.9 s, when the four wind turbines' optimal power are all less than P_{up_lim}, all the wind turbines follow their optimal power, the offshore wind farm power production becomes less than 0.5 p.u. as shown in Fig. 5.29(k). The onshore converters power is shown in Fig. 5.29(l), where the negative onshore converter receives all the wind farm power via the negative pole cable.

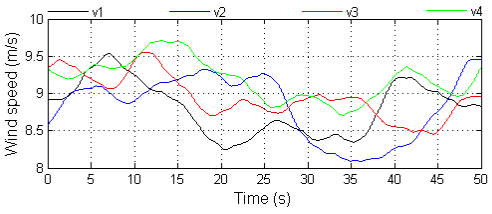

(a)

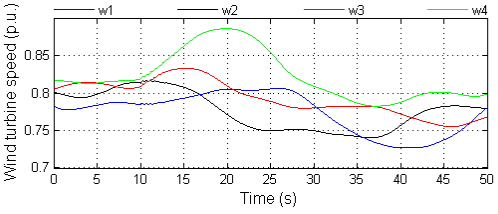

(b)

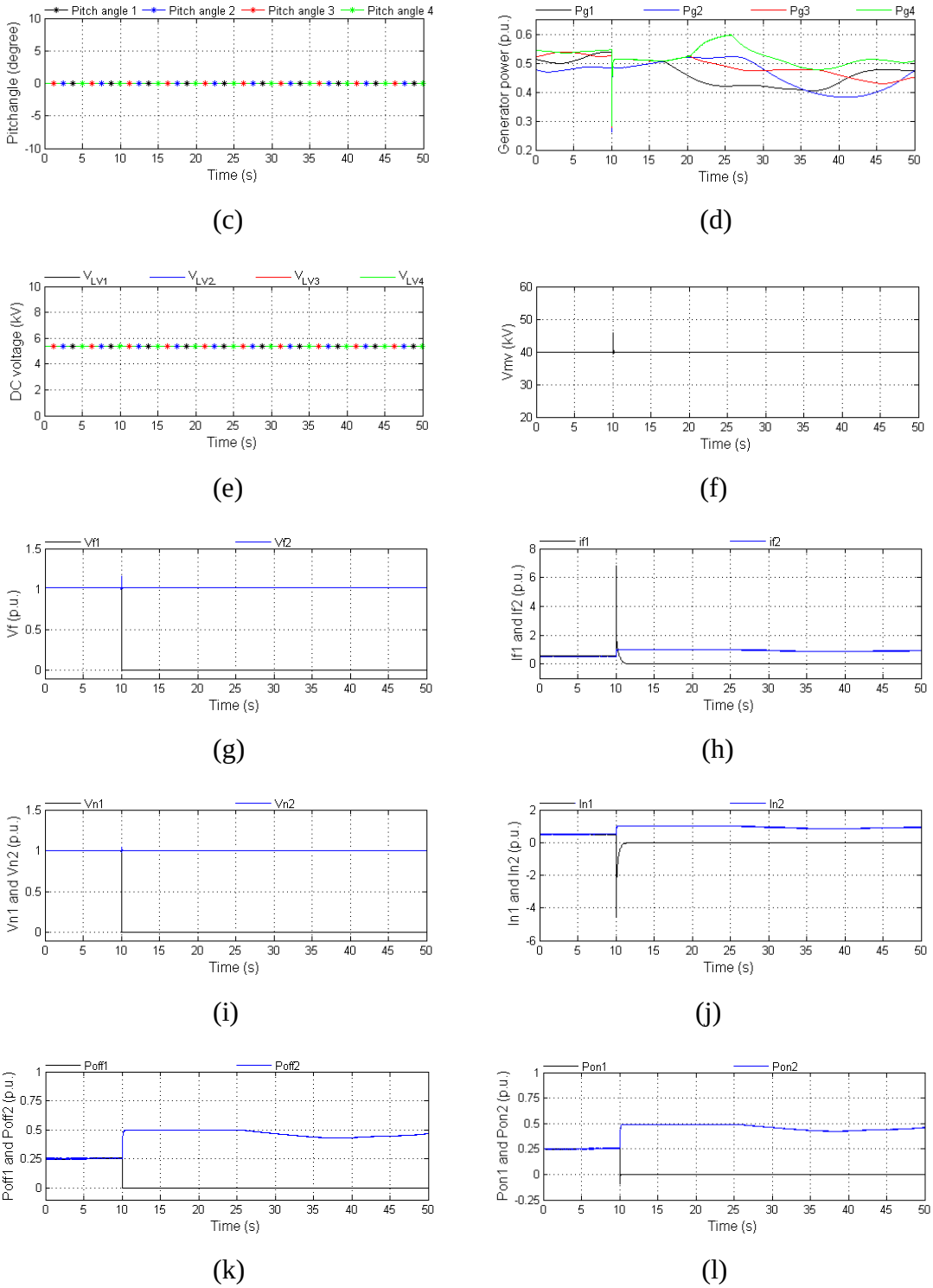

Fig. 5.29. (a) Wind speed. (b) Wind turbine speed. (c) Pitch angle. (d) Generator power P_{g1}, P_{g2}, P_{g3}, P_{g4}. (e) Voltage V_{LV1}, V_{LV2}, V_{LV3} and V_{LV4} in the wind turbines. (f) Collection level voltage V_{MV}. (g) Voltage V_{f1} and V_{f2}. (h) Cable current i_{f1} and i_{f2}. (i) Voltage V_{n1} and V_{n2}. (j) Cable current i_{n1} and i_{n2}. (k) Offshore converters power P_{off1} and P_{off2}. (l) Onshore converters power P_{on1} and P_{on2}.

Fig. 5.30 shows the other simulation results with the high wind speeds, as shown in Fig. 5.30(a). The DC-link voltage V_{f1} and V_{n1}, the cable current i_{f1} and i_{n1}, and the power P_{off1} and P_{on1} are reduced to zero under faults as shown in Figs. 5.30(g)~(i). Owing to the optimal powers of the WT 1~4 are more than the upper limit P_{up_lim}, the WT 1~4 are operated with the P_{up_lim}, as shown in Fig. 5.30(d), which ensures the wind farm power as much as possible, as shown in Fig. 5.30(k). The wind turbine speeds are suddenly increased when the fault happened as shown in Fig. 5.30(b) because of the reduction of the wind turbine power. The action of the pitch angle control, as shown in Fig. 5.30(c), limits the wind turbine speed. The DC-link voltage in the wind turbines are shown in Fig. 5.30(e). There is a fluctuation at the collection level voltage under faults as shown in Fig. 5.30(f).

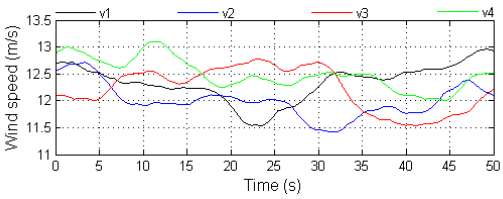

(a)

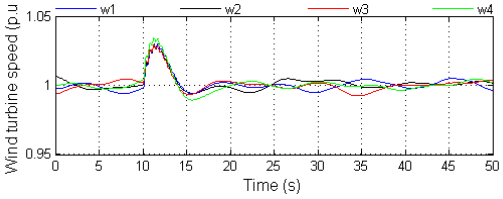

(b)

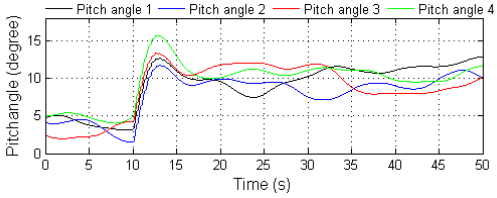

(c)

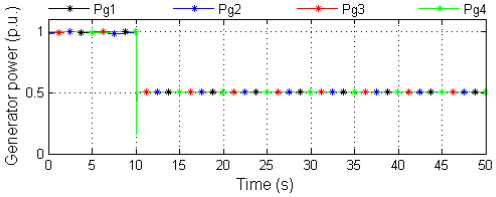

(d)

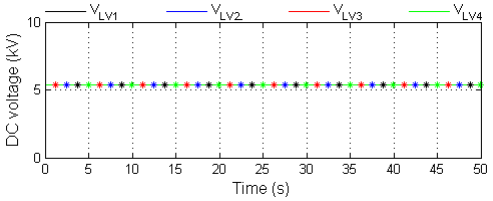

(e)

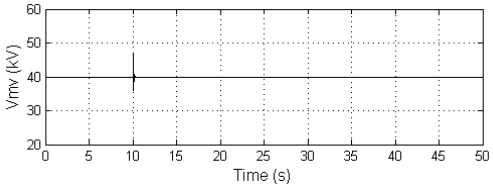

(f)

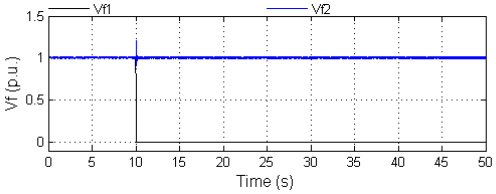

(g)

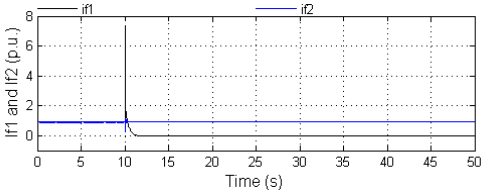

(h)

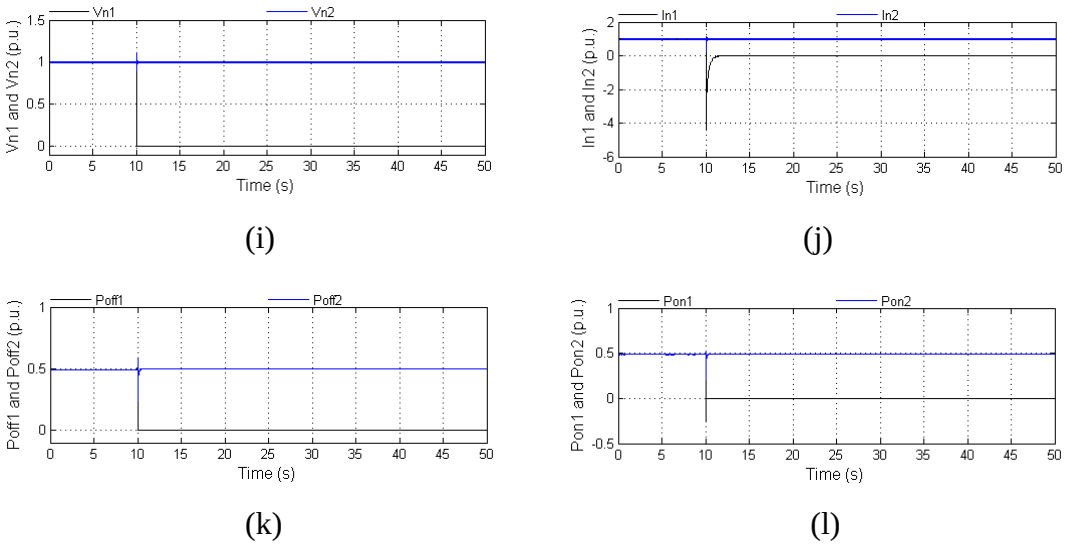

Fig. 5.30. (a) Wind speed. (b) Wind turbine speed. (c) Pitch angle. (d) Generator power P_{g1}, P_{g2}, P_{g3}, P_{g4}. (e) Voltage V_{LV1}, V_{LV2}, V_{LV3} and V_{LV4} in the wind turbines. (f) Collection level voltage V_{MV}. (g) Voltage V_{f1} and V_{f2}. (h) Cable current i_{f1} and i_{f2}. (i) Voltage V_{n1} and V_{n2}. (j) Cable current i_{n1} and i_{n2}. (k) Offshore converters power P_{off1} and P_{off2}. (l) Onshore converters power P_{on1} and P_{on2}.

5.8 Summary

In this chapter, the fault analysis and protection design for the HVDC transmission system under DC cable faults are presented. The transient characteristic of the HVDC system under cable-to-ground fault is analyzed in detail. A huge current may be caused at the onshore and offshore converters during the fault, which may damage the diodes in the converters. The protective inductor is presented and designed for the onshore and offshore converter, which can effectively limit the capacitor discharge current and cable current, therefore, the diode current can also be limited in a small range. The capacity of the diodes in the onshore and offshore converter can also be determined based on the designed protective inductors, which is enough to tolerate the current under faults. On the other hand, the redundancy of the system under HVDC transmission system faults is presented as well, which can be realized with the corresponding switchgears and the control including onshore converter control, offshore converter control, chopper resistor control, and the wind turbine control. With the presented fault ride-through control, the wind farm power can still be sent to the grid as much as possible so as to increase the system efficiency.

Chapter 6

Conclusion

6.1 Summary

In this thesis, a DC grid for offshore wind farms is investigated with focus on the design and control. The DC grid for offshore wind farms is different from the existing offshore wind farm. In the DC grid, the wind turbine output is DC not AC, and the wind turbine can be directly integrated into the DC collection system. Besides, the offshore converter in the DC grid is a DC/DC converter to step up the collection level DC voltage to the transmission level DC voltage. Owing to the mature technology for the wind farm with AC grid, the DC grid structure for the offshore wind farm is similar to the wind farm structure with AC grid. The wind turbines in the offshore wind farm are connected with a few clusters in the DC distribution system. And then, these clusters are collected at the offshore station and the DC level is stepped up by the offshore converter to the transmission level. Through the HVDC transmission link, the offshore wind farm power is sent to the onshore, and integrated into the grid. To implement the DC grid for the offshore wind farm, a few issues should be considered including wind turbine and HVDC transmission system. Especially, the DC/DC converter for the wind turbine and the offshore converters are identified as key components.

An IFBTL isolated DC/DC converter is presented for the wind turbine in the DC grid with the advantages in the aspects of power quality, and EMI for high power applications. In the three-level configuration, the switches in the converter only take half of the DC bus voltage, which effectively reduces the dv/dt. A passive filter is inserted into the IFBTL DC/DC, and improves the performance of the DC/DC converter. As a consequence, the problem caused by the non-linear characteristics of semiconductor devices can be overcome by the IFBTL DC/DC converter. In addition, the harmonics and the voltage

stress of the MFT is reduced, which is very significant for the power converter in the high-power application.

Two types wind turbine configurations are presented. One is with the three-level NPC converter as the generator-side converter and the IFBTL DC/DC converter as the grid-side converter, where the generator is controlled by the three-level NPC converter for the optimal power track, and the DC-link voltage in the wind turbine is kept by the IFBTL DC/DC converter. The other one is with the uncontrollable diode rectifier as the generator-side converter for AC/DC conversion, and the IFBTL DC/DC converter as the grid side converter, where the generator is regulated by the IFBTL DC/DC converter for the optimal power track.

A HVDC transmission system is presented for the DC grid, where the offshore converter is used for DC/DC conversion. In the HVDC transmission system, the MMC is used for the onshore converter with the features of modularity and scalability. Especially, the high number of levels in the MMC enables a great reduction in the device average switching frequency without compromise of power quality. Furthermore, an inductor is in series with the distributed energy storage capacitors in each arm to reduce the damage under faults. The corresponding modulation and control for the onshore converter is presented. A DC/DC converter based on MMC is also presented for the offshore converter, which is composed with a three-level MMC, medium frequency transformer, and diode rectifier. The corresponding control for the offshore converter is also introduced.

The performance of the DC grid under AC grid faults is presented. During the AC grid voltage dip, the overvoltage situation may occur at the HVDC transmission system with the normal control of the DC grid, which may damage the DC grid. A fault ride-through control is introduced for the DC grid, where the normal control in the DC grid for wind turbine and HVDC transmission system is improved. With the presented fault ride-through control, the possible overvoltage situation at the DC grid is avoided, and the redundant power in the wind farm will be stored in the wind turbine mechanical system. As a consequence, the wind turbine speed will be increased. Owing to the big inertia of the wind turbine and the pitch angle control system, the wind turbine speed can be effectively limited.

The DC cable fault in the HVDC transmission system is harmful for the DC grid, which may damage the system. The performance of the DC grid under DC cable faults is studied and analyzed, where a few fault distances are conducted. During the fault, a huge current may be caused, which may flow through the diodes in the onshore and offshore converters and damage the converters. In order to protect the system under faults, the protective inductor is presented and designed, which can limit the cable current and

protect the onshore and offshore converters under faults. Moreover, the redundancy of the HVDC transmission system under faults is presented. Under the action of the switchgears, the faults parts of the HVDC transmission system can be isolated, and the HVDC transmission system can be still operated with the healthy converters and cable. The control of the DC grid under HVDC transmission system faults is proposed. The healthy onshore converter still keeps the transmission level voltage constant, and the healthy offshore converter keeps the collection level voltage constant under faults. A chopper resistor system at the offshore converter may be active to cost the more power at the collection level and limit the collection level voltage. During the fault, the control for the wind turbines will be changed, where a power limiter will be inserted into the controller. A centralized power limit value will be regulated and sent to each wind turbine based on the HVDC transmission system power. With the proposed fault ride-through control for the HVDC transmission system, the wind farm power can be sent to the on land as much as possible under faults, which can effectively improve the system efficiency.

6.2 Proposals for Future Work

As to the DC grid for offshore wind farms, the layout of the wind farm with DC grid is very important. The layout of the wind farm and the collection level voltage value are related to the system cost and loss, which needs further investigation.

For the DC/DC converter in the wind turbine, the modular multilevel technology may be used for the DC/DC converter so as to improve the power quality and increase the converter efficiency, which is very important. In addition, the possible voltage fluctuation at the DC-link of the wind turbine may affect the wind turbine operation under system faults. In order to effectively keep the DC-link voltage, even under the grid faults, the DC/DC converter associated with its control must be investigated further and limit the DC-link voltage fluctuation under faults.

For the DC/DC converter at the offshore station, the frequency of the transformer and the modulation strategy for the DC/DC converter may be researched. A further study may be needed to improve the converter performance and control, so as to enhance the HVDC system reliability.

The HVDC transmission system fault is considered, and the corresponding protection method, redundancy, and the operation and control of the DC grid under faults is presented. The fault located at the DC collection level and the wind turbine system may

be focused in future. The performance of the DC grid under collection system faults and wind turbine faults may be studied and analyzed. And then, the corresponding protection, redundancy, and control strategy may be studied so as to improve the system performance.

In case of super DC grid system, the system layout, the converter characteristic, the DC grid performances under faults, and the system protection may be needed to be studied, as well as the DC grid protection and operation under faults. In addition, the interaction between the DC grid and the power system is very important and worth researching in future.

References

[1] Z. Chen, Y. Hu and F. Blaabjerg, "Stability improvement of induction generator-based wind turbine systems," *Renewable Power Generation, IET*. Vol. 1, pp.81-93, March 2007.

[2] R. Li, S. Bozhko, and G. Asher, "Frequency control design for offshore wind farm grid with LCC-HVDC link connection," *IEEE Transaction on Power Electronics*, vol. 23, no. 3, pp. 1085-1092, May 2008.

[3] P. Bresesti, W. L. Kling, R. L. Hendriks, and R. Vailati, "HVDC connection of offshore wind to the transmission system," *IEEE Transactions on Energy Conversion*, vol. 22, no. 1, pp. 37-43, March 2007.

[4] Y. K. Wu, C. Y. Lee, and G. H. Shu, "Taiwan's first large-scale offshore wind farm connection-A real project case study with a comparison of wind turbine," *IEEE Transactions on Industry Applications*, vol. 47, no. 3, pp. 1461-1469, May/June 2011.

[5] N. Flourentzou, V. G, Agelidis, and G. D. Demetriades, "VSC-Based HVDC power transmission systems: an overview," *IEEE Transactions on Power Electronics*, vol. 24, no. 3, pp. 592-602, March 2009.

[6] C. Du, E. Agneholm, and G. Olsson, "Comparison of different frequency controllers for a VSC-HVDC supplied system," *IEEE Transactions on Power Delivery*, vol. 23, no. 4, pp. 2224-2232, Oct. 2008.

[7] C. Feltes, H. Wrede, F. W. Koch, and I. Erlich, "Enhanced fault ride-through method for wind farms connected to the grid through VSC-based HVDC transmission," *IEEE Transactions on Power System*, vol. 24, no. 3, pp. 1537-1546, August 2009.

[8] O. Gomis-Bellmunt, A. Junyent-Ferre, A. Sumper, and J. Bergas-Jane, "Control of a wind farm based on synchronous generators with a central HVDC-VSC converter," *IEEE Transactions on Power System*, vol. 26, no. 3, pp. 1632-1640, August 2011.

[9] F. Mura, C. Meyer, and R. W. De Doncker, "Stability analysis of high power DC grids," *IEEE Transactions on Industry Applications*, vol. 46, no. 2, pp. 584-592, Mar./Apr. 2010.

[10] C. Meyer, M. Hoing, A. Peterson, and R. W. De Doncker, "Control and design of DC grids for offshore wind farms," *IEEE Transactions on Industry Applications*, vol. 43, no. 6, pp. 1475-1482, Nov./Dec. 2007.

[11] J. Robinson, D. Jovcic, and G. Joós, "Analysis and design of an offshore wind farm using a MV DC grid," *IEEE Transactions on Power Delivery*, vol. 25, no. 4, pp. 2164-2173, Oct. 2010.

[12] W. Lu and B. T. Ooi, "Optimal acquisition and aggregation of offshore wind power by multiterminal voltage-source HVDC," *IEEE Transactions on Power Delivery*, vol. 18, no. 1, pp. 201-206, January 2003.

[13] D. Jovcic and B. T. Ooi, "Developing DC transmission networks using DC transformers," *IEEE Transactions on Power Delivery*, vol. 25, no. 4, pp. 2535-2543, October 2010.

[14] S. Lundberg, "Performance comparison of wind park configurations," Ph.D. dissertation, Chalmers Univ. Technol., Göteborg, Sweden, 2003.

[15] L. Max, "Energy evaluation for DC/DC converters in DC-based wind farms," Ph.D. dissertation, Chalmers Univ. Technol., Göteborg, Sweden, 2007.

[16] M. Tsili and S. Papathanassiou, "A review of grid code technical requirements for wind farms," *IET on Renewable Power Generation*, vol. 3, no. 3, pp. 308-332, September 2009.

[17] G. Ramtharan, A. Arulampalam, J. B. Ekanayake, F. M. Hughes, and N. Jenkins, "Fault ride through of fully rated converter wind turbines with AC and DC transmission," *IET on Renewable Power Generation*, vol. 3, no. 4, pp. 426-438, December 2009.

[18] C. Rahmann, H. -J. Haubrich, A. Moser, R. Palma-Behnke, and L. Vargas, "Justified fault-ride-through requirements for wind turbines in power systems," *IEEE Transactions on Power System*, vol. 26, no. 3, pp. 1555-1563, August 2011.

[19] D. Xiang, R. Li, P. J. Tavner, and S. Yang, "Control of a doubly fed induction generator in a wind turbine during grid fault ride-through," *IEEE Transactions on Energy Conversion*, vol. 21, no. 3, pp. 652-662, September 2006.

[20] C. Wessels, F. Gebhardt, and F. W. Fuchs, "Fault ride-through of a DFIG wind turbine using a dynamic voltage restorer during symmetrical and asymmetrical grid faults," *IEEE Transactions on Power Electronics*, vol. 26, no. 3, pp.807-815, March 2011.

[21] J. Robinson, D. Jovcic, and G. Joós, "Analysis and design of an offshore wind farm using a MV DC grid," *IEEE Transactions on Power Delivery*, vol. 25, no. 4, pp. 2164-2173, Oct. 2010.

[22] S. P. Engel, N. Soltau, H. Stagge, and R. W. De Doncker, "Dynamic and balanced control of three-phase high-power dual-active bridge DC-DC converters in DC-grid applications*," IEEE Transactions on Power Electronics*, Accepted, 2012.

[23] D. Jovcic, "Bidirectional, high-power DC transformer," *IEEE Transactions on Power Delivery*, vol. 24, no. 4, pp. 2276-2283, October 2009.

[24] S. Lundberg, "Wind farm configuration and energy efficiency studies-series DC versus AC layouts," Ph.D. dissertation, Chalmers Univ. Technol., Göteborg, Sweden, 2006.

[25] L. Max and S. Lundberg, "System efficiency of a DC/DC converter-based wind farm," *Wind Energy*, vol. 11, no. 1, pp. 109-120, 2008.

[26] J. Yang, J. E. Fletcher, and J. O' Reilly, "Multiterminal DC wind farm collection grid internal fault analysis and protection design," *IEEE Transactions on Power Delivery*, vol. 25, no. 4, pp. 2308-2318, 2010.

[27] C. M. Franck, "HVDC circuit breakers: a review identifying future research needs," *IEEE Transactions on Power Delivery*, vol. 26, no. 2, pp. 998-1007, Apr. 2011.

[28] B. Sheng, "A synthetic test circuit for current switching tests of HVDC circuit breakers," *Transmission and Distribution Conference and Exposition*, 2008, pp. 1-4.

[29] M. E. Baran and N. R. Mahajan, "Overcurrent protection on voltage-source-converter-based multiterminal DC distribution systems," *IEEE Transactions on Power Delivery*, vol. 22, no. 1, pp. 406-412, January 2007.

[30] L. Tang and B. T. Ooi, "Locating and isolating DC faults in multi-terminal DC system," *IEEE Transactions on Power Delivery*, vol. 22, no. 3, pp. 1877-1884, July 2007.

[31] W. Lu and O. Boon-Teck, "DC overvoltage control during loss of converter in multiterminal voltage-source converter-based HVDC (M-VSC-HVDC)," *IEEE Transactions on Power Delivery*, vol. 18, no. 3, pp. 915-920, July 2003.

[32] A. Hansen and L. Hansen, "Wind turbine concept market penetration over 10 years (1995-2004)," *Wind Energy*, vol. 10, no. 1, pp. 81-97, 2007.

[33] H. Li and Z. Chen, "Overview of different wind generator systems and their comparisons," *IET on Renewable Power Generation*, vol. 2, no. 2, pp. 123-138, 2008.

[34] J. G. Slootweg, S. W. H. de Haan, H. Polinder, and W. L. Kling, "Aggregated modelling of wind parks with variable speed wind turbines in power system dynamics simulations," *in Proc. 14th Power Sys. Comp.* Conf, Sevilla, Spain, Jun 2002.

[35] S. Li, T. A. Haskew, R. P. Swatloski, and W. Gathings, "Optimal and direct-current vector control of direct-driven PMSG wind turbines," *IEEE Transactions on Power Electronics*, vol. 27, no. 5, pp.2325-2337, May 2012.

[36] Z. Chen, J. M. Guerrero, and F. Blaabjerg, "A review of the state of the art of power electronics for wind turbines," *IEEE Transactions on Power Electronics*, vol. 24, no. 8, pp. 1859-1875, August 2009.

[37] S. Zhang, T. King-Jet, D. M. Vilathgamuwa, T. D. Nguyen, and X. Wang, "Design of a robust grid interface system for PMSG-based wind turbine generators," *IEEE Transactions on Industrial Electronics*, vol. 58, no. 1, pp. 316-328, January 2011.

[38] H. Geng, D. Xu, B. Wu, and G. Yang, "Active damping for PMSG-based WECS with DC-link current estimation," *IEEE Transactions on Industrial Electronics*, vol. 58, no. 4, pp. 1110-1119, April 2011.

[39] K. Kim, Y. Jeung, D. Lee, and H. Kim, "LVRT scheme of PMSG wind power systems based on feedback linearization," *IEEE Transactions on Power Electronics*, vol. 27, no. 5, pp. 2376-2384, May 2012.

[40] Z. Chen, X. Xiao, H. Wang, and M. Liu, "Analysis of converter topological structure for direct-drive wind power system with PMSG," in *Proc. 2010 International Conference on Power System Technology*, 2010, pp. 1-5.

[41] C. Janani and K. Rajambal, "Power flow analysis of a grid connected PMSG based direct driven wind electric generator," in *Proc. 2012 International Conference on Advanced in Engineering, Science and Management*, 2012, 123-128.

[42] K. Zhao, G. Li, B. Wang, and M. Zhou, "Grid-connected topology of PMSG wind power system based on VSC-HVDC," in *Proc. 2011 4th International Conference on Electric Unility Deregulation and Restructuring and Power Technologies*, 2011, pp. 297-302.

[43] K. Tan and S. Islam, "Optimum control strategies in energy conversion of PMSG wind turbine system without mechanical sensors," *IEEE Transactions on Energy Conversion*, vol. 19, no. 2, pp. 392-399, June 2001.

[44] P. J. Grbovic, "High-voltage auxiliary power supply using series-connected MOSFETs and floating self-driving technique," *IEEE Transactions on Industrial Electronics*, vol. 56, no. 5, PP. 1446-1455, May 2009.

[45] F. Blaabjerg, F. Iov, Z. Chen, and K. Ma, "Power electronics and controls for wind

turbine systems," in *Proc. 2010 IEEE International Energy Conference and Exhibition*, pp. 333-344.

[46] F. Blaabjerg, Z. Chen, and B. S. Kjaer, "Power electronics as efficient interface in dispersed power generation systems," *IEEE Transactions on Power Electronics*, vol. 19, no. 5, pp. 1184-1194, Sep. 2004.

[47] N. Mohan, T. M. Undeland, and W. P. Robbins, *Power Electronics: Converters, Applications, and Design, 3rd Edition*. New York: Wiley, 2003.

[48] N. Y. Dai, M. C. Wong, and Y. D. Han, "Application of a three-level NPC inverter as a three-phase four-wire power quality compensator by generalized 3DSVM," *IEEE Transactions on Power Electronics*, vol. 21, no. 2, pp. 440-449, Mar. 2006.

[49] X. Ruan, B. Li, Q. Chen, S. C. Tan, and C. K. Tse, "Fundamental considerations of three-level DC-DC converters: topologies, analyses, and control," *IEEE Transactions on Circuits And Systems I: Regular Papers*, vol. 55, no. 11, pp. 3733-3743, Dec. 2008.

[50] Z. Zhang and X. Ruan, "ZVS pwm full-bridge three-level converter," in *Proc. 2004-4th International Power Electronics and Motion Control Conference (IPEMC)*, 2004, pp. 1085-1090.

[51] Z. Zhang, and X. Ruan, "A novel double phase-shift control scheme for full-bridge three-level converter," in *Proc. 2005-20th Annual IEEE Applied Power Electronics Conference and Exposition*, 2005, pp. 1240-1245.

[52] P. J. Grbovic, "High-voltage auxiliary power supply using series-connected MOSFETs and floating self-driving technique," *IEEE Transactions on Industrial Electronics*, vol. 56, no. 5, PP. 1446-1455, May 2009.

[53] P. J. Grbović, P. Delarue, P. Le Moigne, and P. Bartholomeus, "A bidirectional three-level DC-DC converter for the ultracapacitor applications," *IEEE Transactions on Industrial Electronics*, vol. 57, no. 10, pp. 3415-3430, Oct. 2010.

[54] P. M. Barbosa, F. Canales, J. M. Burdío, and F. C. Lee, "A three-level converter and its application to power factor correction*," IEEE Transactions on Power Electronics*, vol. 20, no. 6, pp. 1319-1327, Nov. 2005.

[55] J. R. Pinheiro and I. Barbi, "The three-level zvs-pwm DC-to-DC converter*," IEEE Transactions on Power Electronics*, vol. 8, no. 4, pp. 486-492, Oct. 1993.

[56] S. Inoue and H. Akagi, "A bidirectional isolated DC-DC converter as a core circuit of the next-generation medium-voltage power conversion system," *IEEE Transactions on Power Electronics*, vol. 22, no. 2, pp. 535-542, 2007.

[57] M. Malinowski, K. Gopakumar, J. Rodriguez, and M. A. Pérez, "A survey on cascaded multilevel inverters," *IEEE Transactions on Industrial Electronics*, vol. 57, no. 7, pp. 2197-2206, Jul. 2010.

[58] S. Kouro, M. Malinowski, K. Gopakumar, J. Pou, L. G. Franquelo, B. Wu, J. Rodriguez, M. A. Pére, and J. I. Leon, "Recent advances and industrial applications of multilevel converters," *IEEE Transactions on Industrial Electronics*, vol. 57, no. 8, pp. 2553-2580, Aug. 2010.

[59] J. Rodriguez, S. Bernet, B. Wu, J. O. Pontt, and S. Kouro, "Multilevel voltage-source-converter topologies for industrial medium-voltage drives," *IEEE Transactions on Industrial Electronics*, vol. 54, no. 6, pp. 2930-2945, Dec. 2007.

[60] S. Kenzelmann, A. Rufer, M. Vasiladiotis, D. Dujic, F. Canales, and Y. R. de Novaes, "A versatile DC-DC converter for energy collection and distribution using the modular multilevel converter," in *Proc. 2011-14th European Conference on Power Electronics and Applications*, pp. 1-10.

[61] M. Saeedifard and R. Iravani, "Dynamic performance of a modular multilevel back-to-back HVDC system," *IEEE Transactions on Power Delivery*, vol. 25, no. 4, pp. 2903-2912, Oct. 2010.

[62] M. A. Parker, N. Chong, and R. Li, "Fault-Tolerant control for a modular generator-converter scheme for direct-drive wind turbines," *IEEE Transactions on Industrial Electronics*, vol. 58. No. 1, pp.305-315, Jan. 2011.

[63] R. Melício, V. M. F. Mendes, and J. P. S. Catalão, "Comparative study of power converter topologies and control strategies for the harmonic performance of variable-speed wind turbine generator systems," *Energy*, vol. 36, no. 1, pp. 520-529, Jan. 2011.

[64] P. Samuel, R. Gupta, and D. Chandra, "Grid interface of wind power with large split-winding alternator using cascaded multilevel inverter," *IEEE Transactions on Energy Conversion*, vol. 26, no. 1, pp. 299-309, March 2011.

[65] Z. Chen and E. Spooner, "Grid interface options for variable-speed, permanent-magnet generators," Electric Power Applications, IEE Proceedings, vol. 145, no. 4, pp. 273-283, July 1998.

[66] B. Wu, Y. Lang, N. Zargari, and S. Kouro, *Power Conversion and Control of Wind Energy Systems*. New Jersey: Hoboken, 2011.

[67] H. -J. Knaak, "Modular multilevel converters and HVDC/FACTS: a success story," *in Proc. 2011-14th European Conference on Power Electronics and Applications*, 2011, pp. 1-6.

[68] C. Du, E. Agneholm, and G. Olsson, "VSC-HVDC system for industrial plants with onsite generators," *IEEE Transactions on Power Delivery*, vol. 24, no. 3, pp. 1359-1366, Jul. 2009.

[69] A. Lesnicar and R. Marquardt, "An innovative modular multilevel converter topology suitable for a wide power range," in *Proc. Power Tech Conference, 2003 IEEE Bologna*, vol. 3, Jun. 2003.

[70] M. A. Perez, J. Rodriguez, E. J. Fuentes, and F. Kammerer, "Predictive control of AC-AC modular multilevel converters," *IEEE Transactions on Industrial Electronics*, vol. 59, no. 7, pp.2832-2839, Jul. 2012.

[71] S. Kouro, M. Malinowski, K. Gopakumar, J. Pou, L. G. Franquelo, B. Wu, J. Rodriguez, M. A. Pérez, and J. I. Leon, "Recent advances and industrial applications of multilevel converters," *IEEE Transactions on Industrial Electronics*, vol. 57, no. 8, pp. 2553-2580, Aug. 2010.

[72] J. Duncan Glover and M. Sarma, *Power System Analysis and Design (Second Edition)*, Boston: PWS, 1994, pp.327.

[73] J. G. Slootweg, S.W.H. de Haan, H. Polinder, and W. L. Kling, "General model for representing variable speed wind turbines in power system dynamics simulations," *IEEE Transactions on Power System*, vol. 18, pp. 144–151, February 2003.

[74] E. Koutroulis and K. Kalaitzakis. "Design of a Maximum Power Tracking System for Wind-Energy-Conversion Applications," *IEEE Transactions on industrial electronics*, vol. 53, pp. 486-494, April 2006.

[75] J. Jonkman, S. Butterfield, W. Musial, and G.scott, "Definition of a 5-MW reference wind turbine for offshore system development," National Renewable Energy Laboratory, U. S., Tech. Rep. NREL/TP-500-38060, Feb. 2009.

[76] S. Achilles and M. Poller, "Direct drive synchronous machine models for stability assessment of wind farms," in *Proc. of 4th International Workshop on Large-Scale Integration of Wind Power and Transmission Networks for Offshore Wind Farms*, Billund, 2003, pp. 1-9.

[77] S. M. Muyeen, Md. Hasan, R. Takahashi, T. Murata, J. Tamura, Y. Tomaki, A. Sakahara, and E. Sasano, "Comparative study on transient stability analysis of wind turbine generator system using different drive train models," *IET Renew. on Power Gener.*, vol. 1, no. 2, pp. 131-141, 2007.

[78] L. A. C. Lopes, J. Lhuilier, A. Mukherjee, and M. F. Khokhar, "A wind turbine emulator that represents the dynamics of the wind turbine rotor and drive train," *Power Electronics Specialists Conference, 2005. PESC. IEEE 36th*. pp. 2092-2097, June 2005.

[79] T. Sun, Z. Chen, and F. Blaabjerg, "Voltage recovery of grid-connected wind turbines after a short-circuit fault," in *Proc. The 29th Annual Conf. Of IEEE Ind. Electron. Soc., IECON'03*, Roanoke, VA, USA, vol. 3, pp. 2723-2728, November. 2003.

[80] S. S. Fazel, S. Bernet, D. Krug, and K. Jalili, "Design and comparison of 4-kV neutral-point-clamped, flying-capacitor, and series-connected H-bridge multilevel converters," *IEEE Transactions on Industry Applications*, vol. 43, no. 4, pp. 1032-1040, Jul./Aug. 2007.

[81] C. M. Wu, W. H. Lau, and H. Chung, "A five-level neutral-point-clamped H-bridge PWM inverter with superior harmonic suppression: A theoretical analysis," in *Proc. 1999 IEEE Int. Symp. Circuits and Systems*, Orlando, FL, May 30-Jun. 2 1999, vol. 5, pp. 198-201.

[82] Z. Cheng and B. W, "A novel switching sequence design for five-level NPC/H-bridge inverters with improved output voltage spectrum and minimized device switching frequency," *IEEE Transactions on Power Electronics,* vol. 22, no. 6, pp.2138-2145, Nov. 2007.

[83] K. Hyosung, K. Jang-Hwan, and S. Seung-Ki, "A design consideration of output filters for dynamic voltage restorers," in *Proc. 35th IEEE Power Electronics Specialists Conference*, 2004, pp.4268-4272.

[84] X. Yuan, F. Wang, D. Boroyevich, Y. Li, and R. Burgos, "DC-link voltage control of a full power converter for wind generator operating in weak-grid systems," *IEEE Transactions on Power Electronics*, vol. 24, no. 9, pp. 2178-2192, September 2009.

[85] V. Valtchev, A. Bossche, J. Ghijselen, and J. Melkebeek, "Autonomous renewable energy conversion system," *Renew. Energy*, vol. 19, no. 1, pp.259-275, 2000.

[86] Z. Chen and E. Spooner, "Voltage source inverters for high-power, variable-voltage DC power sources," *IEE Proceedings, Generation, Transmission and Distribution*, vol. 148, no. 5, pp. 439-447, 2001.

[87] G. F. Franklin and J. D. Powell, *Feedback Control of Dynamic Systems (Fourth Edition)*. New Jersey: Prentice Hall, 2002.

[88] C. Du, "VSC-HVDC for industrial power systems," Ph.D. dissertation, Chalmers Univ. Technol., Göteborg, Sweden, 2007.

[89] A. Lesnicar and R. Marquardt, "An innovative modular multilevel converter topology suitable for a wide power range," in *Proc. Power Tech Conference, 2003 IEEE Bologna*, vol. 3, Jun. 2003.

[90] M. A. Perez, J. Rodriguez, E. J. Fuentes, and F. Kammerer, "Predictive control of AC-AC modular multilevel converters," *IEEE Transactions on Industrial Electronics*, vol. 59, no. 7, pp. 2832-2839, Jul. 2012.

[91] S. Kouro, M. Malinowski, K. Gopakumar, J. Pou, L. G. Franquelo, B. Wu, J. Rodriguez, M. A. Pérez, and J. I. Leon, "Recent advances and industrial applications of multilevel converters," *IEEE Transactions on Industrial Electronics*, vol. 57, no. 8, pp. 2553-2580, Aug. 2010.

[92] B. Gemmell, J. Dorn, D. Retzmann, and D. Soerangr, "Prospects of multilevel VSC technologies for power transmission," in *Proc. IEEE/PES T & D Conf. Expo.*, pp. 21-24, Apr. 2008, pp. 1-16.

[93] SIEMENS, Introduction to HVDC Plus, [Online]. Available: https://www.energy-portal.siemens.com/static/hq/en/products_solutions/1652_kn03011203.html

[94] SIEMENS, HVDC PLUS-Basics and Principle of Operation, [Online]. Available: http://www.energy.siemens.com/mx/pool/hq/power-transmission/HVDC/HVDC_ Plus_Basics_and _Principle.pdf

[95] J. Rodr ́guez, S. Bernet, B. Wu, J. O. Pontt, and S. Kouro, "Multilevel voltage-source-converter topologies for industrial medium-voltage drives," *IEEE Transactions on Industrial Electronics*, vol. 54, no. 6, pp. 2930-2945, Dec. 2007.

[96] M. Hagiwara, and H. Akagi, "Control and experiment of pulsewidth-modulated modular multilevel converters*," IEEE Trans. Power Electron*, vol. 24, no. 7, pp. 1737-1746, Jul. 2009.

[97] S. Rohner, S. Bernet, M. Hiller, and R. Sommer, "Modulation, losses, and semiconductor requirements of modular multilevel converters," *IEEE Transactions on Industrial Electronics*, vol. 57, no. 8, pp. 2633-2642, Aug. 2010.

[98] U. N. Gnanarathna, A. M. Gole, and R. P. Jayasinghe, "Efficient modeling of modular multilevel HVDC converter (MMC) on electromagnetic transient simulation programs," *IEEE Transactions on Power Delivery*, vol. 26, no. 1, pp. 316-324, Jan. 2011.

[99] Q. Tu, Z. Xu, and L. Xu, "Reduced switching-frequency modulation and circulating current suppression for modular multilevel converters," *IEEE Transactions on Power Delivery*, vol. 26, no. 3, pp. 2009-2017, Jul. 2011.

[100] Q. Tu and Z. Xu, "Impact of sampling frequency on harmonic distortion for modular multilevel converter," *IEEE Transactions on Power Delivery*, vol. 26, no. 1, pp. 298-306, Jan. 2011.

[101] A. Antonpoulos, L. Angquist, and H. P. Nee, "On dynamics and voltage control of the modular multilevel converter," in *Proc. Eur. Conf. Power Electron. Appl.*, Barcelona, Spain, 2009, pp. 1-10.

[102] G. S. Konstantinou and V. G. Agelidis, "Performance evaluation of half-bridge cascaded multilevel converters operated with multicarrier sinusoidal PWM techniques," in *Proc. IEEE Conf. Ind. Electron. Appl*. Xi'an, China, 2009, pp. 3399-3404.

[103] M. Rahimi and M. Parniani, "Efficient control scheme of wind turbines with doubly fed induction generators for low-voltage ride-through capability enhancement," *Renewable Power Generator, IET*, vol. 4, no. 3, pp. 242-252, 2010.

[104] A. Mullane, G. Lightbody, and R. Yacamini, "Wind-turbine fault ride-through enhancement," *IEEE Transactions on Power Systems*, vol. 20, no. 4, pp. 1929-1937, 2005.

[105] T. Sun, Z. Chen, and F. Blaabjerg, "Transient Stability of DFIG Wind Turbines at an External Short-circuit Fault," *Wind Energy*, vol. 8, no. 3, pp. 345-360, 2005.

[106] C. Cho, S. Nam, S. Kang, and S. Ahn, "Modeling of DFIG wind turbines considering fault-ride-through grid code," in *Proc. Advanced Power System Automation and Protection*, 2011, pp. 1024-1028.

[107] L. Max, "Design and control of a DC collection grid for a wind farm," Ph.D. dissertation, Chalmers Univ. Technol., Göteborg, Sweden, 2009.

[108] T. Worzyk, *Submarine Power Cables: Design, Installation, Repair Environment Aspects*. New York: Springer, 2009, pp. 224.

[109] B. Gustavsen, "Validation of frequency-dependent transmission line models," *IEEE Transactions on Power Delivery*, vol. 20, no. 2, pp. 925-933, Apr. 2005.

[110] J. R. Marti, "Accurate modeling of frequency-dependent transmission lines in electromagnetic transient simulations," *IEEE Trans. on Power App. and Syst.*, vol. PAS-101, no. 1, pp. 147-157, Jan. 1982.

[111] A. Morched, B. Gustavsen, and M. Tartibi, "A universal model for accurate calculation of electromagnetic transients on overhead lines and underground cables," *IEEE Transactions on Power Delivery*, vol. 14, no. 3, pp. 1032-1038, Jul. 1999.

[112] HVDC Light@ Cables, *Submarine and land power cables*, 2010. [Online].Available:http://www05.abb.com/global/scot/scot245.nsf/veritydisplay/1591f139098f62e5c1257154002f9801/$File/HVDC%20Light%20power%20cables.pdf

[113] HVDC Light Cables, *Submarine and Land Power Cables*. [Online]. Available: http://www05.abb.com/global/scot/scot245.nsf/veritydisplay/1591f139098f62e5c1257154002f9801/$File/HVDC%20Light%20power%20cables.pdf, ABB, 2010.

Appendix A

5 MW Wind Turbine System Parameters

TABLE A
5 MW Wind Turbine system Parameters

Parameters	Value
Wind turbine rated power (MW)	5
Rotor diameter (m)	126
Rotating speed (r/m)	6.9~11.94
Nominal wind speed (m/s)	11.4
Generator Rated power (MW)	5
Stator rated line voltage (kV)	3
Rated frequency (Hz)	20
Number of pole pairs	100
Stator winding resistance (p.u.)	0.001
Unsaturated induction X_d (p.u.)	0.15
Unsaturated induction X_q (p.u.)	0.1
Magnetic strength (p.u.)	1
Generator inertia (s)	0.84
Equivalent wind turbine inertia (s)	5.54
Shaft stiffness *K* (p.u.)	2.15
Shaft damping *D* (p.u.)	0.015

Appendix B

2.5 MW Wind Turbine System Parameters

TABLE B
2.5 MW Wind Turbine System Parameters

Parameters	Value
Wind turbine power (MW)	2.5
Rotor diameter (m)	100
Rotating speed (r/m)	9.6~15.5
Gear ratio	26:1
Generator power (MW)	2.5
Rated line-to-line voltage (kV)	4
Frequency (Hz)	40
Number of pole pairs	6
Stator winding resistance R_s (p.u.)	0.0038
Unsaturated induction X_d (p.u.)	0.25
Unsaturated induction X_q (p.u.)	0.62
Magnetic strength (p.u.)	1.1
Capacitors C_g (μF)	150
Capacitors C_{i1} and C_{i2} (mF)	6.8
Turn ratio of the MFT	1:7
Inductance L_s (mH)	0.4
Capacitor C_s (μF)	15
Inductance L_d (mH)	1
Capacitor C_o (μF)	330
Cable inductance L_c (mH/km)	0.5
Cable resistance R_c (Ω/km)	0.15
Cable length (km)	10
DC network voltage V_o (kV)	40
Switching frequency (kHz)	2

Appendix C

Experimental Circuit Parameters

TABLE C
IFBTL DC/DC Converter Experimental Parameters

Parameters	Value
Capacitors C_{i1} and C_{i2} (uF)	330
Inductance L_s (mH)	0.4
Capacitor C_s (μF)	3
Turn ratio of the MFT	1:2.6
Inductance L_d (mH)	0.4
Capacitor C_o (μF)	1000
DC network voltage V_o (V)	250
DC network inductance (mH)	0.4
DC network resistance (Ω)	0.1
Switching frequency (kHz)	5

Appendix D

Cable Parameters

The frequency dependent phase model is applied as the simulation model for cable in PSCAD/EMTDC [109-101]. The cable layout is shown in Fig. A.1, which consists of a copper core conductor with a cross section of 1200 mm^2, a lead sheath, a steel armor, and insulating layers. All relevant data are listed in Table I, which is based on a cable design that is assembled from [9], [112] and [113].

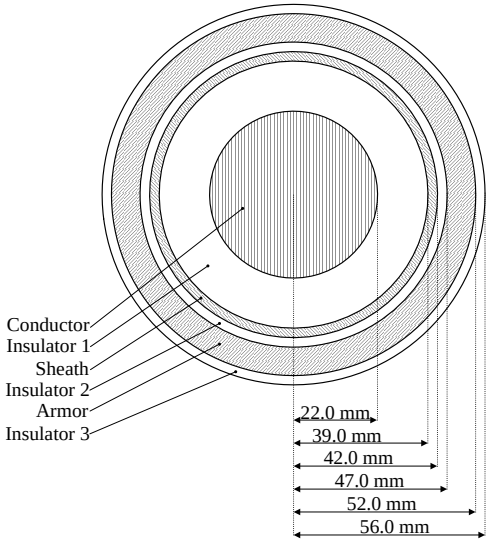

Fig. D.1. Dimensions of the cable model

TABLE D
Properties of the Cable

Layer	Material	Thickness (mm)	Resistivity (Ω·m)	Rel. per-mittivity	Rel. per-meability
Core	copper	22	$1.68 \cdot 10^{-8}$	-	1
Insulator	XLPE	17	-	2.3	1
Sheath	Lead	3	$2.2 \cdot 10^{-7}$	-	1
Insulator	XLPE	5	-	2.3	1
Armor	Steel	5	$1.8 \cdot 10^{-7}$	-	10
Insulator	PP	4	-	2.1	1

Appendix E

HVDC Transmission System Parameters

TABLE E
HVDC Transmission System Parameters

Parameters	Value
Rated power for each positive (negative) converter (MW)	200
DC-link voltage V_{n1} and V_{n2} (kV)	150
Capacitor C_{n1}, C_{n2}, C_{f1} and C_{f2} (uF)	35.5
Reactor inductor L_f (mH)	16
Reactor resistor R_f (Ω)	0.16
AC Transformer leakage reactance	20 %
Onshore converter switching frequency (Hz)	1950
Offshore converter switching frequency (Hz)	1950
Offshore converter reference frequency (Hz)	200